Structure and function in glaucoma: OCT/A and ERG investigations

Dissertation
zur Erlangung des akademischen Grades

doctor rerum naturalium (Dr. rer. nat.)

genehmigt durch die Fakultät für Naturwissenschaften
der Otto-von-Guericke-Universität Magdeburg

von: **M.Sc., Khaldoon Omer Ali Al-Nosairy**
geb. am 02. November 1984 in Sana'a, Jemen

Gutachter: apl. Prof. Dr. rer. nat. Michael Hoffmann
Prof. Dr. rer. nat. Peter Heiduschka

eingereicht am: 21. Januar 2021
verteidigt am: 31. August 2021

Table of contents

List of figures & tables

List of abbreviations

AUC	Area under receiver operating characteristic curve
CRT	Cathode ray tube
CDR	Cup disc ratio
ERG	Electroretinogram/graphy
IO	Eyemate intraocular pressure sensor
IOP/IOD	Intraocular pressure/ Intraocular Druck
GCL	Ganglion cell layer
INL	Inner nuclear layer
IPL	Inner plexiform layer
LGB	Lateral geniculate body
LDP	Lateral decubitus posture/position
mfERG	Multifocal electroretinogram
mGCIPL	Macular ganglion cell inner plexiform layer
mfPhNR	Multifocal photopic negative response
NFL	Nerve fiber layer
NTG	Normal tension glaucoma
OAG	Open angle glaucoma
OCT/A	Optical coherence tomography/angiography
PERG	Pattern electroretinogram
pfVD	Parafoveal vessel density
PhNR	Photopic negative response
POAG	Primary open angle glaucoma
pRNFL	Peripapillary retinal nerve fiber layer
pVD	Peripapillary vessel density
RGC	Retinal ganglion cell
RNFL	Retinal nerve fiber layer
RPE	Retinal pigment epithelium
SAP	Standard automated perimetry
SD-OCT	Spectral domain optical coherence tomography
SS-OCT	Swept source optical coherence tomography
ssPERG	Steady state PERG

Zusammenfassung

Die klinische Beurteilung des Glaukoms wird durch das begrenzte Verständnis der zugrundeliegenden Pathophysiologie und durch die suboptimale diagnostische Leistung der etablierten Methoden erschwert. Elektrophysiologische Maße der Sehfunktion ermöglichen nicht nur Glaukomärzten und Glaukomforschern einen intuitiven Ansatz zur Entschlüsselung der Struktur-Funktions-Beziehung von Glaukomschäden, sondern tragen auch dazu bei, die Erkennung von Glaukomen in frühen Stadien zu beschleunigen. In dieser Arbeit wurden state-of-the-art wie auch innovative Technologien der Ophthalmologie und Glaukomforschung angewandt, um i) unser Verständnis der Beziehung zwischen intraokularem Druck und retinaler Ganglienzellfunktion (IOD-RGC) zu fördern, ii) die Detektion von Glaukomen zu verbessern und iii) die Struktur-Funktions-Beziehung bei Glaukomen zu ermitteln.

i) IOD-RGC Beziehung. Der IOD ist ein Hauptrisikofaktor beim Glaukom und unterliegt unter anderem tageszeitlichen, langfristigen und positionsabhängigen Fluktuationen. Eine kombinierte Bewertung der IOD-RGC-Funktion kann einen umfassenden Ansatz zur Beurteilung solcher Fluktuationen bieten. Kontinuierliche und simultane IOD-RGC- und Muster-Elektroretinogramm (PERG) Messungen werden mit der Verfügbarkeit eines telemetrischen Augeninnendrucksensors (eyemate-IO Sensor) ermöglicht. In dieser Studie wurde zum ersten Mal die Machbarkeit der gleichzeitigen und kontinuierlichen IOD- und RGC-Funktionsmessungen demonstriert und die Auswirkungen von IOD-Änderungen auf die RGC-Funktion während IOD-Manipulationen anhand eines Positionierungsmodells untersucht. Hier wurde gezeigt, dass während der lateralen Dekubitus-Lagerung (LDP, Seitenlagerung) der IOD im unteren Auge der Kontroll- [+1,6 mmHg, P = 0,02] und der eyemate-IO Glaukompatienten [+5,1 mmHg, P = 0,00004] anstieg, während die PERG-Amplitude abnahm [-17%, P = 0,005 bzw. -25%, P = 0,02], was auf reduzierte RGC-Antworten hinweist. Die experimentellen Ergebnisse dieses Testprotokolls könnten die LDP zu einem provokativen Test für die frühzeitige Erkennung von Glaukomverdachtsfällen machen und somit helfen, rechtzeitig entsprechende Therapien einleiten. Darüber hinaus könnte die LDP ein Modell sein, um spezifische Schädigungsmechanismen beim Glaukom zu entschlüsseln, wie beispielsweise die einseitige Glaukomschädigung.

ii) Diagnose des Glaukoms. Zwei Tests sind von besonderem Interesse für die Beurteilung der RGC-Funktion: die photopische negative Antwort (PhNR) und das PERG. Die multifokale PhNR (mfPhNR) ist eine Ergänzung der fokalen ERG-Ableitungen und ermöglicht die Beurteilung von multiplen Gesichtsfeld-Antworten innerhalb der zentralen 40-50° Netzhautareals. Die Ergebnisse dieser Studie legen nahe, dass die mfPhNR/-Ratio im Vergleich zur globalen Netzhautantwort keinen Vorteil für die topographische Analyse von Gesichtsfelddefekten bietet. Die mfPhNR Ratio der Globalantwort zeigte dennoch die höchste diagnostische Leistung [AUC = 0,84, P = 0,008] zur Erkennung von Glaukomverdachtsfällen gegenüber anderen etablierten Methoden, d.h. pRNFL [AUC = 0,74, P ≤ 0,05] und PERG [AUC = 0,78, P = 0,039]. Es wurde auch festgestellt, dass jede Veränderung der peripapillären retinalen Nervenfaserschicht (pRNFL), die mittels optischer Kohärenztomographie (OCT) erhoben wurde, signifikante Veränderungen in diesen ERG-Messungen anzeigt. Die ERG-Indizes der Sehfunktion bieten die Möglichkeit, frühe Veränderungen beim Glaukom zu erkennen und möglicherweise die strukturellen Veränderungen im Falle einer glaukomatösen Progression zu verfolgen.

iii) Struktur-Funktions-Verhältnis beim Glaukom. Eine substanzielle Anzahl von Glaukompatienten weist einen normalen IOD auf, während sich bei anderen, trotz guter Kontrolle des IODs, eine Verschlechterung einstellt, was zunehmend die Bedeutung anderer Risikofaktoren als des IODs in der Glaukom-Pathogenese belegt. Vaskuläre Dysfunktion steht an erster Stelle unter den nicht-IOD-Risikofaktoren. Die OCT-Angiographie (OCT-A) baut auf der OCT-Technologieplattform auf und fügt den aktuellen strukturellen Methoden [Makula-Ganglienzell-Plexiformschicht (mGCIPL) und pRNFL] eine robuste Dimension hinzu, indem sie erlaubt den vaskulären Status verschiedener Netzhautschichten [parafoveale (pfVD) und peripapilläre Gefäßdichte (pVD)] zu beurteilen. Hier wurde durch eine multimodale Untersuchung eine stärkere Assoziation zwischen funktionell/strukturellen Maßnahmen festgestellt [mfPhNR Ratio/mGCIPL Korrelation von 0.58 (P = 0. 001) und mfPhNR Ratio/pRNFL Korrelation von 0,66 (P ≤ 0,001)] als zwischen funktionell/vaskulären Maßnahmen [mfPhNR Ratio/pfVD Korrelation von 0,29 (P = 0,13) und mfPhNR Ratio/pVD Korrelation von 0,54 (P = 0,003)]. Dieser Befund könnte dazu beitragen, Aspekte der zeitlichen Abfolge der glaukomatösen Schädigung aufzudecken, die für effizientere Behandlungsschemata relevant sind.

Zusammenfassend lässt sich sagen, dass die Integration von OCT/A- und ERG-Messungen eine präzise Beurteilung des Glaukomschadens mit einer daraus resultierenden Früherkennung ermöglicht, die entscheidend ist, um glaukombedingte Beeinträchtigungen zu reduzieren und zu verhindern. Daher kann die Anwendung eines solchen multimodalen Ansatzes in der klinischen Praxis die Genauigkeit der Glaukomdiagnose erhöhen und somit Spätentdeckungen von Glaukomfällen vermeiden.

Abstract

The clinical assessment of glaucoma is hampered by the limited understanding of the underlying pathophysiology and by the suboptimal diagnostic performance of the established methods. Electrophysiological measures of visual function not only empower glaucoma clinicians and researcher alike with an intuitive approach to decipher the structure-function relationship of glaucoma damage, but also contribute to expedite the detection of glaucoma at early stages. In this thesis, state of the art and emerging technologies in ophthalmology and glaucoma research were applied i) to promote our understanding of the relationship of intraocular pressure and retinal ganglion cell function (IOP-RGC), ii) to improve the detection of glaucoma and iii) to ascertain the structure-function relationship in glaucoma.

i) IOP-RGC relationship. The IOP is a major risk factor in glaucoma and subjects to diurnal, long-term and positional fluctuations. A combined assessment of the IOP-RGC relationship may provide a comprehensive approach to assess such fluctuations. Continual simultaneous IOP-RGC measurements are deemed possible with the availability of the telemetric intraocular pressure sensor (eyemate-IO sensor) combined with pattern electroretinogram (PERG) measurements. For the first time, this study demonstrated the feasibility of simultaneous and continual IOP and RGC-function readouts and studied the impact of IOP changes on the RGC function during IOP manipulations using a positional model. Here, it was demonstrated that during lateral decubitus posture (LDP), the IOP increased in the lower eye of the control [+1.6 mmHg, P = 0.02] and eyemate-IO glaucoma patients [+5.1 mmHg, P = 0.00004] while the PERG amplitude decreased [-17%, P = 0.005 and -25%, P = 0.02, respectively], indicating reduced RGC responses. The experimental results of this testing protocol might render the LDP a provocative test for the early detection of glaucoma suspects and initiate timely the appropriate therapy. Furthermore, the LDP may be a model to decipher damage mechanisms in glaucoma such as unilateral glaucomatous damage.

ii) Detection of glaucoma. Two tests are of a particular interest in the assessment of the RGC function: the photopic negative response (PhNR) and the PERG. The multifocal PhNR (mfPhNR) has supplanted the focal ERG recordings and allows for the assessment of multiple visual field responses elicited within the central 40-50° of the retina. The findings of this study suggest that mfPhNR/-ratio did not offer any privilege for the

topographical analysis of visual defects in comparison to the global, i.e. summed, mfPhNR/-ratio. The mfPhNR ratio of the global response showed yet the highest discriminatory performance [AUC = 0.84, P = 0.008] to detect glaucoma suspects vs other established methods, i.e. pRNFL [AUC = 0.74, P ≤ 0.05] and PERG [AUC = 0.78, P = 0.039]. It was also found that any change of the peripapillary retinal nerve fiber layer (pRNFL) obtained from optical coherence tomography (OCT) imaging reflected corresponding changes in these ERG measures. The ERG indices of the visual function offer the ability to detect early changes in glaucoma and to possibly track the structural changes in cases of glaucomatous progression.

iii) Structure-function relationship in glaucoma. A substantial number of glaucoma patients presents with normal IOP while others still deteriorate albeit the good control of the IOP supporting the increasingly clear role of other risk factors than the IOP in glaucoma pathogenies. Vascular dysfunction is foremost among those non-IOP risk factors. The OCT-Angiography (OCT-A) builds on the OCT technology platform and adds a robust dimension to the current structural methods by assessing the vascular status of different retinal layers. Here, by multimodally scrutinizing the interrelationship of ERG measures vs surrogate clinical structural [macular ganglion cell plexiform layer (mGCIPL) and pRNFL] and vascular measures [parafoveal (pfVD) and peripapillary vessel density (pVD)], a stronger functional/structural measures association [mfPhNR ratio/mGCIPL correlation of 0.58 (P = 0.001) and mfPhNR ratio/pRNFL correlation of 0.66 (P ≤ 0.001)] than functional/vascular measures association [mfPhNR ratio/pfVD correlation of 0.29 (P = 0.13) and mfPhNR ratio/pVD of 0.54 (P = 0.003)] was reported. This finding might help to uncover aspects of the temporal sequence of glaucomatous damage with relevance for efficient treatment schemes.

In conclusion, the integration of OCT/A and ERG measures provides a careful assessment of glaucoma damage with the resultant early detection which is critical to minimize and hinder glaucoma related visual disability. Therefore, the application of such a multimodal approach in clinical settings may increase the accuracy of glaucoma diagnosis and thus obviate error prone late detections of glaucoma cases.

Chapter 1

Introduction

A vital element to a functioning visual system is the retinal and optic nerve integrity. In glaucoma, the “silent theft of vision”, patients have constricted visual fields due to apoptosis of the retinal ganglion cells (RGCs) and the associated loss of the retinal nerve fiber layer (RNFL). In glaucoma, many RGCs may be lost before any detectable defects appear on the standard visual field tests mandating an enhanced approach for the early glaucoma diagnosis and the understanding of damage mechanisms. As objective measures of visual function, electrophysiological indexes not only offer the promise for early detection but also complement other diagnostic methods for the assessment of the glaucoma pathogenesis.

The glaucomatous damage might be a consequence of the interplay of several factors on the RGCs, e.g. the IOP and the vascular dysfunction. Therefore, the development of more efficient techniques to evaluate these risk factors might render the understanding of the damage cascades possible and hence carry out a timely and an appropriate intervention. The continuous quantification of IOP levels is one technique that could improve the care for glaucoma. Another relatively recent method is the evaluation of retinal microvasculature using the optical coherence tomography (OCT) platform [OCT angiography (OCT-A)] that will expand the means to probe the anatomical damage seen in glaucoma. The combined use of functional and anatomical (structural/vascular) methods is of promise for an efficient assessment of this prevalent eye disease.

In this thesis, I explored the application of the electroretinography (ERG) along with these contemporary methods in the management of glaucoma. In chapter 5, I investigated a glaucoma provocative test model by studying the influence of postural changes on the intraocular pressure (IOP) and the RGC function using the simultaneous novel IOP measurement (eyemate-IO® sensor, Implandata) and the pattern electroretinogram recording, respectively. Using the ERG coupled with multifocal techniques (chapter 6), i.e. multifocal photopic negative response (mfPhNR), I carried out a topographical analysis of the visual field defects and assessed the diagnostic performance in glaucoma especially to

detect glaucoma suspects. Finally, employing a multimodal approach of the ERG along with OCT/A measures (chapter 7), I studied the temporal relationship of the glaucomatous damage as well as evaluated the discriminatory power of these measures. In brief, these studies might may contribute to optimizing the diagnosis and the elucidation of the pathophysiology of glaucoma (chapter 5, 6 & 7).

Chapter 2

Background

2.1 Human visual system

The visual system consists of three major parts i) the eye in which light strikes the retina and signals are generated and carried through the optic nerve and the optic tract to synapse in ii) the lateral geniculate body (LGB) that projects to iii) the visual cortex.

2.1.1 The eye

The eye is a complex organ with more than 80% of human sensory input coming through the sight (Brar et al., 2019). Moreover, it is an anatomical window into the nervous and the vascular systems. The eyeball or globe consists of 3 concentric layers, an outer protective, a middle vascular and an inner neural layer (Figure 1). The outer layer comprises the clear cornea anteriorly and the opaque posterior sclera whose role is to protect the internal ocular tissues. The uvea, i.e. the middle layer, consists of the choroid, the ciliary body and the iris and it serves supportive and nutritive roles, such as oxygen supply to the outer part of the neural layer. Inner to the uvea is a photosensitive layer that initiates visual processing. These coats surround the lens, the aqueous humor and the vitreous body (Brar et al., 2019; Girkin et al., 2019; Snell and Lemp, 2013).

The eye also comprises three compartments: the anterior chamber, the posterior chamber and the vitreous cavity. The anterior and the posterior chamber contain the aqueous humor. The latter is secreted by the ciliary body and drains either into the Schlemm canal through the trabecular meshwork (Figure 2) or into the suprachoroidal space through the iris and ciliary muscle, i.e. the conventional or uveoscleral pathways, respectively. The third compartment is the vitreous cavity that makes up two thirds of the volume of the eye and is filled with the vitreous gel. (Brar et al., 2019; Girkin et al., 2019; Snell and Lemp, 2013).

2.1.1.1 The retina and optic nerve

The retina is a remarkable modification of the forebrain that collects, codes and transmits information through the optic nerve to further processing areas in the brain.

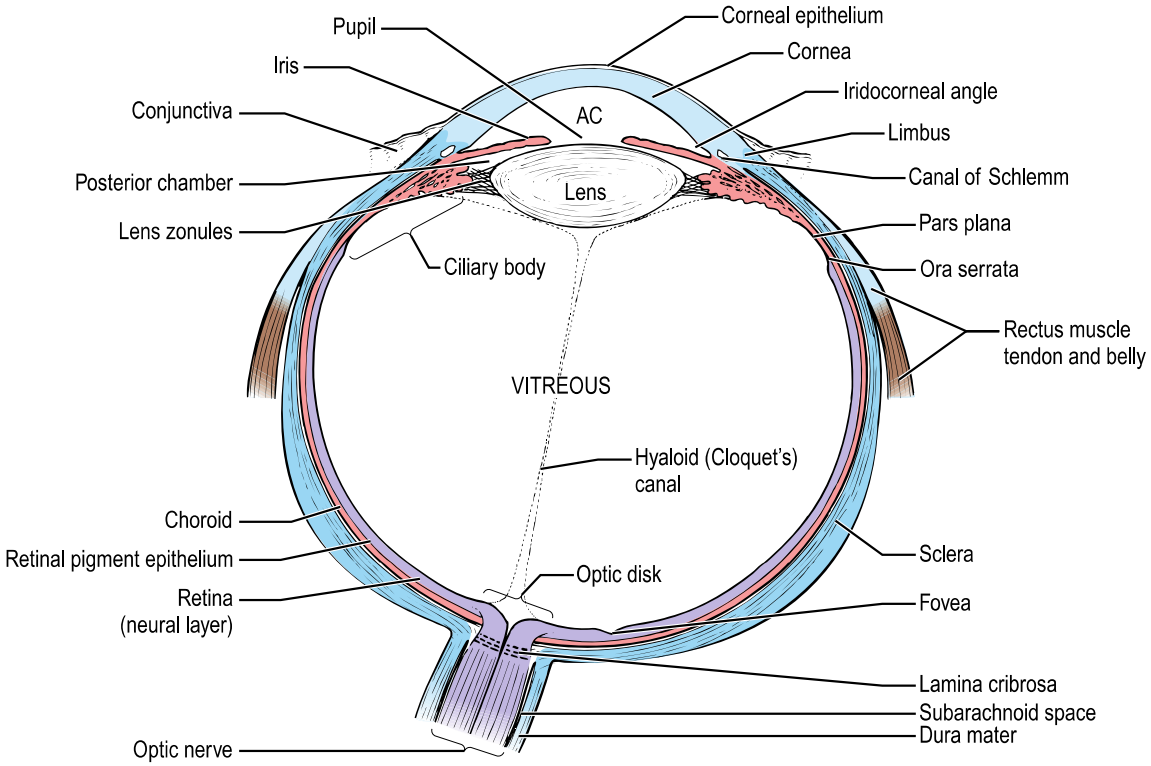

Figure 1. Horizontal section of an eye with major components.
The outer layer (blue), the middle vascular layer-uveal tract (orange/red) and the inner neural layer (purple). Reprinted with permission from (Forrester et al., 2015); The Eye; Elsevier copyright: 2015.

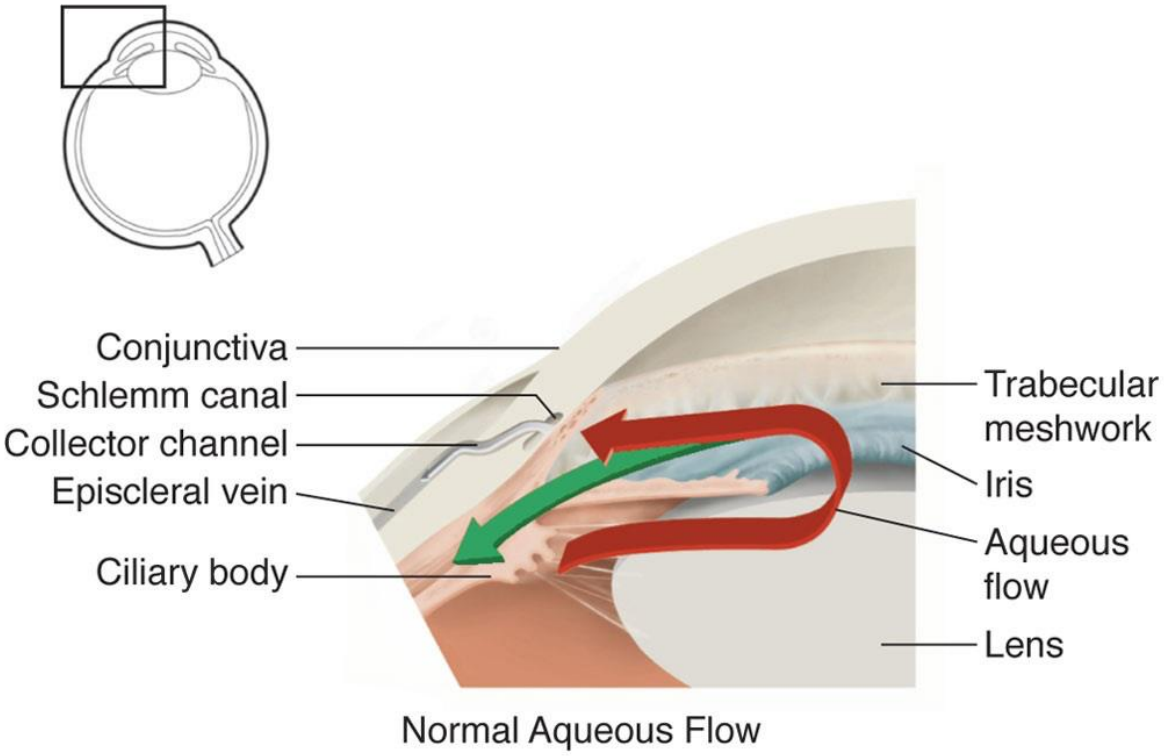

Figure 2. Anterior segment of a healthy eye showing aqueous humor production and drainage.
Red and green arrows: sites of conventional aqueous and the uveoscleral outflow pathway, respectively Reprinted with permission from (Girkin et al., 2019); Glaucoma; American Academy of Ophthalmology (AAO) copyright: 2019.

Embryologically, the retina has a neuroectodermal origin, i.e. the optic vesicle, and consists of an outer layer that becomes the retinal pigment epithelium (RPE) and an inner layer that becomes the neurosensory retina (Brar et al., 2019; Girkin et al., 2019; McCannel et al., 2019; Snell and Lemp, 2013).

The RPE is a single layer of hexagonal cells extending from the optic nerve to the ora serrata and involved in many functions such as the formation of the outer blood ocular barrier and the absorption of excess light (Brar et al., 2019; Girkin et al., 2019; McCannel et al., 2019; Snell and Lemp, 2013).

The neurosensory layer contains various neuronal, vascular and glial components. It is divided histologically into 9 layers (Figure 3 A) and encompasses highly specialized cells, rods (≈ 120 million) and cons (≈ 6 million) photoreceptors with ≈ 20:1 ratio. Other components (Figure 3 B) are the integrators (bipolar, horizontal, amacrine and ganglion cells), the output retinal nerve fiber layer (RNFL) and the supporting Müller glial cells (Brar et al., 2019; Denniston and Murray, 2018; Girkin et al., 2019; McCannel et al., 2019; Snell and Lemp, 2013).

Topographically, the central part of the retina is referred to as the macula which is bordered by the temporal vascular arcades (also known as posterior pole or area centralis). The macula is 5-6 mm in size and histologically defined by the presence of more than one layer of RGCs. It is subdivided (Figure 4) further into the foveal (a 1.5 mm-diameter), parafoveal (0.5 mm diameter with 6 layers of bipolar cells) and perifoveal region (1.5 mm wide, defined by 7-11 layers of bipolar cells).

The central part of the macular, the fovea, contains the 0.35 mm-diameter foveola with only one layer of photoreceptors. Within the fovea lies also the foveal avascular zone which is a 250-600 μm region devoid of retinal capillaries (Brar et al., 2019; Denniston and Murray, 2018; Girkin et al., 2019; McCannel et al., 2019; Salmon, 2019; Snell and Lemp, 2013).

Above and nasal to the macula by 0.8 and 0.3 mm, respectively, is a 1.8 mm pale pinkish area, i.e. the optic disc. The neuroretinal rim of the optic disc is an orange/pink tissue between the outer cup edge and the disc margin. The optic disc is evaluated using the 'ISNT' rule which describes the normal contour of disc rim being of decreasing thickness: Inferior, superior, nasal and temporal. The cup disc ratio (CDR) is the fraction of cup / disc

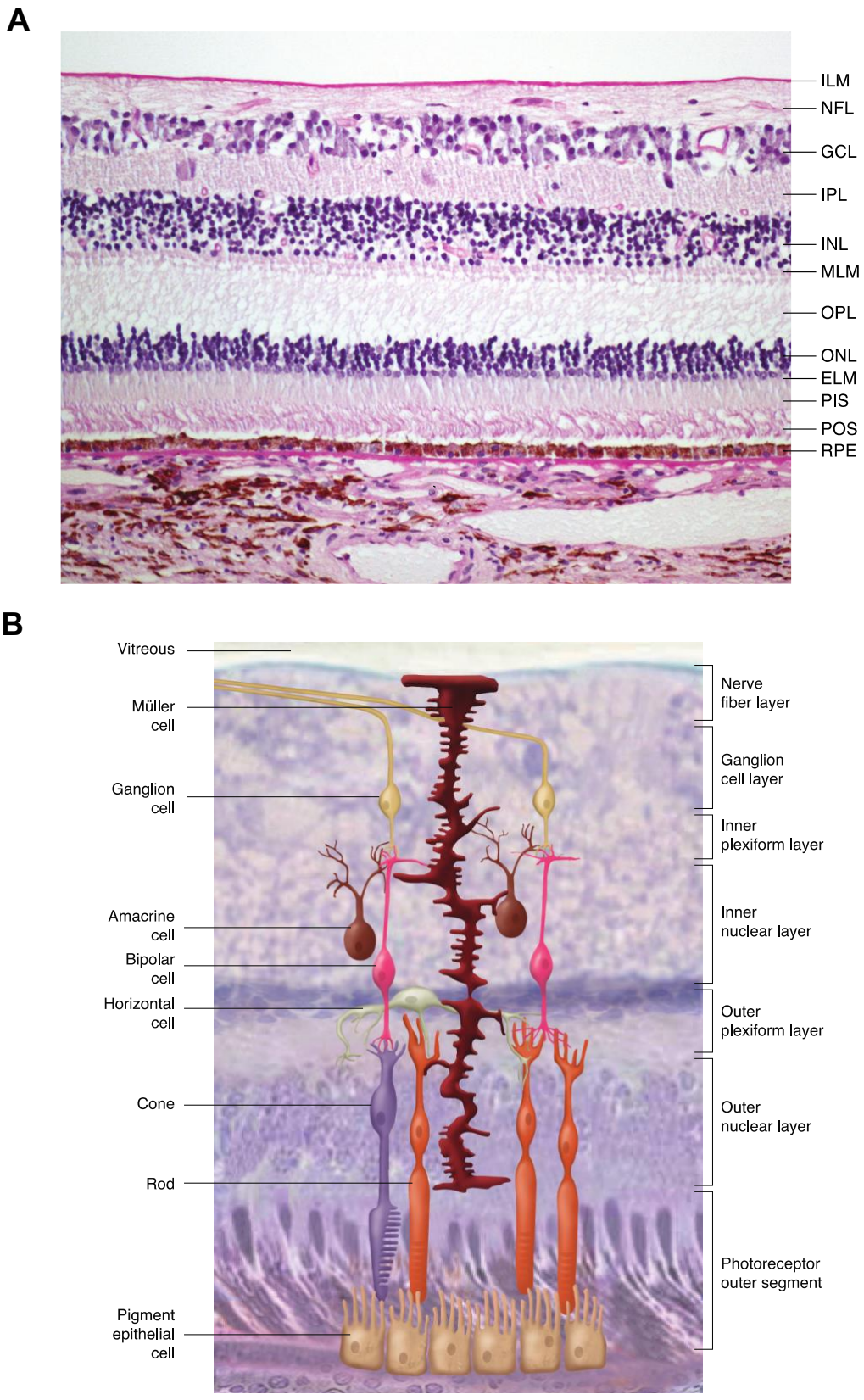

Figure 3. Microstructure of the retina.
(A) Retinal layers. From outer to inner layers: RPE = retinal pigment epithelium; POS/PIS = photoreceptor outer/inner segment; ELM=external limiting membrane; ONL=outer nuclear layer; OPL=outer plexiform layer; MLM=middle limiting membrane; INL=inner nuclear layer; IPL=inner plexiform layer; GCL = ganglion cell layer; NFL = nerve fiber layer; ILM = internal limiting membrane. (B) Different retinal cells. Reprinted with permission from (Brar et al., 2019); Fundamentals and Principles of Ophthalmology; AAO copyright: 2019.

diameters and in 98% of population CDR is ≤ 0.7 in which the vertical rather than the horizontal ratio is generally considered (Figure 4). The optic disc is devoid of retinal layers and photoreceptors (blind spot) through which the RNFL leaves to form the optic nerve. (Brar et al., 2019; Denniston and Murray, 2018; Girkin et al., 2019; McCannel et al., 2019; Salmon, 2019; Snell and Lemp, 2013).

The optic nerve is about 5 cm long and contains 1.2 million nerve fiber axons and extends to the LGB. Anatomically, it begins at the optic disc but functionally it begins from the ganglion cell layer covering the entire retina and continues to the optic chiasm (Brar et al., 2019; Denniston and Murray, 2018; Girkin et al., 2019; McCannel et al., 2019; Salmon, 2019; Snell and Lemp, 2013).

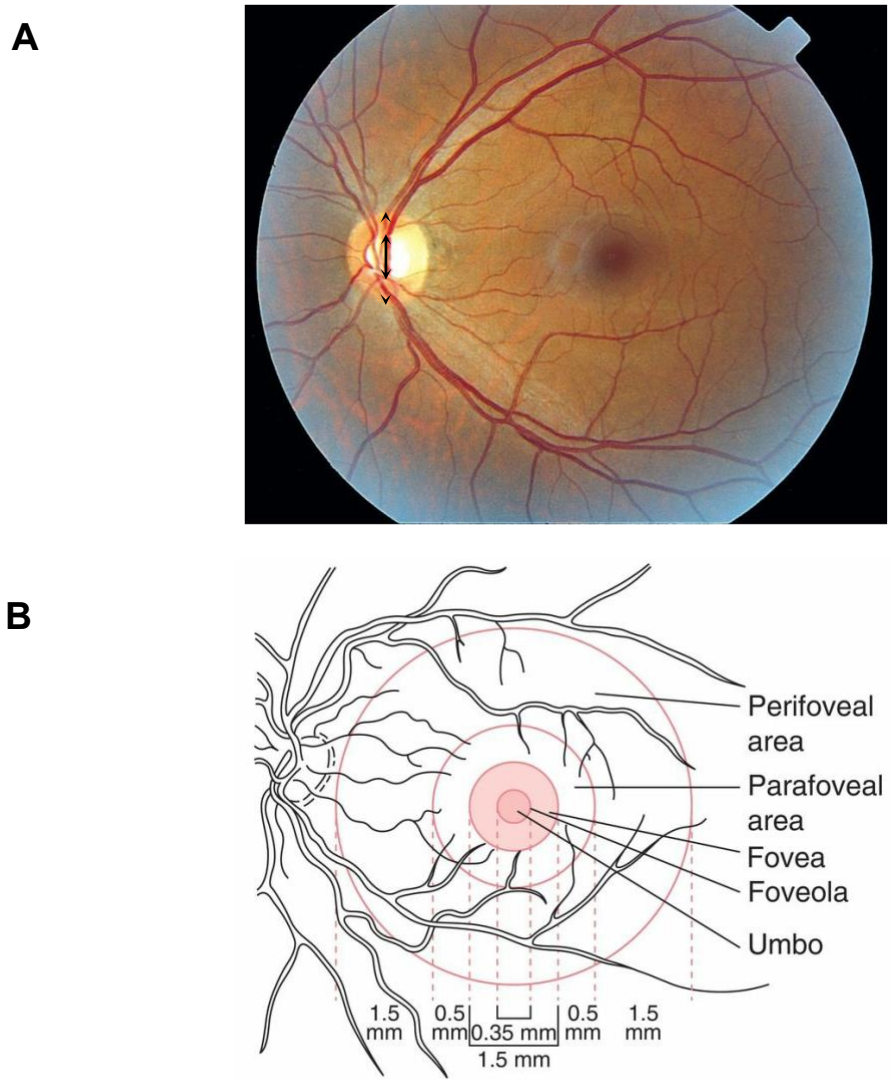

Figure 4. Fundus photo and nomenclature.
(A) Normal fundus. Arrow shows the cup and arrowheads show edge of optic disc; (B) classification and nomenclature of posterior pole. Reprinted with permission from (Trattler et al., 2016); Review of Ophthalmology; Elsevier copyright: 2018. And reprinted with permission from (Yanoff and Duker, 2018); Ophthalmology; Elsevier copyright: 2018.

2.1.2 The visual pathway

The visual pathway originates in the retina where the electrical signals are generated in the photoreceptors (first order neurons) and transmitted through the bipolar cells to the RGCs (second and third order neurons, respectively). The axons of the latter form the optic nerve where fibers decussate at the optic chiasm into the right and the left optic tracts. Each optic tract conveys information from the ipsilateral temporal retina and the contralateral nasal retina. The optic tract terminates and synapses in the LGB. The fourth order neuron of the visual pathway stems from the LGB which projects via the optic radiation to the primary visual cortex (Figure 5), also known as V1, striate cortex or Brodmann area 17 (Brar et al., 2019; Joukal, 2017).

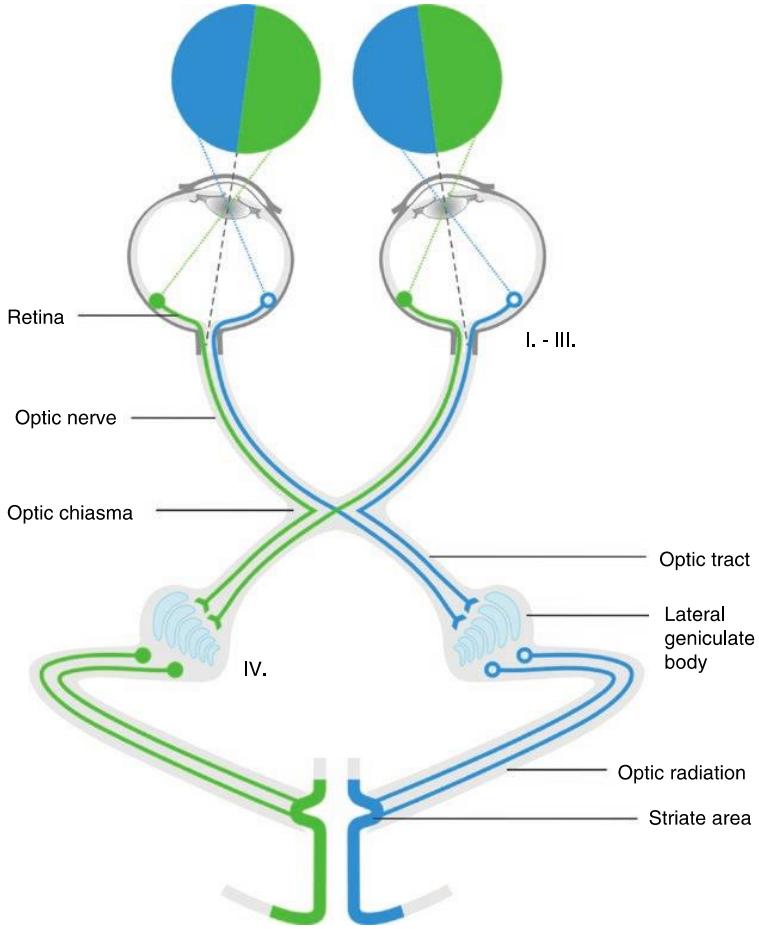

Figure 5. Visual pathway.
I-III: Three order neurons stem within the retina: photoreceptors to bipolar cells and ganglion cells. IV: Fourth order neurons stem from the LGB. Reprinted with permission from (Joukal, 2017); Anatomy of the Human visual Pathway; Springer Nature copyright: 2017.

2.2 Glaucoma

Glaucoma is a panoply group of diseases characterized by RGCs loss with characteristic optic disc changes, retinal nerve fiber layer (RNFL) thinning and loss of visual field (Figure 6). Glaucoma is leading worldwide as the most frequent cause of irreversible blindness (Quigley and Broman, 2006; Tham et al., 2014; Bourne et al., 2016). It is estimated that the number of people (aged 40-80 years old) affected by glaucoma would increase from 76 million in 2020 to 112 million in 2040 highlighting an increasing burden of glaucoma globally where the primary open angle glaucoma (POAG) is the most common form (Tham et al., 2014). Early diagnosis is therefore essential to prevent the glaucoma related irreversible loss of vision (Jonas et al., 2017). The identification of risk factors for glaucoma could potentially lead to an enhanced detection and hindrance of damage progression (Heijl et al., 2002; Leske et al., 2003).

2.3 Glaucoma pathophysiology

Although the glaucoma pathophysiology is not fully understood, the two main mechanisms, i.e. elevated intraocular pressure and vascular dysfunction, are implicated in the development and progression of glaucoma (Flammer, 1994; Flammer et al., 2002; Halpern and Grosskreutz, 2002; Mansouri, 2016).

2.3.1 The role of IOP in glaucoma

The only proven therapy to halt glaucoma progression is to lower the IOP (Heijl et al., 2002; Kass et al., 2002) which is the most important and modifiable risk factor from the pathophysiological and therapeutic perspectives of glaucoma (Jonas et al., 2017).

The IOP is maintained through the secretion of the aqueous humor from the ciliary processes of the ciliary body and the drainage through either the outflow pathways (Figure 2). A high impedance to the aqueous outflow results in an increase of the IOP (Jonas et al., 2017). The elevated IOP exerts strain and stress on the structures of the optic disc at the lamina cribrosa resulting in the loss of the neuroretinal rim and the widening of the optic cup (Figure 7), i.e. glaucomatous optic neuropathy (Burgoyne et al., 2005; Jonas et al., 2017).

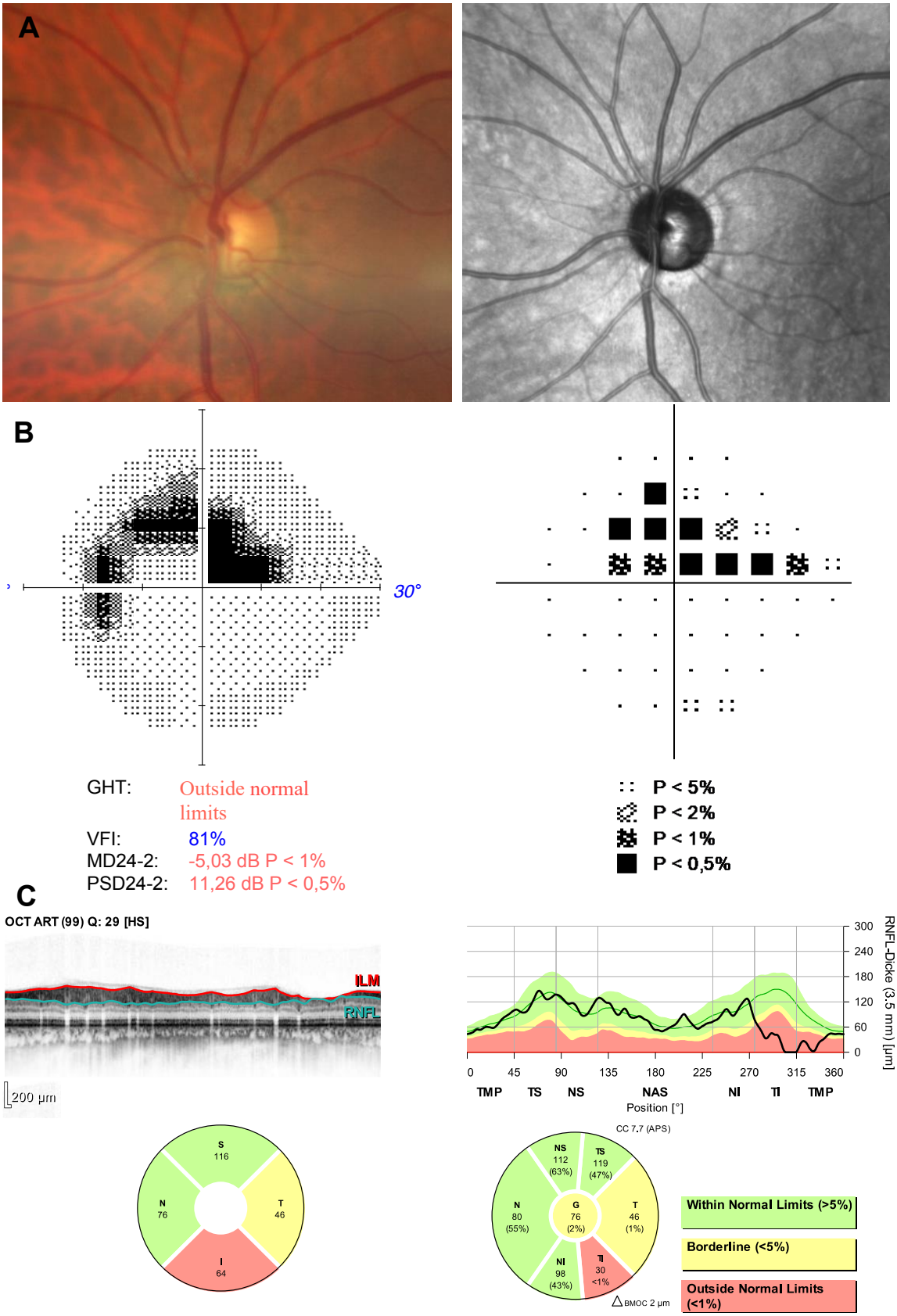

Figure 6. Glaucomatous damage assessment.
(A) A fundus photograph of optic disc with an inferior notch consistent with the superior visual field defect seen on the grey scale and corrected pattern standard deviation of the visual field (B) and with abnormal pRNFL thickness in inferior quadrant (C). GHT = Glaucoma hemifield test; VFI = Visual field index; MD/PSD = Mean/pattern standard deviation; S = superior; I = Inferior; N = Nasal; T= Temporal.

Along with the high IOP, several other factors are presumed to be contributing factors to glaucomatous optic neuropathy, e.g. gene mutations and vascular dysfunction, which warrant further work to establish associations with the glaucomatous damage (Jonas et al., 2017).

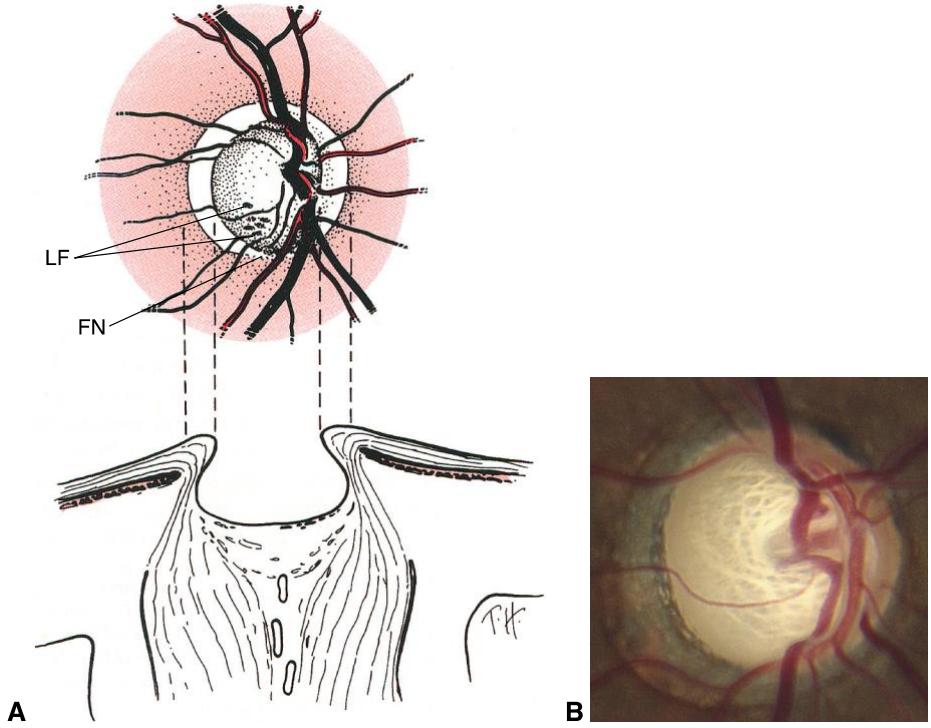

Figure 7. Glaucomatous optic neuropathy.
A) Right eye anterior and transverse view of the optic nerve. Thinning of neuroretinal rim with inferior focal notching (FN); enlarged central cup with clear laminar fenestrations (LF); shift of retinal vessels nasally; and peripapillary atrophy. B) Clinical view showing extensive loss of the neuroretinal rim. Part A reprinted with permission from (Wright, 1997);Textbook of Ophthalmology; Lippincott copyright: 1997. Part B reprinted with permission from (Girkin et al., 2019); Glaucoma; AAO copyright: 2019.

2.3.2 Role of vascular dysfunction in glaucoma

The direct causality of glaucoma is still unclear, but there is a considerable evidence of glaucoma damage being linked to the loss of retinal and the optic nerve blood flow. The "vascular theory" resolves some inconsistencies in the glaucoma pathogenesis, such as prevailed visual deterioration albeit good IOP control, by implicating reduced ocular blood flow in glaucoma (Flammer et al., 2002). The latter induces periods of ischemic and reperfusion damage to the optic nerve. Studies with imaging technologies e.g. optical coherence tomography angiography (OCT-A) despite inconsistent results support the vascular role in glaucoma damage (Mansouri, 2016).

2.4 Glaucoma classification

Based on the aqueous outflow dynamics, glaucoma is traditionally classified into an open angle glaucoma (OAG), i.e. with an open anterior chamber angle and free access to the drainage pathways, or a closed angle glaucoma with a contact between the peripheral iris and the outflow structures such as the trabecular meshwork. From the etiological perspectives, the open angle glaucoma can be either primary (POAG) with no identifiable anatomical cause of the aqueous flow obstruction, or secondary OAG with a putative role of an abnormality in the pathogenesis e.g. pseudoexofoliative glaucoma (Girkin et al., 2019). In POAG, IOP can be as low as 10 mmHg with damage to the optic nerve, a category termed normal tension glaucoma (NTG). An angle closure glaucoma, on the other hand, may be primary without any apparent cause while in a secondary closure glaucoma a recognizable cause, e.g. an angle neovascularization, is the culprit in an iridocorneal contact (Jonas et al., 2017).

2.5 Glaucoma diagnostics

Glaucoma detection is established with an appropriate clinical examination, i.e. characteristic changes at the RNFL and the optic disc (Figure 7) and corresponding VF (Figure 8) loss (Jonas et al., 2017). These glaucomatous changes, i.e. the glaucoma triad (Denniston and Murray, 2018), are intuitively assessed in each glaucoma case (Table 1).

Table 1. Glaucoma triad

Glaucomatous changes	**Evidence**
Abnormal optic disc	Large CDR for disc size
	Neuroretinal rim notch/thinning ‘ISNT rule’
	CDR asymmetry
	Disc hemorrhage
	Vessel bayoneting/nasally displaced
	Peripapillary atrophy (beta zone)
VF loss	Nasal step
	Paracentral scotoma
	Arcuate scotoma
	Altitudinal scotoma
	Central island of vision or residual temporal crescent
Raised IOP	> 21 mmHg*

CDR: Cup/disc ratio; ISNT described disc contour with decreasing thickness in the following order Inferior, superior, nasal and temporal. IOP: Intraocular pressure.
*IOP cutoff should be individualized.

Structural changes in glaucoma seen by the ophthalmoscopy might also be investigated using the optical coherence tomography (OCT) imaging which is complementary especially for follow up examinations (see section 4.1.2). Another useful technique for glaucoma diagnosis and follow-up is the assessment of retinal microvasculature using the OCT angiography (OCT-A; section 4.1.3).

The second technique used for glaucoma diagnosis and follow up is to characterize the visual field (VF; see section 4.1.1.1). The VF is 'an island of vision enclosed by a sea of darkness'. The clinical perimetry has for decades been the standard method of choice to identify/quantify glaucomatous visual fields (Figure 8) as well as assess the damage stability or progression (Girkin et al., 2019).

The IOP is a part of the glaucoma triad and is important for the diagnosis and follow-up. The IOP measurement, tonometry, is a non-invasive technique and most commonly measured with the Goldmann applanation tonometry in the clinics. This technique is safe and precise in most situations. Although the IOP value of 21 mmHg was used to separate normal from abnormal pressure, there is no clear level below which IOP is normal and above which IOP level is considered abnormal. The IOP elevation yet is the most important risk factor in glaucoma (Girkin et al., 2019; Jonas et al., 2017).

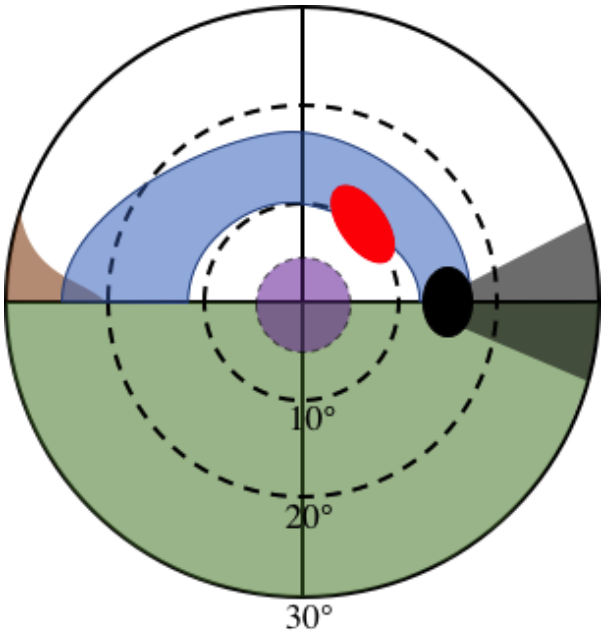

Figure 8. Visual field defects of the right glaucomatous eye.
Color coded visual field defects: 1) nasal step; 2) paracentral defect; 3) arcuate scotoma; 4) altitudinal defect; 5) temporal wedge scotoma and 6) central visual field defect.

2.5.1 Enhanced glaucoma detection

Certain diagnostic challenges exist in the assessment of glaucoma. The clinical detection of structural changes during ophthalmoscopy could be challenging especially at the early stages of the disease (Weinreb et al., 2014). Furthermore, the perimetric VF examination is highly variable and many optic nerve axons might be lost before the appearance of any detectable VF defects (Jonas et al., 2017). The IOP is another diagnostic dilemma because many glaucomatous patients present with normal IOP levels or their VFs deteriorate albeit good IOP control (Asrani et al., 2000; Jonas et al., 2017).

2.5.1.1 Optimization of IOP measurements

The emergence of telemetric IOP sensors enabled continual IOP measurements which may revolutionize implement telemedicine glaucomatous care. Currently, there are two technologically available sensors empowering 24 IOP measurement: a contact lens sensor (Sensimed Triggerfish) (Aptel et al., 2017; Tojo et al., 2017) and an implantable intraocular pressure sensor (eyemate-IO sensor) (Koutsonas et al., 2018, 2016; Melki et al., 2014).

The commercially available eyemate-IO sensor (eyemate-IO sensor®, Implandata Ophthalmic products GmbH, Hannover, Germany) is a ring shape sensor (Figure 9) co-implanted in the ciliary sulcus during cataract surgery. For the eyemate-IO sensor read-out, typically an external reader device (Mesograph), which emits an electromagnetic connection toward the implant upon button press of the device, is held in front of the eye with distance of < 5 cm to power the eyemate-IO sensor. A non-contact prototype reading system, where the coil antenna of the reading device is incorporated in a sleep mask or a modified eyepatch during night and at day time, respectively, enables the continual readings of the IOP. The eyemate-IO sensor proved to be functional and safe (Koutsonas et al., 2018). The utility of continual IOP measurements opens the possibility to reveal IOP-related pathomechanisms such as the influence of various risk factors on the IOP, e.g. body position and hemodynamics.

Figure 9. The eyemate-IO sensor®.
The external reader device (Mesograph) emission of radiofrequencies to couple with the ring-shaped IO-sensor implant (Image courtesy of Implandata GmbH, Hannover, Germany).

2.5.1.2 Multimodal approach

Electrophysiology indexes offer an optimized and reliable approach for objective visual function assessment, which may complement the current methods of the VF-based testing methods. It is reported that the detection of glaucoma would be improved upon the combined assessment of the functional and structural damage (Shah et al., 2006). A relatively new imaging modality that might also boost glaucoma diagnosis is the use of OCT-A especially as structural changes reach a floor effect in advance glaucoma hindering close follow up for these patients. A multidisciplinary approach, therefore, with the use of objective functional tests along with OCT-A and the current standard methods of glaucoma diagnosis will enhance the diagnostic performance and reduce the variability of results.

Chapter 3

Research questions - Aims and outlines

I investigated the open angle glaucoma by studying the interrelationship between. physiological, functional and anatomical measures to elucidate the pathogenesis of glaucoma. Further, I compared the diagnostic performance of these measures to assess their role in glaucoma detection. Specifically, I addressed the questions detailed below.

3.1 Do continuous IOP readings enhance our understanding of glaucoma?

In chapter 5, I investigated the plausibility of simultaneous measurement of RGC function and IOP and studied the short-term influence of postural changes on both measures in open angle glaucoma and healthy participants by taking the following steps:

- Adapt a novel device (the eyemate-IO sensor) to continuously tap the IOP during simultaneous recording with the PERG.
- Assess the potential confounding effects of simultaneous IOP and PERG measurements.
- Ensure the functionality of the sensor when coupled with ERG, i.e. the interference with outcome measures, i.e. PERG amplitudes.
- Evaluate the influence of LDP on IOP and RGC function on all groups:
    a. Controls participants
    b. Glaucoma participants
    c. Glaucoma with eyemate-IO sensor

3.2 What is the role of mfPhNR in glaucoma detection?

In chapter 6, I studied the effect of the stimulus length of the mfPhNR on the detection of glaucoma and evaluates the diagnostic performance of mfPhNR vs PERG and OCT by taking the following steps:

- Design of an appropriate stimulus and an application of a range of stimulation protocols to:
    d. Assess different components of mfERG including mfPhNR characteristics, e.g. peak time, normalization of mfPhNR to b wave in the following groups:
        i. Controls
        ii. Glaucoma suspects
        iii. Glaucoma
    e. Study responses between different visual field locations in glaucoma, i.e. topographical analysis.
    f. Determine the most sensitive stimulation protocol to differentiate between groups.
- Compare the diagnostic performance of the selected mfPhNR protocol vs other established methods, i.e. peripapillary retinal nerve fiber layer thickness (pRNFL) and PERG.

3.3 Does a multimodal approach help to optimize glaucoma detection?

In chapter 7, I applied a multimodal approach in glaucoma diagnosis by assessing functional, structural and vascular parameters of RGCs using ERG, optical coherence tomography and angiography (OCT and OCT-A), respectively, and by taking the following steps:

- Optimize the testing protocol for vascular retinal imaging and use a custom script to analyze OCT-A images.
- Acquire and prepare ERG, OCT measures and OCT-A images for offline analysis to:
    a. Estimate the loss of vision metrics in glaucoma vs controls based on ERG and OCT/A measures, i.e. pRNFL, macular ganglion cell inner plexiform layer

thickness (mGCIPL), vessel density of parafoveal (pfVD) and peripapillary areas (pVD).

b. Study the vascular damage of different retinal layers in glaucoma vs controls.
c. Appraise the inter-correlation between functional vs structural and vascular measures both at the macula and optic disc.
d. Compare the diagnostic performance of the mfPhNR and vascular parameters, i.e. pfVD and pVD, vs other established methods, i.e. pRNFL, PERG, and mGCIPL.

Chapter 4

Methods

4.1 Tools for human visual system investigation – An overview

Given the irreversible nature of the glaucoma-yielded visual disability, glaucoma is, therefore, comprehensively investigated by assessing not only the visual function, i.e. visual field and electrophysiology, but also the anatomical measures, i.e. structural and vascular indices. This might contribute to the early detection of damage and prevent permanent functional and structural deterioration.

4.1.1 Functional assessment of glaucoma

Several methods (detailed below) are at hand to tap visual system in order to clinically evaluate the function and integrity of the visual system.

4.1.1.1 Visual field

The visual field (VF) resembles a 3-D structure akin to a hill of increasing sensitivity. The sensitivity of VF is highest at fovea (the sharpest visual acuity) which declines progressively toward the periphery where the nasal step is steeper than the temporal (Salmon, 2019).

In glaucoma diagnostics, the VF is usually tested using the standard automated perimetry (SAP). In the SAP, a stimulus of differential light sensitivity at different locations of the visual field with a uniform background is being projected till the sensitivity of the eye in each point is found. Decibels (dB) are used as unit of clinical perimetry where 10 dB = 1 log unit. With increasing dB readings, the retinal sensitivity increases (Salmon, 2019). The retinal sensitivity is measured at preselected locations in the VF including the central 24° or 30°, 10° or full-field (Denniston and Murray, 2018). Automated perimeters commonly used are the Humphrey field analyzer (Figure 6 B) and the Octopus. The most common testing protocols for glaucoma are the central 24 and 30° programs which test the central

VF using a 6° grid with 3° points above and 3° points below the horizontal line to detect defects respecting this line as in glaucoma (Girkin et al., 2019).

In fact, when the glaucomatous damage is detectable on SAP, already a significant number of RGCs (up to 50%) might have been lost (Harwerth et al., 2010; Harwerth and Quigley, 2006; Kerrigan-Baumrind et al., 2000) necessitating the application of more sensitive methods such as electrophysiology measures of vision for the early detection of glaucoma damage.

4.1.1.2 Non-invasive clinical electrophysiology in vision

The visual electrophysiology provides a non-invasive evaluation of different parts of the visual pathway (Figure 10). The ERG metrics of vision, i.e. an objective assessment of the visual function, have the potential to elucidate the pathophysiological processes underlying glaucoma. Two ERG measures are of special interests in glaucoma research, the pattern electroretinogram (PERG) and the multifocal photopic negative response (mfPhNR); see Figure 11 for the recording and stimulation setup.

4.1.1.2.1 Pattern electroretinography

The PERG is a direct indicator of the RGC function and has an established role in the early detection of glaucoma (Bach and Hoffmann, 2006, 2008). The PERG is reported to detect glaucomatous changes in glaucoma suspects ahead of any demonstrable visual field loss (Bach et al., 2006; Bode et al., 2011) or predict a future higher rate of pRNFL thinning in glaucoma suspects (Banitt et al., 2013). It is recorded via corneal (Bach and Hoffmann, 2008) or skin electrodes (Porciatti and Ventura, 2004) and as the name indicates a pattern stimulus is used for the stimulation. A checkerboard or gratings stimulus reverses its luminance contrast, i.e. the reversal of white and black checks without a net luminance change and the resulted space-averaged luminance forces the outer retinal layers' response to cancel each other allowing RGCs responses to dominate the recording. The PERG waveform depends on the frequency of stimulation. Less than 4 reversals per seconds (rps) induce a transient response with two dominant waves: i) P50, a positive response peaked around 50 ms and ii) N95, a negative response peaked around 95 ms. A faster stimulation (≥7 rps) induces a steady state PERG (ssPERG) yielding a sinusoidal response (Figure 12) where responses are merged (Bach and Hoffmann, 2008; Bach and Poloschek, 2013). The

ssPERG is reported to be more effective in glaucoma detection than the slower stimulation PERG (Hiss and Fahl, 1991; Trick, 1985).

One important consideration in the PERG recording is to ensure the integrity of outer/middle retinal layers using another ERG method e.g. PhNR. Also, the patient should maintain an exquisite fixation with a proper refraction to the stimulus distance (Wilsey and Fortune, 2016).

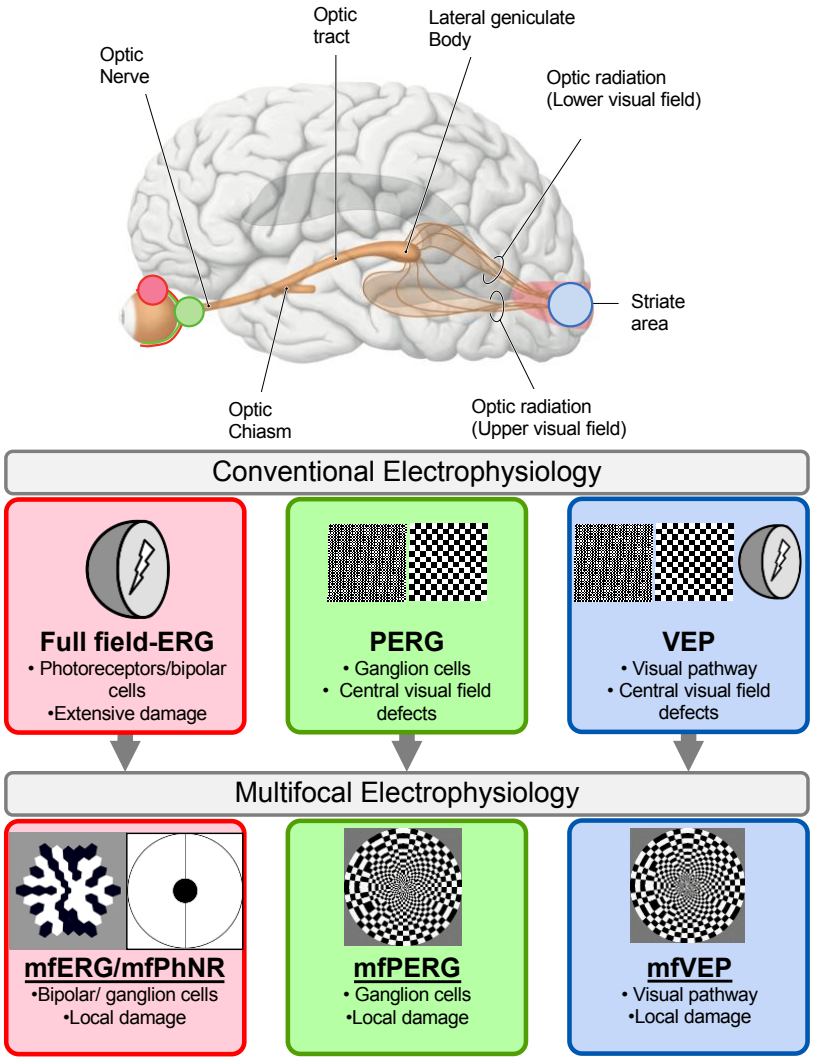

Figure 10. ERG diagnostics of the visual pathway.
Conventional electrophysiology stimulation of photoreceptors and bipolar cells (red), retinal ganglion cells (green) and visual cortex (blue) using full field electroretinogram, pattern electroretinogram (PERG) and visual evoked potential (VEP), respectively, vs multifocal stimulation (mf). mfPhNR = multifocal photopic negative response of mfERG has responses of photoreceptors, bipolar and ganglion cells. Adapted and reprinted with permission from (Hoffmann et al., 2018); Mit klinischer Elektrophysiologie hinter die Netzhaut; Georg Thieme Verlag KG copyright: 2018.

4.1.1.2.2 Multifocal photopic negative response

The photopic negative response of the full field ERG (PhNR) originated, according to animal studies, from the neural activity of RGCs (Viswanathan et al., 2000, 1999). Similar to PERG, the PhNR is an RGC dependent response with an additional assessment of outer retinal layers (cone photoreceptors and bipolar cells). Further, the PhNR response is independent from the clarity of optical media, proper refraction and good fixation (Wilsey and Fortune, 2016).

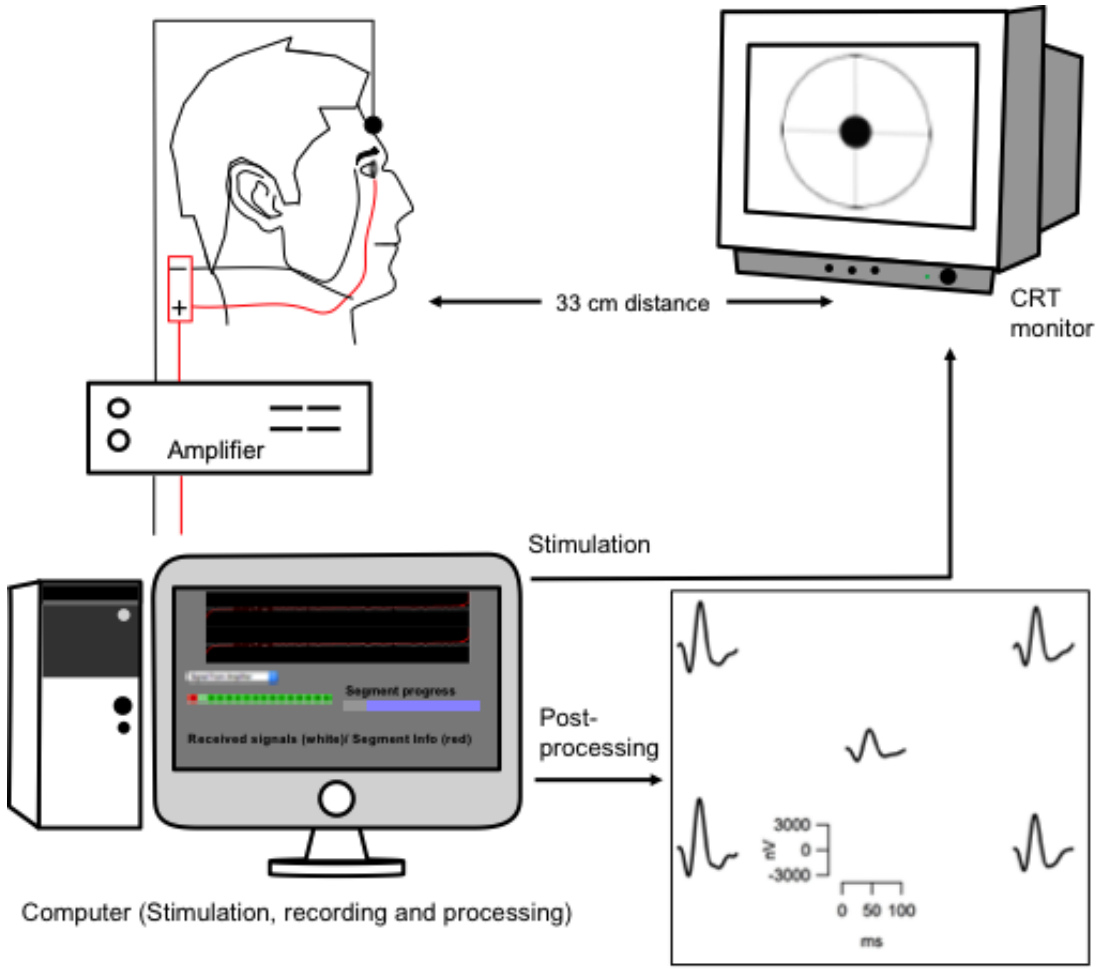

Figure 11. The recording and stimulation set-up of mfPhNR and PERG.
The participant views a stimulus, e.g. here mfPhNR stimulus, generated by the computer and projected on a cathode ray tube (CRT) monitor with a 33-cm viewing distance. An active electrode (red) is a corneal electrode with a reference and ground electrodes fixed at ipsilateral outer canthus and forehead, respectively. The measured signals are sent to the computer via an amplifier system. The computer then outputs the measured signal on a control monitor.

The PhNR is recorded with corneal electrodes and dilated pupils (Bach and Poloschek, 2013). It is elicited by a uniform flash stimulus in a Ganzfeld bowl with a background stimulation to trigger a cone response. Stimulation modes could be a white stimulus on white background or a chromatic stimulation protocol, i.e. a red stimulus to selectively stimulate long wavelength cones on a blue background to saturate rods responses (Bach and Poloschek, 2013; Viswanathan et al., 1999). The PhNR is a slow response following the b wave of the photopic ERG (Viswanathan et al., 2000, 1999). The PhNR amplitude and PhNR/b wave ratio is found to be significantly reduced in glaucoma (Machida et al., 2015; Viswanathan et al., 2001). The conventional PhNR might be submerged by the global healthy retinal response that may miss localized RGCs dysfunctions.

Topographical analysis of retinal responses is deemed feasible with the use of multifocal electrophysiology (Figure 12). Sutter and coworkers (Sutter, 2001; Sutter and Tran, 1992) employed a multifocal stimulation technique using the pseudorandom m-sequences, a binary sequence of two states (1 = stimulus and 0= no stimulus). The m-sequence generation, despite a random appearance, follows a strict role employing a strict shift register with a linear feedback (Müller and Meigen, 2016; Sutter and Tran, 1992).

Using the multifocal stimulation, the PhNR of mfERG (mfPhNR) was found to be reduced in glaucoma, a finding replicated in few studies (Kaneko et al., 2015; Kato et al., 2015; Tanaka et al., 2020). There are still no standards regarding the recording of this promising technique and the paucity of studies about the diagnostic efficacy (Wilsey and Fortune, 2016).

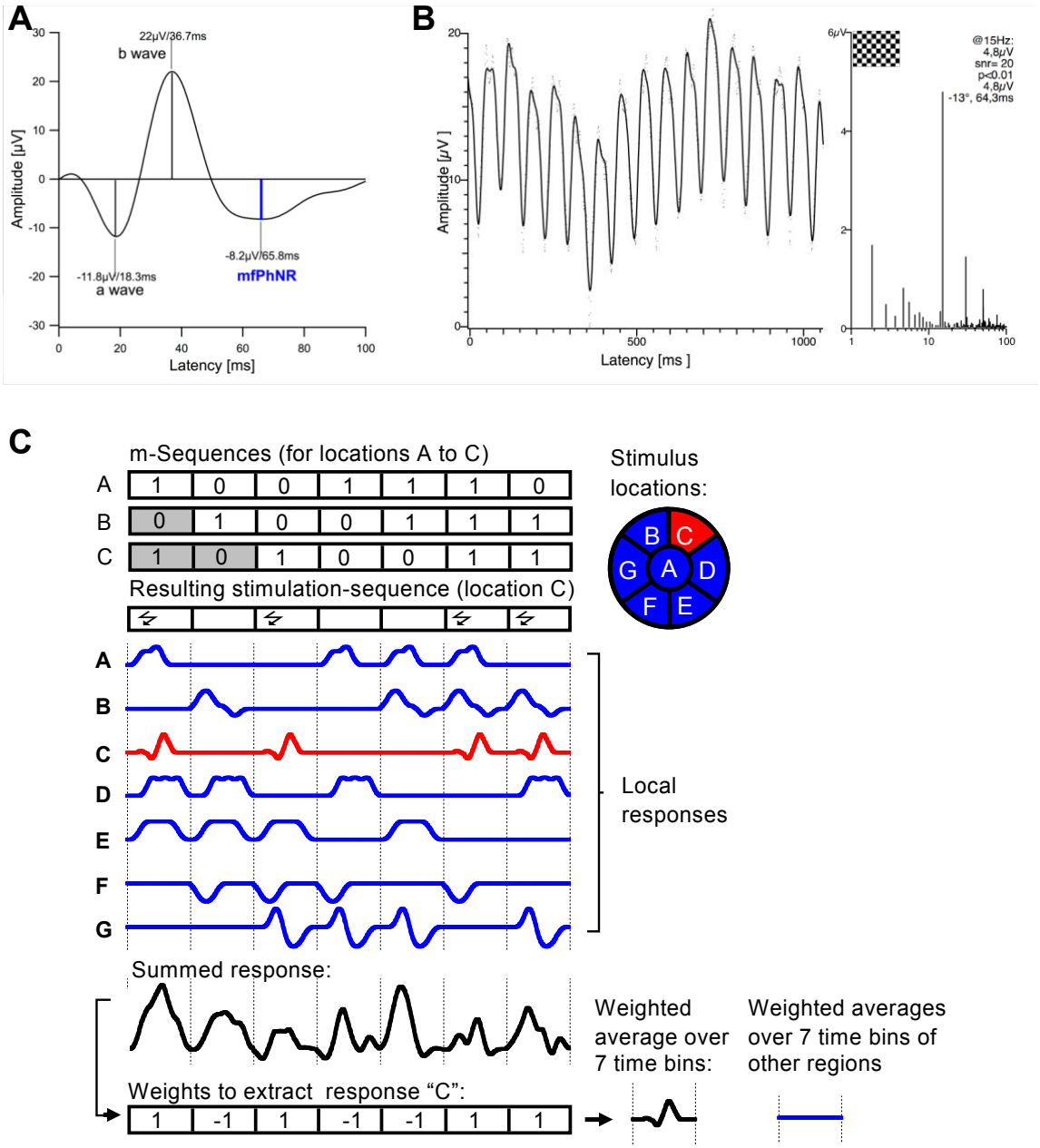

Figure 12. ERG traces (A & B) and multifocal ERG principle (C).
A) mfPhNR stimulation with 1st negative wave (a wave) followed a positive response (b wave) and 2nd negativity wave (PhNR response) that stem from photoreceptors, bipolar cells and retinal ganglion cells (RGCs), respectively.
B) PERG response dominated by the stimulus fundamental frequency (left panel) with checksize stimulation of 15 rps to the small checksize stimulus (0.8°) and amplitudes extracted at the frequency 15 Hz (right panel).
C) mfERG principle (Hoffmann, 2008): Schematics of 7-field stimulations with the same binary m-sequence, e.g. 7 (1: stimulus, 0: no stimulus, but shifted in time). A sequence of responses (blue traces) for each location is elicited; for illustrative purposes each location is given a different response shape. The summed response represents the response of all locations (black trace). To extract the first order kernel response for location c (indicated in red) each bin of the response sequence is assigned the weight –1 or 1, for 0 (no stimulus) or 1 (stimulus) in the m-sequence for c, respectively. The weighted average over the seven-time bins yields the response of location C, as the responses from the other locations cancel out. Part C reprinted with permission from (Hoffmann, 2008); Investigating Visual Function with Multifocal Visual Evoked Potentials; Springer Nature copyright: 2008.

4.1.2 Structural assessment of glaucomatous damage

Besides functional tests, glaucoma is evaluated by estimating the structural loss in the retina and optic disc, especially the retinal ganglion cell layer (GCL) and peripapillary retinal nerve fiber layer (pRNFL) thickness. The presence and the extent of the structural damage can be assessed by computerized imaging; the most common of which is OCT.

The OCT is a non-contact and non-invasive modality with a micrometer-resolution, typically 3-10 µm. A near infrared light, i.e. a low coherence light, is projected to a tissue and a reference arm and interferogram is created by the combination of the light returning from the tissue and the reference arm (McCannel et al., 2019). Different optical signals being transmitted through or reflected by the tissue are used to reconstruct the OCT images (Sharma, Priya and Sergott, 2016). Spectral domain (SD-OCT, light wavelength around 800 nm) and swept source (SS-OCT, light wavelength around 1050 nm) techniques, facilitates more efficient approaches for an image acquisition (McCannel et al., 2019), resulting in a provision of ultrafine structures of the retina in details (Figure 13 A). Both SD- and SS-OCT provide A scans through tissues and a collection of which forms B scans providing a cross sectional structural image. Researchers and clinicians in glaucoma alike aim to benefit from the full potential of the OCT (Figure 13 B & C) that provides vital insights of the structural damage in glaucoma not only of the usual peripapillary , i.e. pRNFL, scans, but also of the macula scans (Hood, 2017; Wang et al., 2015).

Most recently, advances in the field of OCT imaging have enabled the reconstruction of angiographical images in different retinal layers and sites using the OCT angiography (OCT-A) which transforms the OCT technology into an indispensable tool in ophthalmology practice (Sharma, Priya and Sergott, 2016).

4.1.3 Vascular assessment of glaucomatous damage

The OCT-A is considered a valuable breakthrough in ophthalmology practice to investigate and shed light on the pathophysiology of glaucoma (Mansouri, 2016). The OCT-A allows for the non-invasive visualization and assessment of the retinal capillary networks of different retinal layers (Figure 13 C). Without the use of dyes, OCT-A uses light reflectance from the moving red blood cells to detect the vessels of the retina (Koustenis et al., 2017). The same tissue is being scanned repeatedly and the scan differences over time depicted as high flow (marked differences between scans) or low/no flow areas (no changes between scans) (Spaide et al., 2015).

The current OCT-A technologies can scan the optic disc and the macula. The OCT-A scans of the optic disc are performed using volumetric scans typically covering a 4.5x4.5 mm area centered around the disc. The macular volumetric OCT-A scan is performed covering typically 3x3 mm or 6x6 mm scans (Figure 13 C). Several vascular layers can be then assessed and analyzed (Rao et al., 2020). Radial retinal plexus supplying the RNFL and the superficial vascular plexus supplying the GCL are two layers of interest in glaucoma research. OCT-A can also offer evaluation of deeper vascular layers and choroid vasculature (Kd et al., 2019). One of the OCT-A measures reported in the literate is the vessel density (VD) defined as: the percentage of the area occupied by capillaries over the imaged area. In short, OCT-A offers quantitative and qualitative assessment of macular and optic head vasculature that might fill the gap in the understanding of glaucomatous damage.

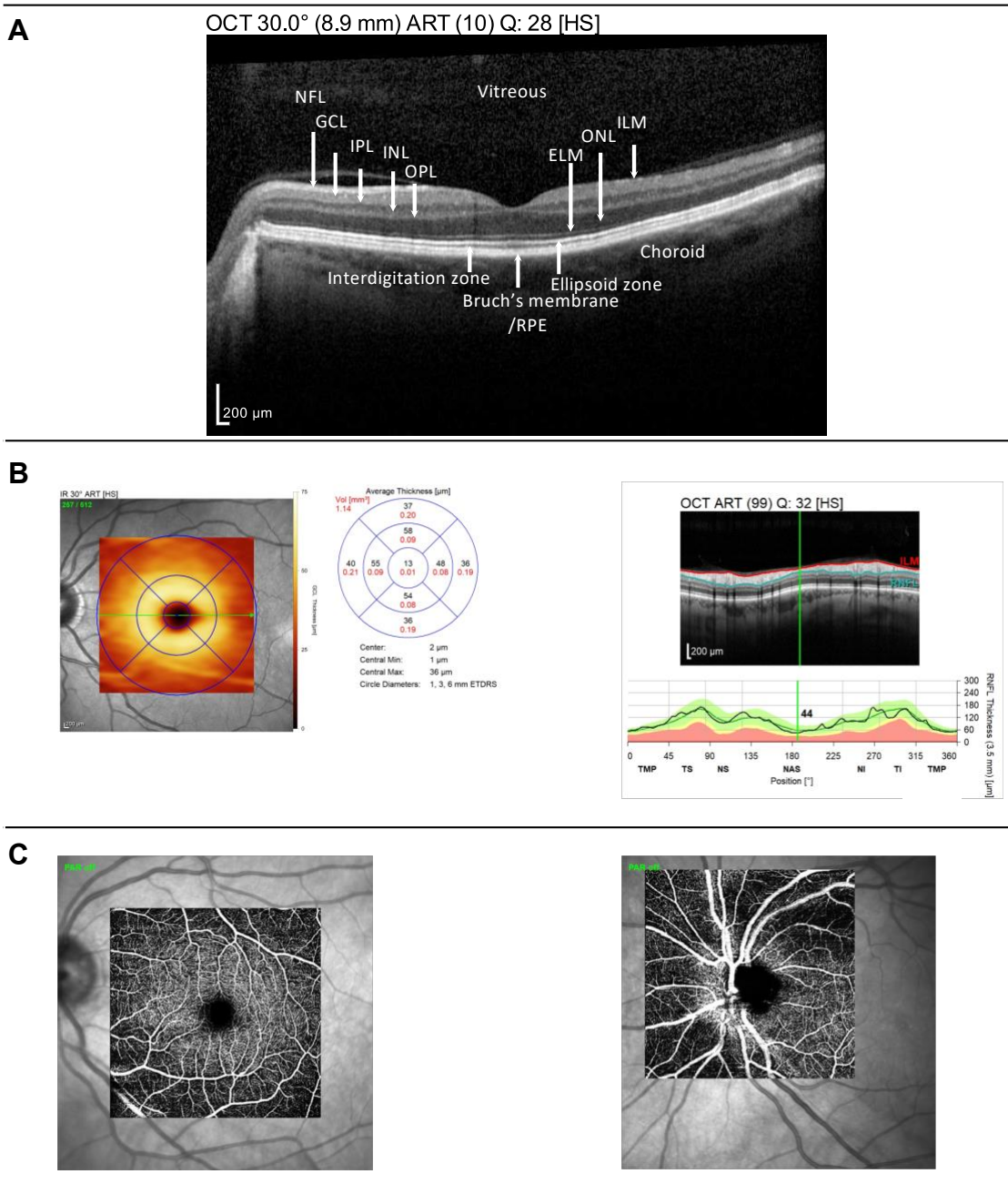

Figure 13. OCT/A scans with structural and vascular assessment of the macula and peripapillary areas. OCT cross sectional scan (A) showing retinal layers, for abbreviations see Figure 3. B) macular scan showing retinal ganglion cell thickness within 1,3 and 6 mm ETDRS areas (left) and peripapillary retinal nerve fiber layer thickness (right) assessment. C) OCT-A vascular scans of the macula within 20º x 20º of the central retina (left) and disc with peripapillary area scans (right).

Chapter 5

Postural influence on glaucoma

This study has been published in the British Journal of Ophthalmology - Br J Ophthalmol. 2021 May;105(5):661-668 - and entitled "**Use of a novel telemetric sensor to study interactions of intraocular pressure and ganglion-cell function in glaucoma**" and has been reprinted in this thesis with permission and is cited as follows:

Al-Nosairy, K. O., Bosch, J. J. O. N. van den, Pennisi, V., Mansouri, K., Thieme, H., Choritz, L., & Hoffmann, M. B. (2020). Use of a novel telemetric sensor to study interactions of intraocular pressure and ganglion-cell function in glaucoma. British Journal of Ophthalmology. https://doi.org/10.1136/bjophthalmol-2020-316136

Use of a novel telemetric sensor to study interactions of intraocular pressure and ganglion-cell function in glaucoma

Khaldoon O Al-Nosairy,[1] Jacqueline J O N van den Bosch,[1,2] Vincenzo Pennisi,[1] Kaweh Mansouri,[3,4] Hagen Thieme,[1] Lars Choritz,[1] Michael B Hoffmann [1,5]

► Supplemental material is published online only. To view please visit the journal online (http://dx.doi.org/10.1136/bjophthalmol-2020-316136).

[1]Department of Ophthalmology, Otto von Guericke University, Magdeburg, Germany
[2]Department of Research and Development, Implandata Ophthalmic Products GmbH, Hannover, Germany
[3]Glaucoma Research Centre, Montchoisi Clinic, Swiss Visio, Lausanne, Switzerland
[4]Department of Ophthalmology, University of Colorado School of Medicine, Denver, Colorado, USA
[5]Center for Behavioral Brain Sciences, Otto von Guericke University, Magdeburg, Germany

Correspondence to
Michael B Hoffmann, Visual Processing Laboratory, University Eye Clinic, Leipziger Str. 44, 39120 Magdeburg, Germany; michael.hoffmann@med.ovgu.de

Received 25 February 2020
Accepted 3 June 2020
Revised 7 May 2020

To cite: Al-Nosairy KO, van den Bosch JJON, Pennisi V, *et al. Br J Ophthalmol* Epub ahead of print: [*please include* Day Month Year]. doi:10.1136/bjophthalmol-2020-316136

ABSTRACT

Aims (1) To test the feasibility of simultaneous steady-state pattern electroretinogram (ssPERG) and intraocular pressure (IOP) measurements with an implanted IOP sensor. (2) To explore the scope of this approach for detecting PERG changes during IOP manipulation in a model of lateral decubitus positioning (LDP; lateral position).

Methods 15 healthy controls and 15 treated glaucoma patients participated in the study. 8 patients had an IOP sensor (Eyemate-IO, Implandata Ophthalmic Products GmbH) in the right eye (GLA_{IMP}) and 7 had no sensor and with glaucoma in the left eye. (1) We compared PERGs with and without simultaneous IOP read-out in GLA_{IMP}. (2) All participants were positioned in the following order: sitting1 (S1), right LDP (LD_R), sitting2 (S2), left LDP (LD_L) and sitting3 (S3). For each position, PERG amplitudes and IOP were determined with rebound tonometry (Icare TA01i) in all participants without the IOP sensor.

Results Electromagnetic intrusions of IOP sensor read-out onto ssPERG recordings had, due to different frequency ranges, no relevant effect on PERG amplitudes. IOP and PERG measures were affected by LDP, for example, IOP was increased during LD_R versus S1 in the lower eyes of GLA_{IMP} and controls (5.1±0.6 mmHg, $P_{0.025}$ =0.00004 and 1.6±0.6 mmHg, $P_{0.025}$=0.02, respectively) and PERG amplitude was reversibly decreased (−25±10%, $P_{0.025}$=0.02 and −17±5%, $P_{0.025}$, respectively).

Conclusions During LDP, both IOP and PERG changed predominantly in the lower eye. IOP changes induced by LDP may be a model for studying the interaction of IOP and ganglion-cell function.

INTRODUCTION

Targeting the interplay of intraocular pressure (IOP) and ganglion-cell function is a promising approach to understand the pathogenesis of glaucoma. An attractive manoeuvre to elucidate these mechanisms comprises the manipulation of IOP, for example, by using posture-induced IOP-changes, and the examination of its impact on ganglion-cell responses, as reflected by the pattern electroretinogram (PERG).[1–4] Importantly, recent investigations revealed that IOP is much more variable than initially assumed.[5 6] As a consequence, continual IOP read-outs that accompany simultaneous electrophysiological recordings would be the ideal approach to study the impact of IOP on retinal function. Recent developments in telemetric IOP sensors open the possibility to pursue this approach. At present, two technologies are commercially available for continual IOP monitoring: a contact lens sensor (Sensimed Triggerfish)[5 7 8] and an implantable IOP sensor (Eyemate-IO, Implandata Ophthalmic Products GmbH, Hannover, Germany).[9–12] With the latter approach, a wireless ring-shaped sensor, that allows for continual IOP read-out, is placed in the ciliary sulcus during co-implantation of an intraocular lens during cataract surgery.[10] Studies have demonstrated the Eyemate-IO sensor to be safe, well tolerated and of good functionality for continual IOP read-outs.[10 12–14]

In the present study, we first assessed the feasibility of PERG recordings during IOP readings. Subsequently, we aimed to outline the potential of the rewarding application field of simultaneous IOP and PERG measurements. For this purpose, we tested an innovative combination of this approach with a simple manoeuvre to manipulate IOP via postural changes, that is, lateral decubitus positioning (LDP).[15–19]

METHODS

Participants

This prospective observational study was conducted at the University Eye Hospital of Otto von Guericke University Magdeburg. The participants gave their written consent to participate in the study. The procedures followed the tenets of the Declaration of Helsinki, and the protocol was approved by the ethical committee of the Otto von Guericke University Magdeburg, Germany. All participant groups underwent complete ophthalmic examinations, best corrected visual acuity (BCVA) testing (ETDRS chart), and visual field testing (Humphrey Field Analyzer 3 (Carl Zeiss Meditec AG, Jena, Germany); Swedish Interactive Threshold Algorithm 24-2 protocol (SITA Fast)). Exclusion criteria were any systemic diseases, ocular diseases or surgeries that might affect electrophysiology recordings except cataract surgery and, in the glaucoma group, glaucoma surgery or incipient cataract that did not decrease BCVA<0.8[20] and refractive error exceeding −6 or +3 D or astigmatism ≥2 D.

GLA_{IMP} group

Eight patients (age range: 62–77 years; mean: 71.1 years), diagnosed with open-angle glaucoma (OAG) who had previously been implanted with

a telemetric IOP sensor in the right eye (Eyemate-IO, Implandata Ophthalmic Products GmbH), were enrolled in the study. A subset of five patients participated in experiment 1 to test the influence of Eyemate-IO sensor electromagnetic radiation on PERG recordings in both eyes. All eight patients participated in experiment 2 to determine the LDP effect on PERG amplitudes. IOP and PERG measurements were included only for the right eye as not all left eyes had glaucoma. The Eyemate-IO sensor had previously (at least 3 years prior to the present measurements) been implanted in glaucomatous patients as part of a preceding study.[13] Participant characteristics are summarised in online supplementary table 1.

GLA_{LE}-group

The left eyes of seven patients (age range: 34–78 years; mean age: 51.4 years) with OAG were included and compared to controls' left eyes (CON_{LE} as defined below). As not all right eyes of this group were glaucomatous, right eyes were not included in the analysis. OAG eyes had an open anterior chamber angle and a glaucomatous appearance of the optic disc, that is, with a general enlargement of the cupping defined as vertical cup-to-disc ratio ≥ 0.7, retinal fibre layer defect or a local notching of the rim. In addition, OAG eyes met one of the following glaucomatous visual field defect criteria: (1) glaucoma hemifield test results outside normal limits; (2) a cluster of three or more non-edge points all depressed on the pattern deviation plot to <5% and one of which depressed to <1%; and (3) an abnormal corrected pattern SD, that is, <5%, of normal fields.[21] All patients with glaucoma were under IOP-lowering treatment.

Normal controls (CON_{RE}/CON_{LE})

Fifteen participants (age range: 33–65 years; mean age: 52.4 years) with normal visual acuity in the absence of ocular diseases were included in the study. Eight participants were included in experiment 1, 11 in experiment 2. In experiment 2, the controls' right eyes (CON_{RE}) were compared to the right eye in GLA_{IMP} whereas left eyes of controls (CON_{LE}) were compared to the GLA_{LE} group.

IOP sensor (Eyemate-IO sensor) and external reader device (mesograph)

The Eyemate-IO sensor is a Micro-Electro-Mechanical System Application-Specific Integrated Circuit (MEMS ASIC) comprising pressure-sensitive sensor cells, temperature sensors, analog-to-digital converters, and telemetry. The ASIC is bonded to a gold-made circular micro-coil antenna. Both parts are silicon-encapsulated.[22] For read-out of the sensor, a reader device is connected to a coiled circular antenna that is positioned and attached around the eye with a plaster (figure 1A). When sufficient power is made available by the reader via radio frequency emission, a pressure reading is performed by the ASIC and digitised data are transferred back to the reader. This way, a continual IOP read-out[23] was obtained at an average sampling rate of 9.2 Hz and recorded with a computer via a USB connection.

Visual stimuli, procedure and recordings

The EP2000 evoked potential system was used for stimulation, recording and analysis of steady-state PERGs (ssPERGs).[24] The recording procedures followed the International Society for Clinical Electrophysiology of Vision standards for PERG recordings.[25] The stimuli were presented binocularly at a frame rate of 75 Hz on a monochrome cathode ray tube (CRT) monitor (MDG403, Philips; P45 phosphor) in a dimly lit room. The participants maintained fixation at the centre of the monitor using a fixation cross (1° diameter), which was replaced by a 200 ms duration digit randomly appearing every 5–20 s. Contrast-inverting (reversal frequency of 15 Hz, ie, 15 reversals per second) checkerboard patterns (visual field: 25° × 25°; mean luminance: 45 cd/m^2; contrast: 98%) with two check sizes, 0.8° and 15°, were presented at a viewing distance of 57 cm. Two PERG blocks were recorded for each sitting position and four PERG blocks were recorded for each LDP. Repeated blocks were averaged offline using Igor (IGOR Pro, WaveMetrics, Portland). Each PERG block contained eight stimulus cycles of 10 trials per check size (80 sweeps of 1.066 s trail duration). PERGs were recorded binocularly using active skin electrodes as detailed in the online supplementary methods. The pupils were not dilated.

Experiment 1: effect of Eyemate-IO sensor read-out on PERG recordings

As the Eyemate-IO sensor functions employ electromagnetic radiation coupling with the antenna, we tested for possible interferences and effects of the Eyemate-IO sensor on the PERG recordings. To confirm any changes detected in patients, we additionally simulated IOP read-out in controls, which required the reader to detect a sensor. For this purpose, the sensor was placed externally next to the eye, that is, without IOP-functionality. Specifically, the Eyemate-IO sensor was fixed below the right lateral third of the lower eyelid with the antenna placed in front of it. Participants in experiment 1 underwent four blocks of PERG binocular recordings, two with read-out switched on, that is, IO-$Reader_{ON}$, and two with read-out switched off, that is, IO-$Reader_{OFF}$, in a counterbalanced sequence ('A-B-B-A'-scheme). The two PERG blocks (2 × 80 sweeps) acquired per condition and same read-out status were averaged. To assess the raw electrophysiological recordings prior to averaging in EP2000, the recordings were acquired with the PowerLab recording system (Model M880, ADInstrument Pty, Australia).

Experiment 2: effect of LDP on PERG

PERGs were recorded binocularly while the participants were positioned in the following sequence: Sitting (S1), right LDP (LD_R), sitting (S2), left LDP (LD_L) and sitting (S3). The CRT monitor used for stimulation was not rotated, resulting, due to sequential phosphor excitation, in slightly different spatiotemporal stimulation patterns during frame-build-up for S and LDP conditions, which are expected to be of no or minor influence. Five minutes after taking each position, the IOP was measured with an Icare tonometer (Icare TA01i Tonometer, Helsinki, Finland) for the control and the GLA_{LE} groups or simultaneously during PERG recording with Eyemate-IO sensor for the GLA_{IMP} group. Pillows were used to support the head during lateral decubitus and to assure that the head was parallel to the ground. Care was taken that the pillow did not compress the lower eye during LDP. The IOP was measured in the centre of the cornea and started always with the right eye followed by the left eye; the IOP value was an automatic average of one set comprising six measurements. As a measure to reduce the probability of erroneous IOP readings (ie, tilting of the device and misalignment), we asked the patient to always look straight ahead. In addition, we kept the orientation of Icare TA01i parallel to the ground in both sitting position and LDP. Due to unclear compatibility issues of the Icare TA01i tonometer and the Eyemate-IO sensor, no simultaneous Icare TA01i measurements were performed for the GLA_{IMP} group.

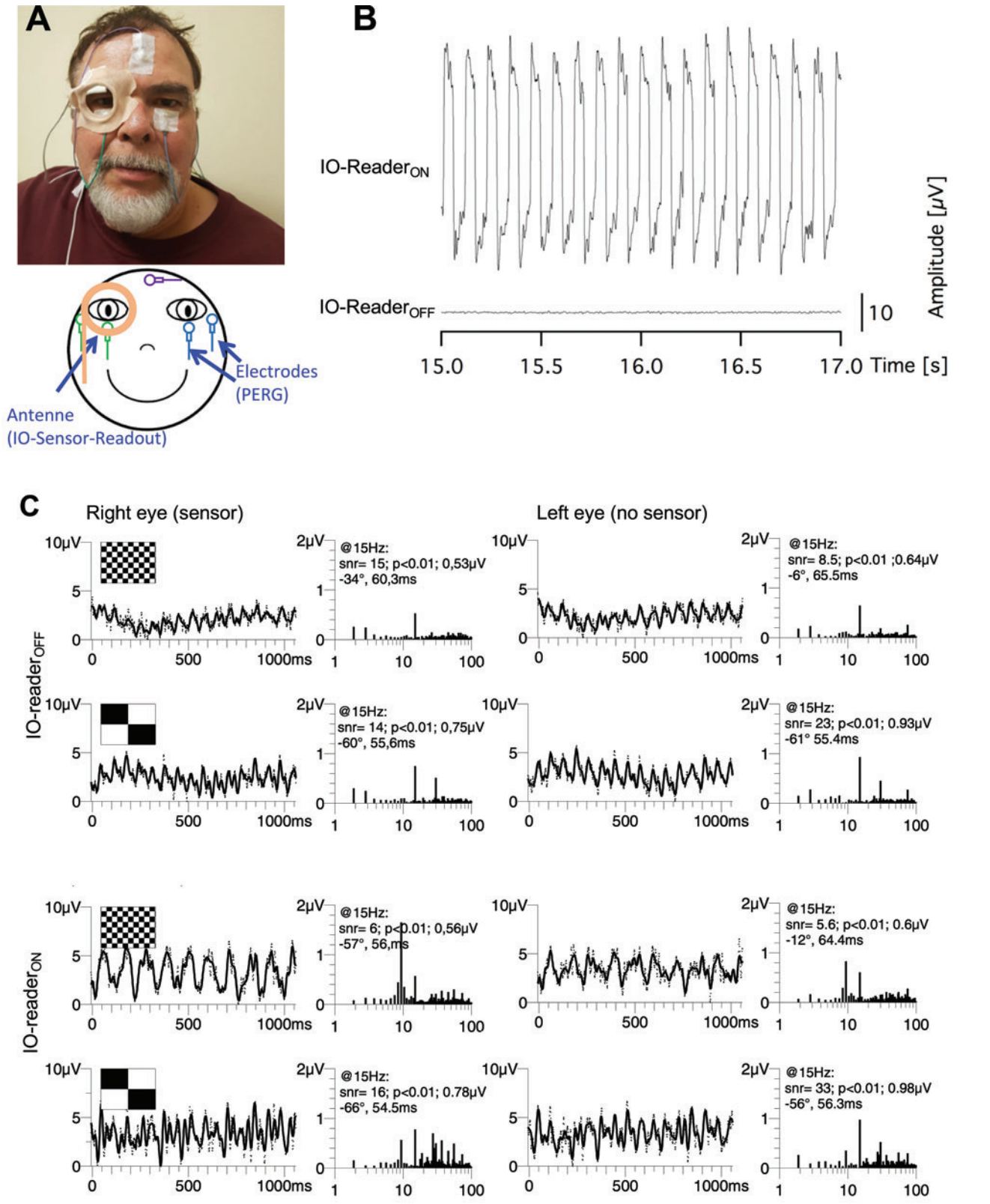

Figure 1 (A) Recording set-up for GLA_{IMP} participants with binocular electrodes for ssPERG recordings and the antenna around the right eye for simultaneous continuous read-out of IOP responses in experiments 1 and 2 (top: photograph of the set-up; bottom: schematic, illustration by MBH and KOA with obtained permission to use it). (B) and (C) Effect of IO-read-out on ssPERG recordings. (B) Raw (non-averaged) ssPERG recording trace for Eyemate-IO sensor on/off states. For IO-$Reader_{ON}$ (top trace), the applied electromagnetic field induced a noise intrusion of around 9.2 Hz, that is, at the read-out frequency (see the Methods section). For IO-$Reader_{OFF}$ (bottom trace), the noise intrusion was absent. (C) ssPERGs and frequency spectra for IO-$Reader_{ON/OFF}$ -states for both eyes for two check sizes (0.8° and 15°). Noise intrusions were reduced due to non-phase locked averaging but still evident for both the eye with Eyemate-IO sensor and -reader and for the fellow eye. As a consequence, a response at around 9.2 Hz was evident in the frequency spectra for IO-$Reader_{ON}$, in addition to the stimulus-evoked response at 15 Hz. GLA_{IMP}, glaucoma patients with Eyemate-IO implant; IOP, intraocular pressure; ssPERGs, steady-state pattern electroretinograms.

Analysis and statistics

The ssPERGs were Fourier-analysed and the response amplitude at the reversal frequency of 15 Hz was determined and corrected for the noise estimate, that is, an average of the neighbouring frequencies below and above 15 Hz.[26 27]

The non-averaged traces acquired during experiment 1 were digitised with PowerLab and exported to Igor (IGOR Pro, WaveMetrics, Portland) for subsequent analyses and the determination of the intrusion frequency during IOP read-out from the Eyemate-IO sensor. The ssPERG recordings were analysed using Igor. To test the effect of LDP on IOP and ganglion-cell function, these measures were compared for S1 versus LD_R and S2 versus LD_L with paired t-tests using SPSS 24 (statistical Package for the Social Sciences, IBM). P values were reported together with α-levels as adjusted according to Bonferroni-Holm correction[28] for multiple comparisons (Pα). We also determined the test–retest reliability of our IOP and PERG measurements and estimated the coefficient of reliability (= 1.96 × SD of difference between test–retest measurements).

RESULTS

Experiment 1: feasibility of simultaneous Eyemate-IO sensor read-out and ssPERG recordings

A qualitative overview of the ssPERG recordings with (IO-Reader$_{ON}$) and without simultaneous Eyemate-IO sensor read-out (IO-Reader$_{OFF}$) is given in figure 1B,C for a representative participant of the GLA_{IMP} group, that is, with an Eyemate-IO sensor implant. In figure 1B, non-averaged recording traces for IO-Reader$_{ON}$ and IO-Reader$_{OFF}$ are depicted. It is evident that there is a periodic high amplitude intrusion into the recordings only for IO-Reader$_{ON}$, which was in the order of 80 µV (peak-to-peak) and at a frequency centred around 9.2 Hz, that is, the known approximate read-out frequency (see the Methods section). A set of averaged ssPERGs from the same participant is given in figure 1C for both check sizes, for both conditions (IO-Reader$_{ON}$ and IO-Reader$_{OFF}$), and both eyes (with and without sensor implant for the right and left eye, respectively). Significant responses ($P<0.01$) are evident at the reversal frequency (15 Hz) for all ssPERGs obtained, as underlined by the peak in the spectrum at 15 Hz. For the IO-Reader$_{ON}$ condition, a second peak is observed at around 9 Hz, that is, corresponding to the read-out frequency (see the Methods and results section). It is also evident that there is an overspill of this intrusion to neighbouring frequencies.[26] This can be attributed to slight variations in the read-out frequency and to ssPERG averaging that is not locked to the read-out frequency. These intrusions are expected to have minimal effect on the amplitude obtained at the reversal frequency of 15 Hz, as it is not a directly neighbouring frequency, and as noise estimates allow for the subtraction of the noise from the actual response amplitude.[27]

To test this directly, we performed a quantitative comparison of ssPERG amplitudes for IO-Reader$_{ON/OFF}$ in five participants with an Eyemate-IO implant and in an additional eight controls without the actual implant, but with the generation of the intrusions of the IO-Reader as described in the Methods section. For this purpose, we analysed the effect of the conditions IO-Reader$_{ON/OFF}$ on ssPERG amplitudes for both check sizes, that is, 0.8° and 15° as depicted in figure 2A. On average, only small trends were observed, which did not reach significance with statistical testing (t-test) for neither eye nor check sizes as shown in online supplementary table 2 for the right eyes of GLA_{IMP} group and of controls with an attached Eyemate-IO sensor/reader antenna. Taken together, these results indicate a lack of relevant impact of the Eyemate-IO sensor on ssPERG recordings. As a final check, we assessed the reproducibility of the recordings, by correlating the amplitudes obtained for the two repetitions for each conditions, that is, 0.8° and 15° check size and for IO-Reader$_{ON}$ and IO-Reader$_{OFF}$ (see figure 2B). High r^2 values, that is, >0.5, were obtained for each condition. Importantly, r^2 values for IO-Reader$_{ON}$ were ≥0.9; consequently, the PERG amplitude reproducibility for IO-Reader$_{ON}$ did not fall short of those for IO-Reader$_{OFF}$.

Experiment 2: influence of postural change on IOP

We investigated the effect of posture (lateral decubitus vs sitting) on IOP and PERG amplitudes. For a representative participant of the GLA_{IMP} group, figure 3A illustrates that continual IOP read-outs were strongly affected by the postural changes made in our study. We were particularly interested in the effects observed for the glaucomatous eyes of the participants with simultaneous IOP and PERG read-out, that is, the right eye of the GLA_{IMP} group (figure 3B.i). For GLA_{IMP}, the IOP increased for LD_R versus S1 by 5.1±0.6 mmHg ($P_{0.025}=0.00004$), and for LD_L versus S2 by 2.7±0.8 mmHg ($P_{0.05}=0.01$; table 1). In CON_{RE}, the IOP increased by 1.5±0.6 mmHg for LD_R versus S1 ($P_{0.025}=0.023$) and for LD_L versus S2 ($P_{0.05}=0.04$). In summary, effects of posture on IOP were evident for both groups and particularly pronounced for LD_R in the GLA_{IMP} group, that is, IOP increase in the lower eye.

The above findings might be due either to the recorded right eye being the lower in LD_R, or to a sequential effect, as LD_R was the second and LD_L the fourth condition. The former is clearly supported by figure 3B.ii, where the simultaneously recorded data from the controls' left eyes (CON_{LE}) are depicted. Here, the IOP increase was significant in controls for the lower eye during LD_L versus S2 by 3.5±0.9 mmHg ($P_{0.025}=0.003$), while a trend for increased IOP for LD_R versus S1 did not reach significance (figure 3B.ii, table 1). As the left eye of the GLA_{IMP}-group was not glaucomatous for all subjects, we confirmed this effect in the GLA_{LE}-group, that is, participants with glaucomatous left eyes (figure 3B.iii and table 1). In GLA_{LE}, the statistical power of our design was not sufficient to resolve a significant difference of IOPs of left eye between sitting and LDP.

Experiment 2: influence of postural change on PERG

For the right eye of GLA_{IMP} (figure 3B.i), 0.8° and 15° PERG amplitudes decreased (by 0.24 µV ($P_{0.025}=0.0007$) and 0.16 µV ($P_{0.025}=0.024$), respectively) for LD_R versus S1, but not for LD_L versus S2. Similarly, for CON_{RE}, 0.8° and 15° PERG amplitudes decreased for LD_R vs S1 by 0.31 µV ($P_{0.025}=0.001$) and by 0.14 µV ($P_{0.025}=0.0049$), respectively, but not for LD_L versus S2 (table 2). Similar effects, but as expected for LD_L versus S2, were evident for CON_{LE} as a significant amplitude decrease by 0.29 µV ($P_{0.025}=0.0004$) and 0.11 µV ($P_{0.025}=0.0098$) for 0.8° and 15° PERG amplitudes, respectively, and for GLA_{LE} (figure 3B.iii) as a significant amplitude decrease, which reached significance only for 0.8° ($P_{0.025}=0.0003$; table 2).

Taken together, LDP induced an IOP increase and PERG decrease predominantly in the lower eye.

DISCUSSION

We demonstrated the feasibility of simultaneous ssPERG and continual IOP recordings. This opens novel directions for the investigation of the relationship between IOP and ganglion-cell function. Our findings corroborate the hypothesis that LDP-induced IOP increase in the lower eye is accompanied by reduced

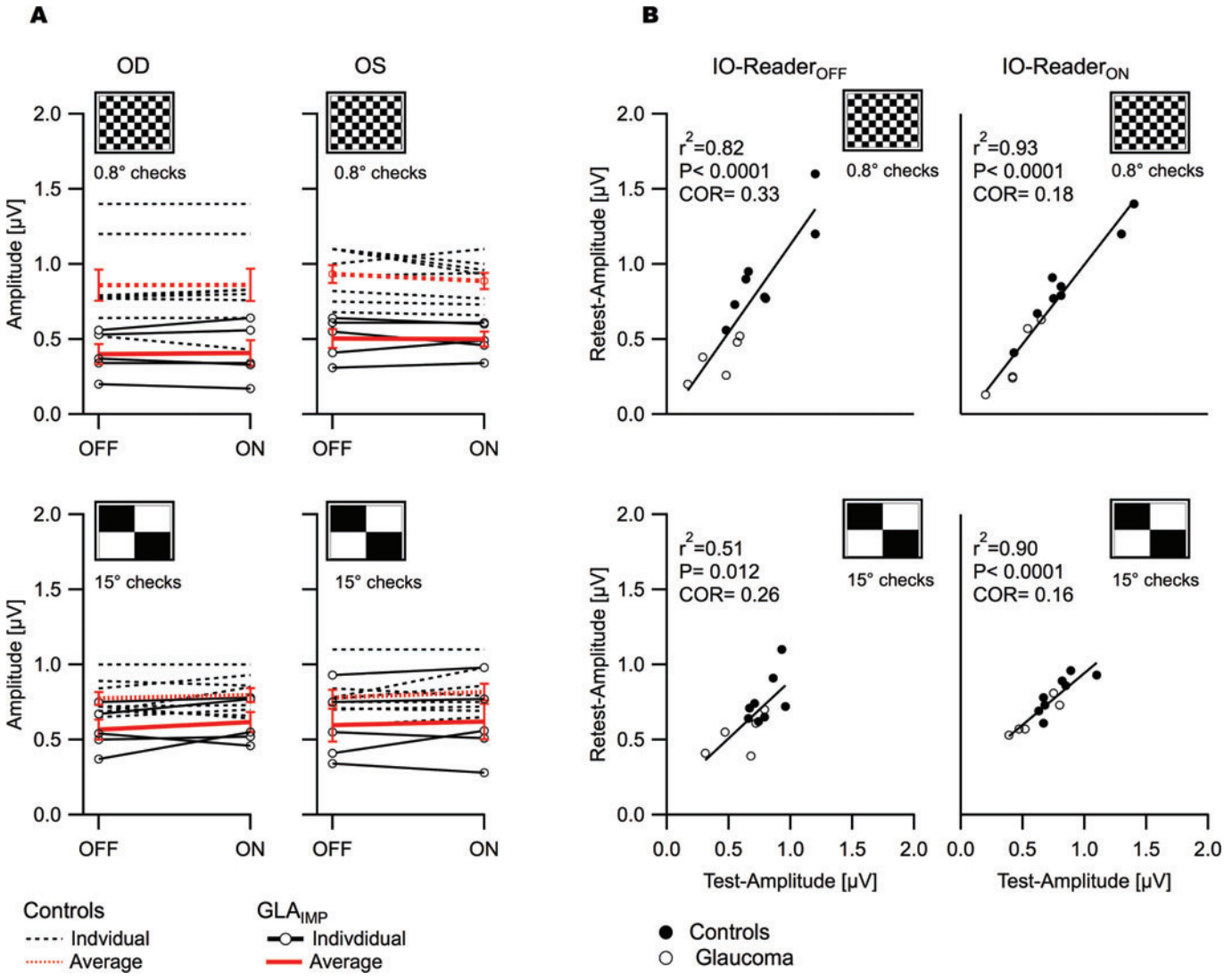

Figure 2 (A) PERG amplitudes for 0.8° and 15° check sizes and IO-Reader$_{ON}$ and IO-Reader$_{OFF}$ in GLA$_{IMP}$ (n=5) and controls (n=8). No significant differences between IO-Reader$_{ON}$ and IO-Reader$_{OFF}$ were evident. Group averages ±SEM (red) and single-subject effects are depicted. (B) Mean test–retest of pattern electroretinogram (PERG) measurements during experiment 1 (IO-Reader$_{ON/OFF}$). PERG check sizes 0.8° and 15° test–retest amplitudes in µV along with r^2, coefficient of reliability (=1.96 × SD of difference) and statistical significance calculation by Pearson correlation. GLA$_{IMP}$, glaucoma patients with Eyemate-IO implant.

ganglion responses as determined with ssPERG, both in control and glaucoma eyes.

In our study, LDP induced significantly higher IOPs in the lower eye compared to the reference condition, that is, sitting, in both controls and GLA$_{IMP}$. This is in accordance with previous studies that demonstrated LDP induced IOP increase of the lower eye in comparison to either sitting and/or supine postures in either healthy participants[16 29 30] or untreated glaucoma patients.[17 18] The GLA$_{IMP}$-group showed higher IOP fluctuations and rise than healthy participants during the posture change from sitting to LDP. This is in line with other studies that reported higher LDP- or supine-induced IOP changes to be associated with stronger progression or asymmetrical visual field defects of untreated and treated glaucoma patients.[15 17 19 31 32] We observed a reversible reduction of ganglion-cell responses as reflected by the ssPERG for LDP, especially in the lower eye. This is supported by a previous report on the effect of recumbent posture on the ssPERG after head-down body tilt of −10°.[33 34] There is no prior report characterising electrophysiological changes during LDP. This is of importance, as LDP does, in contrast to supine posture, not require adapted stimulation set-ups. Due to its simplicity, the LDP paradigm therefore opens the possibility of a widespread use of PERG recordings during posture changes to uncover the relation between glaucoma damage and LDP. For example, this approach might serve as a provocative test to assess the interplay of LDP-induced IOP changes and retinal ganglion-cell function. Further, the ability to obtain continual IOP and PERG recordings enables us to assess the relevance of previously underestimated everyday IOP fluctuations for the responsiveness of retinal ganglion cells. For such follow-up projects, it would be of interest to study the IOP continuously for both eyes. However, at present, no patients were implanted with the Eyemate-IO sensor in both eyes, neither were any healthy controls implanted with the sensor.

In conclusion, we demonstrated that continuous IOP monitoring with the Eyemate-IO sensor can be used for simultaneous IOP measurements and ssPERG recordings. Further, we reported reduced ssPERG in the lower eye during LDP and thus

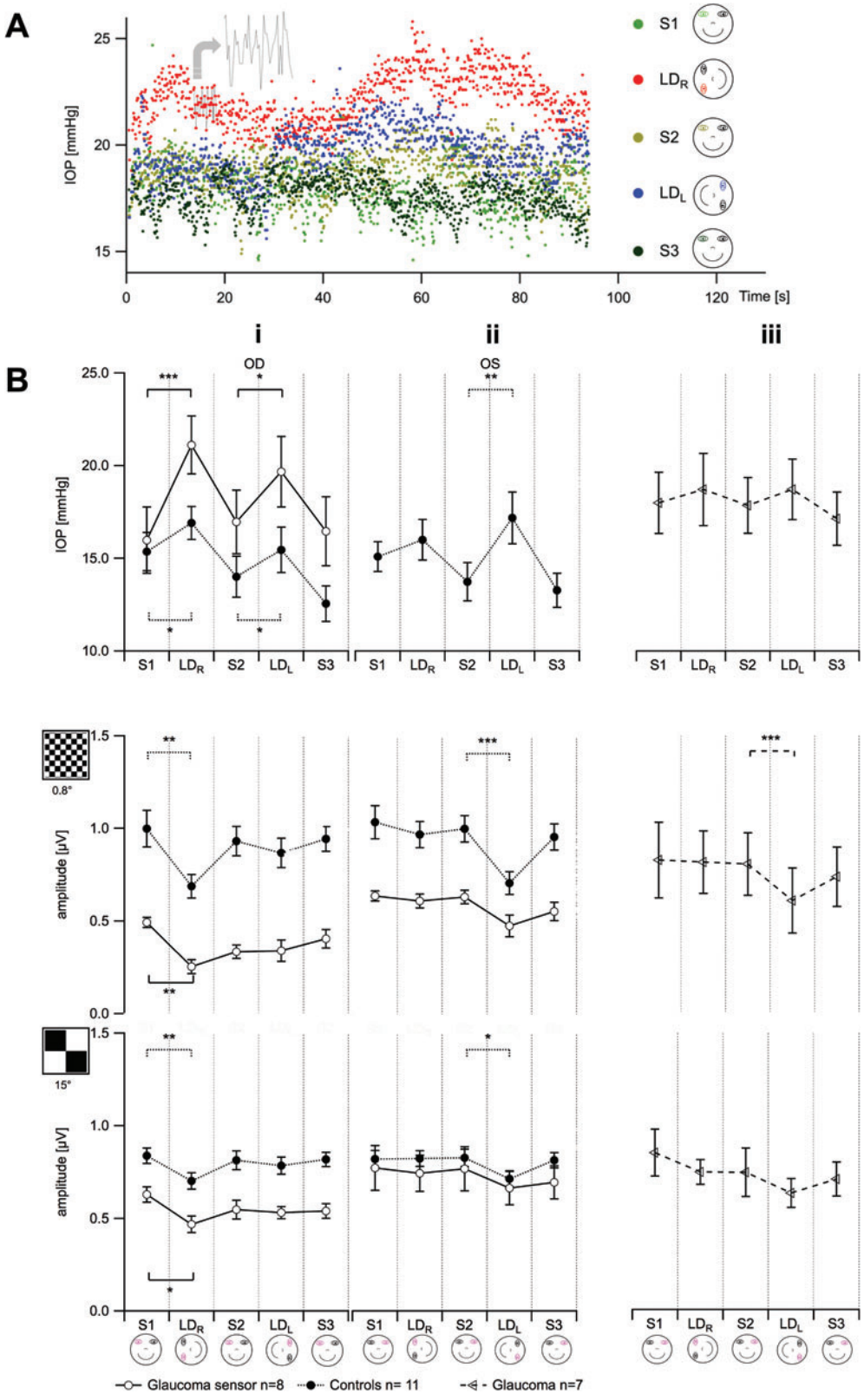

Figure 3 (A) Intraocular pressure (IOP) continuous read-out in a representative participant of the GLA_{IMP} group, that is, with an Eyemate-IO sensor implant, during different postures (see legend and icon for colour-code) plotted as a function of time. A clear effect of posture on IOP was evident. It should be noted, that the apparent scatter of the data points within each condition did not reflect random noise, but reflected regular pulses (see grey error for magnified 5 s time course of LD_R) reminiscent of the ocular pulse. (B) Mean±SEM IOP (top row) and mean±SEM ssPERG amplitudes (0.8° check size: middle row; 15° check size: bottom row) for different postures (S1=sitting 1; LD_R=right lateral decubitus; S2=sitting 2; LD_L=left lateral decubitus; S3=sitting 3). Data were plotted for control right eyes (CON_{RE}), GLA_{IMP}-group' right eyes, control left eyes (CON_{LE}), GLA_{IMP}-group's left eyes (i and ii) and GLA_{LE}-group left eyes (iii) and t-tests were performed for conditions S1 versus LD_R and S2 versus LD_L. *P<0 .05; ** P<0.01; ***P<0.001. GLA_{IMP}, glaucoma patients with Eyemate-IO implant.

Table 1 Intraocular pressure during different body postures

OD	CON_{RE} (N=11)				GLA_{IMP} (N=8)			
Posture	**Mean IOP ±SE**	**M. diff.±SE**	**t(10)**	**P**	**Mean IOP ±SE**	**M. diff. ±SE**	**t(7)**	**P**
S1	15.36±1.04	−1.55 ±0.58	−2.68	$P_{0.025}$=0.023	15.98±1.79	−5.14±0.57	−8.96	$P_{0.025}$=0.00004
LD_R	16.91±0.89				21.12±1.57			
S2	14.00±1.10	−1.45±0.62	−2.33	$P_{0.05}$=0.04	16.97±1.72	−2.71±0.78	−3.47	$P_{0.05}$=0.01
LD_L	15.45±1.23				19.68±1.91			
OS	CON_{LE} (N=11)				GLA_{LE} (N=7)			
Posture	**Mean IOP ±SE**	**M. diff. ± SE**	**t(10)**	**P**	**Mean IOP ±SE**	**M. diff. ±SE**	**t(6)**	**P**
S1	15.09±0.80	−0.91±0.59	−1.53	0.16	18.00±1.65	−0.71±0.89	−0.8	0.45
LD_R	16.00±1.10				18.71±1.95			
S2	13.73±1.03	−3.45±0.88	−3.94	$P_{0.025}$=0.003	17.86±1.50	−0.86±0.59	−1.44	0.20
LD_L	17.18±1.40				18.71±1.63			

CON_{RE}, controls' right eye; CON_{LE}, controls' left eye; diff., difference; GLA_{IMP}, Eyemate-IO sensor patients' right eye; GLA_{LE}, left eye glaucoma patients; IOP, intraocular pressure; M., mean; LD_R, right lateral decubitus posture; LD_L, left lateral decubitus posture; OD, right eyes; OS, left eyes; S1 and S2, sitting 1 and 2; Pα, α denotes α-level according to Bonferroni-Holm correction.

Table 2 PERG amplitude changes during different body postures

OD		CON_{RE} (N=11)				GLA_{IMP} (N=8)			
Checksize	**Posture**	**M. Amp.± SE**	**M. diff.± SE**	**t(10)**	**P**	**M. Amp.±SE**	**M. diff. ±SE**	**t(7)**	**P**
0.8°	S1	1.00±0.10	0.31±0.07	4.58	$P_{0.025}$=0.001	0.49±0.03	0.24±0.04	5.78	$P_{0.025}$=0.0007
	LD_R	0.69±0.06				0.25±0.04			
15°	S1	0.84±0.04	0.14±0.04	3.59	$P_{0.025}$=0.0049	0.63±0.04	0.16±0.06	2.87	$P_{0.025}$=0.024
	LD_R	0.70±0.04				0.47±0.05			
0.8°	S2	0.93±0.08	0.06±0.04	1.67	0.12	0.33±0.04	−0.01±0.04	−0.13	0.89
	LD_L	0.87±0.08				0.34±0.06			
15°	S2	0.81±0.05	0.03±0.04	0.74	0.47	0.55±0.05	0.02±0.06	0.29	0.78
	LD_L	0.78±0.05				0.53±0.03			
OS		CON_{LE} (N=11)				GLA_{LE} (N=7)			
Checksize	**Posture**	**M. Amp.± SE**	**M. diff.±SE**	**t(10)**	**P**	**M. Amp.± SE**	**M. diff.±SE**	**t(6)**	**P**
0.8°	S1	1.04±0.09	0.07±0.05	1.31	0.217	0.82±0.20	0.01±0.09	0.12	0.91
	LD_R	0.97±0.07				0.81±0.17			
15°	S1	0.82±0.05	−0.002±0.04	−0.07	0.949	0.85±0.13	0.10±0.07	1.48	0.19
	LD_R	0.82±0.04				0.75±0.07			
0.8°	S2	1.01±0.07	0.29±0.06	5.17	$P_{0.025}$=0.0004	0.80±0.17	0.20±0.03	7.31	$P_{0.025}$=0.0003
	LD_L	0.71±0.06				0.60±0.18			
15°	S2	0.83±0.05	0.11±0.04	3.18	$P_{0.025}$=0.0098	0.75±0.13	0.11±0.09	1.31	0.24
	LD_L	0.71±0.04				0.63±0.08			

Amp., amplitude; CON_{RE}, controls' right eye; CON_{LE}, controls' left eye; diff., difference; GLA_{LE}, left eye glaucoma patients; GLA_{IMP}, Eyemate-IO sensor patients' right eye; LD_R, right lateral decubitus posture; LD_L, left lateral decubitus posture; M., mean; OD, right eyes; OS, left eyes; PERG, pattern electroretinogram; S1 and S2, sitting 1 and 2; Pα, α denotes α-level according to Bonferroni-Holm correction.

demonstrated the impact of IOP changes on retinal ganglion-cell function. This opens the possibility to perform investigations to scrutinise the relationship of IOP and ganglion-cell function with the novel approach of simultaneous IOP and PERG measurements as tested in the present study. Further studies with bigger sample size are required to detail the observed effects and their relationship to glaucoma asymmetry and progression.

Contributors MBH and LC obtained funding and supervised the study. MBH, LC and KOA contributed to study concept and design. KOA, JJONvdB and VP collected the data. KOA analysed the data. MBH and KOA drafted the manuscript. All authors critically discussed the results, commented on and revised the manuscript.

Funding This work was supported by European Union's Horizon 2020 research and innovation programme under the Marie Sklodowska-Curie grant agreement (No. 675033) to MBH and LC and by funding of the German research foundation to MBH (DFG; HO2002/20-1).

Competing interests JJONvdB is currently employed at Implandata as PhD student within EGRET+ supported by EU-funded postgraduate training programme under the Marie Sklodowska-Curie grant agreement (No. 675033). KM is currently working as consultant for Implandata.

Provenance and peer review Not commissioned; externally peer reviewed.

Data sharing statement Data are available upon reasonable request.

ORCID iD
Michael B Hoffmann http://orcid.org/0000-0002-6452-9638

REFERENCES

1 Bach M, Hoffmann M. The origin of the pattern electroretinogram. In: Heckenlively JR, Arden GB, eds. *Principles and practice of clinical electrophysiology of vision*. MIT Press, 2006: 185–96.

2 Bach M, Cuno A-K, Hoffmann MB. Retinal conduction speed analysis reveals different origins of the P50 and N95 components of the (multifocal) pattern electroretinogram. *Exp Eye Res* 2018;169:48–53.
3 Porciatti V, Ventura LM. Normative data for a user-friendly paradigm for pattern electroretinogram recording. *Ophthalmology* 2004;111:161–8.
4 Bach M, Hoffmann MB. Update on the pattern electroretinogram in glaucoma. *Optom Vis Sci* 2008;85:386.
5 Tojo N, Abe S, Ishida M, *et al.* The fluctuation of intraocular pressure measured by a contact lens sensor in normal-tension glaucoma patients and nonglaucoma subjects. *J Glaucoma* 2017;26:195–200.
6 Itoh Y, Nakamoto K, Horiguchi H, *et al.* Twenty-four-hour variation of intraocular pressure in primary open-angle glaucoma treated with triple eye drops. *J Ophthalmol* 2017;2017:1–6.
7 Leonardi M, Leuenberger P, Bertrand D, *et al.* First steps toward noninvasive intraocular pressure monitoring with a sensing contact lens. *Invest Ophthalmol Vis Sci* 2004;45:3113–7.
8 Aptel F, Musson C, Zhou T, *et al.* 24-hour intraocular pressure rhythm in patients with untreated primary open angle glaucoma and effects of selective laser trabeculoplasty. *J Glaucoma* 2017;26:272–7.
9 Melki S, Todani A, Cherfan G. An implantable intraocular pressure transducer: initial safety outcomes. *JAMA Ophthalmol* 2014;132:1221–5.
10 Koutsonas A, Walter P, Roessler G, *et al.* Implantation of a novel telemetric intraocular pressure sensor in patients with glaucoma (ARGOS Study): 1-year results. *Invest Ophthalmol Vis Sci* 2015;56:1063–9.
11 Koutsonas A, Walter P, Plange N. Selbsttonometrie mit einem telemetrischen, intraokularen drucksensor bei patienten mit Glaukom. *Klin Monatsblätter Für Augenheilkd* 2016;233:743–8.
12 Koutsonas A, Walter P, Roessler G, *et al.* Long-term follow-up after implantation of a telemetric intraocular pressure sensor in patients with glaucoma: a safety report. *Clin Experiment Ophthalmol* 2018;46:473–9.
13 Choritz L, Mansouri K, van den Bosch J, *et al.* Telemetric measurement of intraocular pressure via an implantable pressure sensor—12-month results from the ARGOS-02 trial. *Am J Ophthalmol* 2019;
14 Enders P, Hall J, Bornhauser M, *et al.* Telemetric intraocular pressure monitoring after boston keratoprosthesis surgery. *Ophthalmology* 2019;126:322–4.
15 Park J-H, Yoo C, Yoo E, *et al.* Intraocular pressure elevation during lateral body posture in side-sleeping glaucoma patients. *Optom Vis Sci Off Publ Am Acad Optom* 2019;96:62–70.
16 Lee JY, Yoo C, Jung JH, *et al.* The effect of lateral decubitus position on intraocular pressure in healthy young subjects. *Acta Ophthalmol (Copenh)* 2012;90:e68–72.
17 Lee JY, Yoo C, Kim YY. The effect of lateral decubitus position on intraocular pressure in patients with untreated open-angle glaucoma. *Am J Ophthalmol* 2013;155:329–335.e2.
18 Piven I, Glovinsky Y. Intraocular pressure curves of untreated glaucoma suspects and glaucoma patients in sitting and lateral decubitus positions using the goldmann applanation tonometer. *J Glaucoma* 2014;23:541–6.
19 Kim KN, Jeoung JW, Park KH, *et al.* Effect of lateral decubitus position on intraocular pressure in glaucoma patients with asymmetric visual field loss. *Ophthalmology* 2013;120:731–5.
20 Bach M, Mathieu M. Different effect of dioptric defocus vs. Light scatter on the pattern electroretinogram (PERG). *Doc Ophthalmol* 2004;108:99–106.
21 Anderson DR, Patella VM. *Automated static perimetry*. Mosby, 1999.
22 Todani A, Behlau I, Fava MA, *et al.* Intraocular pressure measurement by radio wave telemetry. *Invest Ophthalmol Vis Sci* 2011;52:9573–80.
23 Koutsonas A, Walter P, Kuerten D, *et al.* Automated, noncontact intraocular pressure home monitoring after implantation of a novel telemetric intraocular pressure sensor in patients with glaucoma: a feasibility study. *Biomed Res Int* 2018;2018:1–5.
24 Bach M. Bach: Freiburg evoked potentials. Available http://localhost:4000/ep2000/ (accessed 14 Jan 2019)
25 Bach M, Brigell MG, Hawlina M, *et al.* ISCEV standard for clinical pattern electroretinography (PERG): 2012 update. *Doc Ophthalmol* 2013;126:1–7.
26 Bach M, Meigen T. Do's and don'ts in fourier analysis of steady-state potentials. *Doc Ophthalmol* 1999;99:69–82.
27 Meigen T, Bach M. On the statistical significance of electrophysiological steady-state responses. *Doc Ophthalmol* 1999;98:207–32.
28 Holm S. A simple sequentially rejective multiple test procedure. *Scand J Stat* 1979;6:65–70.
29 Malihi M, Sit AJ. Effect of head and body position on intraocular pressure. *Ophthalmology* 2012;119:987–91.
30 Lee T-E, Yoo C, Kim YY. Effects of different sleeping postures on intraocular pressure and ocular perfusion pressure in healthy young subjects. *Ophthalmology* 2013;120:1565–70.
31 Kiuchi T, Motoyama Y, Oshika T. Relationship of progression of visual field damage to postural changes in intraocular pressure in patients with normal-tension glaucoma. *Ophthalmology* 2006;113:2150–5.
32 Kiuchi T, Motoyama Y, Oshika T. Postural response of intraocular pressure and visual field damage in patients with untreated normal-tension glaucoma. *J Glaucoma* 2010;19:191–3.
33 Ventura LM, Golubev I, Lee W, *et al.* Head-down posture induces PERG alterations in early glaucoma. *J Glaucoma* 2013;22:255–64.
34 Porciatti V, Feuer WJ, Monsalve P, *et al.* Head-down posture in glaucoma suspects induces changes in IOP, systemic pressure, and PERG that predict future loss of optic nerve tissue. *J Glaucoma* 2017;26:459–65.

Chapter 6

mfPhNR in glaucoma diagnosis

This study has been published in the Experimental Eye Research (EER) Journal - Exp Eye Res. Volume 200, November 2020, 108242- and entitled "**Diagnostic performance of multifocal photopic negative response, pattern electroretinogram and optical coherence tomography in glaucoma**" and has been reprinted in this thesis with permission and is cited as follows:

Al-Nosairy, K. O., Thieme, H., & Hoffmann, M. B. (2020). Diagnostic performance of multifocal photopic negative response, pattern electroretinogram and optical coherence tomography in glaucoma. Experimental Eye Research, 108242. https://doi.org/10.1016/j.exer.2020.108242

Experimental Eye Research 200 (2020) 108242

Contents lists available at ScienceDirect

Experimental Eye Research

journal homepage: www.elsevier.com/locate/yexer

Diagnostic performance of multifocal photopic negative response, pattern electroretinogram and optical coherence tomography in glaucoma

Khaldoon O. Al-Nosairy [a], Hagen Thieme [a], Michael B. Hoffmann [a,b,*]

[a] Department of Ophthalmology, Otto-von-Guericke University, Magdeburg, Germany
[b] Center for Behavioral Brain Sciences, Magdeburg, Germany

ARTICLE INFO

Keywords:
Multifocal
ERG
Photopic negative response
Glaucoma
Pattern electroretinogram
Retinal ganglion cells

ABSTRACT

The photopic negative response of the electroretinogram reflects retinal ganglion cell function and consequently aids diagnosis of optic nerve diseases including glaucoma. In this study, we assessed the efficacy of stimulation parameters for electroretinographic recordings of the multifocal photopic negative response (mfPhNR) for the detection of glaucoma and compared the diagnostic accuracy of electrophysiological, structural and functional measures of glaucoma. We compared the diagnostic performance of the mfPhNR for 6 different stimulation rates in a cohort of 24 controls, 10 glaucoma suspects (GLA_S) and 16 glaucoma participants (GLA_G). A cross-modal comparison of the mfPhNR/b wave ratio was performed with the pattern electroretinogram (PERG), and the peripapillary retinal nerve fiber layer (pRNFL) thickness. These analyses were based on area under curves (AUC) obtained from receiver-operating-characteristics (ROC) and step-wise regression analyses. We found that compared to the other mfPhNR-conditions, the PhNR/b-wave ratio for the fastest stimulation condition had the highest AUC for GLA_S (0.84, $P = 0.008$, 95%CI: 0.71- 0.98), while the other modalities, i.e., PERG-amplitude and pRNFL had AUCs of 0.78 ($P= 0.039$), and 0.74 ($P < 0.05$), respectively. For GLA_G , the respective AUCs were 0.78 ($P= 0.004$), 0.85 ($P< 0.001$) and 0.87 ($P< 0.001$). pRNFL was the significant predictor for both mfPhNR/b-wave ratio [$t (48) = 4$, $P = 0.0002$] and for PERG amplitude [$t (48) = 3.4$, $P = 0.001$]. In conclusion, fast mfPhNR protocols outperform other multifocal PhNR protocols in the identification of glaucomatous damage especially for GLA_S and thus aid the early detection of glaucoma, indicating its value as a surrogate marker of early stage ganglion cell dysfunction.

1. Introduction

Glaucoma is leading as an irreversible cause of visual impairment (Flaxman et al., 2017) and early detection is of great importance. Several methods are at hand to tap functional and structural damage in glaucoma. Standard automated perimetry (SAP) allows for an assessment of visual function in glaucoma that might be linearly correlated with (Harwerth et al., 2004) or preceded (Quigley et al., 1989; Kerrigan-Baumrind et al., 2000) by structural damage in retina. However, the subjective nature and high variability of SAP might hinder its ability to assess changes in visual function (Chauhan et al., 2008). Electrophysiological measures of vision, on the other hand, allows for an objective assessment of visual function.

An important tool for the assessment of retinal ganglion cell function is the steady state pattern electroretinogram (ssPERG), which can detect glaucoma prior to visual field loss (Bach and Hoffmann, 2006, 2008). In fact, previous studies demonstrated that PERG could predict glaucoma conversion of ocular hypertension 4 years before conversion, i.e. before detectable visual field defects on SAP (Bach et al., 2006; Bode et al., 2011). The full-field ERG (ff-ERG) recorded under light adaptation is another method of particular interest as it provides assessment of inner retinal functions (i.e., ganglion cells) via a component termed the photopic negative response (PhNR) (Viswanathan et al., 1999, 2001). It has the additional benefit, that it is, compared to the PERG, more robust to optic media opacities and refractive errors. PhNRs to full field stimulation do not allow for the detection of focal or localized retinal damage, as the response is the sum response of both healthy and diseased retinal areas (Viswanathan et al., 1999).

Focal PhNRs from multiple retinal areas were reported to detect early functional loss in diseases affecting retinal ganglion cells' functions (Machida et al., 2010). The multifocal stimulation approach introduced by Sutter et al. (Sutter and Tran, 1992; Sutter, 2001) allows

* Corresponding author. Department of Ophthalmology, Otto-von-Guericke University, Leipziger Str. 44, 39120, Magdeburg, Germany.
E-mail address: michael.hoffmann@med.ovgu.de (M.B. Hoffmann).

https://doi.org/10.1016/j.exer.2020.108242
Received 27 March 2020; Received in revised form 31 July 2020; Accepted 8 September 2020
Available online 11 September 2020

Table 1
Overview of participants' characteristics.

	Control (n = 24)	GLA_S (n = 10)	GLA_G (n = 17)	P value[a]
	Mean ± SE	Mean ± SE	Mean ± SE	
Age [years]	52.12 ± 2.25	61.84 ± 1.79	57.90 ± 3.73	0.080
BCVA [decimal]	1.11 ± 0.04	1.73 ± 0.70	0.99 ± 0.04	0.172
VF-MD [dB][b]	0.85 (1.48)[b]	1.8 (0.7)[b]	4.2 (4.9)[b]	<0.001[b]
VF-PSD [dB]	3.9 (3.63)[b]	8.4(6.30)[b]	15.7 (51.6)[b]	<0.001[b]

GLA_S = Glaucoma suspects; **GLA_G** = Glaucoma group; BCVA= Best-corrected visual acuity in decimal; VF-MD = visual field mean deviations, VF-PSD = visual field pattern standard deviations.
[a] ANOVA test.
[b] Kruskal-Wallis test. Results reported as median and interquartile range.

obtaining visual field topographies of retinal and cortical function within short time. Therefore, combining PhNR-recordings with the multifocal approach might enhance its scope in identifying retinal ganglion cell dysfunction. In fact, several studies employing PhNRs recorded with adapted multifocal ERG protocols (mfPhNR) were conducted in glaucoma and optic nerve lesions (Kamei and Nagasaka, 2010, 2014; Kamei et al., 2011; Rajagopalan et al., 2014; Kaneko et al., 2015; Kato et al., 2015; Tanaka et al., 2020) and regional PhNR-changes were demonstrated. Different multifocal stimulation modes were used in these studies, i.e., fast (Kamei and Nagasaka, 2010, 2014; Kamei et al., 2011; Kaneko et al., 2015; Kato et al., 2015; Tanaka et al., 2020) (1–9 interleaved frames) or slow stimulation sequences (Rajagopalan et al., 2014; Van Alstine and Viswanathan, 2017) (around 30 interleaved frames). It is not clear at present, whether any of these modes are of specific advantage for the detection of ganglion cell damage. This prompted our present investigation. In accordance with previous studies (Kaneko et al., 2015; Kato et al., 2015; Tanaka et al., 2020), we applied mfPhNR-protocols with 5 sectors to address our primary objective, i.e. to determine (i) which of the slow and fast stimulation modes yields highest mfPhNR and (ii) which condition performs best for the differentiation of controls and glaucoma patients. As a secondary objective, we investigated how the mfPhNR compares to other established diagnostic methods [i.e., PERG and peripapillary retinal fiber layer thickness (pRNFL)]. We found the fastest mfPhNR-protocol to be the superior multifocal protocol for the discrimination of GLA_S (glaucoma suspects).

2. Materials and methods

2.1. Participants

We included 50 participants in the study as detailed below. The participants gave their written consent to participate in the study. The procedures followed the tenets of the declaration of Helsinki and the protocol was approved by the ethical committee of the Otto-von-Guericke University of Magdeburg, Germany. The participants underwent complete ophthalmic examinations and subjective and objective refractions were assessed for both near and far visual acuity to determine best corrected visual acuity (BCVA). Exclusion criteria were any eye diseases or surgeries except cataract and glaucoma surgery, incipient cataract that did not decrease BCVA <0.8 (Bach and Mathieu, 2004) and refractive error exceeding ± 5 D or astigmatism > ± 2 D. There was no significant difference between age across groups [ANOVA, F (2, 48) = 2.7, P = 0.08]. Demographic and clinical characteristics of each group are shown in Table 1. All glaucoma participants were under either medical and/or surgical treatment.

Controls: Twenty-four participants [mean age ± standard error (SE): 52.1 ± 2.3 years] with normal visual acuity (VA≥1.0) were included in the study. According to the selection criteria for the glaucoma patients' eyes (see below) incidentally only their left eyes (with one exception, see below) were included and, consequently, compared to the left eyes of the controls. One participant had neither PERG nor OCT measurements.

Primary open angle glaucoma suspects' group (GLA_S). Left eyes of 10 patients (mean age ± SE: 61.8 ± 1.8 years) were included in the study. In accordance with and following the respective guidelines of American Academy of Ophthalmology (Prum et al., 2016a) glaucoma suspects in our study had any of the clinical findings: (i) a suspicious appearance of glaucomatous damage in optic disc or RNFL, (ii) a visual field defect suspicious for glaucoma damage (i.e., as defined for GLA_G group below) without any other apparent causes (n = 4), or (iii) consistently elevated intraocular pressure (IOP) > 21 mmHg (n = 6). All glaucoma suspects' eyes in our study had an open anterior chamber angle with normal appearance of optic disc and RNFL.

Glaucoma group (GLA_G). Sixteen glaucoma patients (mean age ± SE: 57.90 ± 3.7 years) were included in the study. Ten patients with primary open angle glaucoma, 5 patients with normal tension glaucoma and 1 patient with pigment dispersion glaucoma. Glaucoma severity ranges from preperimetric to severe stages. For most patients both eyes had the same damage stages and the eye with more severe damage was included. For one participant, damage stages differed between eyes, such that both eyes were included (i.e., 17 eyes were included in the analysis). GLA_G patients met the following criteria (Preiser et al., 2013): 1) Local notching of optic disc rim or vertical cup disc ratio ≥7; 2) Visual field defect with 3 or more adjacent points of ≥5 dB loss or two or more adjacent points of ≥10 dB loss detected in Standard static white-on-white perimetry (SAP). Four POAG eyes have definite optic disc or RNFL abnormalities consistent with glaucoma but has no VF defects tested in SAP, i.e. mild stage of glaucomatous damage following the American Academy guidelines for POAG (Prum et al., 2016b).

2.2. Standard automated perimetry

Standard automated perimetry (dG2; dynamic strategy; Goldmann size III; OCTOPUS® Perimeter 101, Haag-Streit International, Switzerland) was tested to the central 30° of VF. Higher mean deviation values indicate more decrease of visual function.

2.3. SD-OCT

Peripapillary retinal nerve fiber layer thickness (pRNFL) from a 3.5 mm circle scan centered on optic disc (12° diameter) with 768 A-scan Spectral domain optical coherence tomography (OCT) was performed with the OCT Spectralis (Heidelberg Engineering, Heidelberg, Germany).

2.4. Electrophysiological testing

Procedure. Two types of ERG-recordings, mfPhNR and PERG, were applied in separate sessions, for better comparability both at the same viewing distance of 33 cm. Binocular mfPhNR and PERG were recorded using DTL electrodes (DTL Electrode ERG, Unimed electrode Supplies, Ltd, UK) placed in the upper margin of lower lid. The reference electrode (10 mm diameter; Golden EEG Cup Electrodes, Natus Manufacturing Limited, Ireland), filled with conductive paste (Ten20, WEAVER and Company, USA), was attached to the temple ipsilateral of the corresponding eye. The ground electrode filled with conductive paste was pasted on the forehead. Reference and ground electrodes were attached after skin cleaning with a cleaning paste (skinPure, NIHON KODEN Corporation, Tokyo, Japan) to reduce the resistance of the skin below 5 kOhm. Pupils were dilated when recording mfPhNR with Tropicamide 0.5% (Mydriaticum Stulln® UD, Pharma Stulln GmbH, Germany) to approximately 7 mm. Corneas were locally anaesthetized with Oxybuprocain hydrochlorid 0.4% (Conjuncain® EDO®, Bausch&Lomb

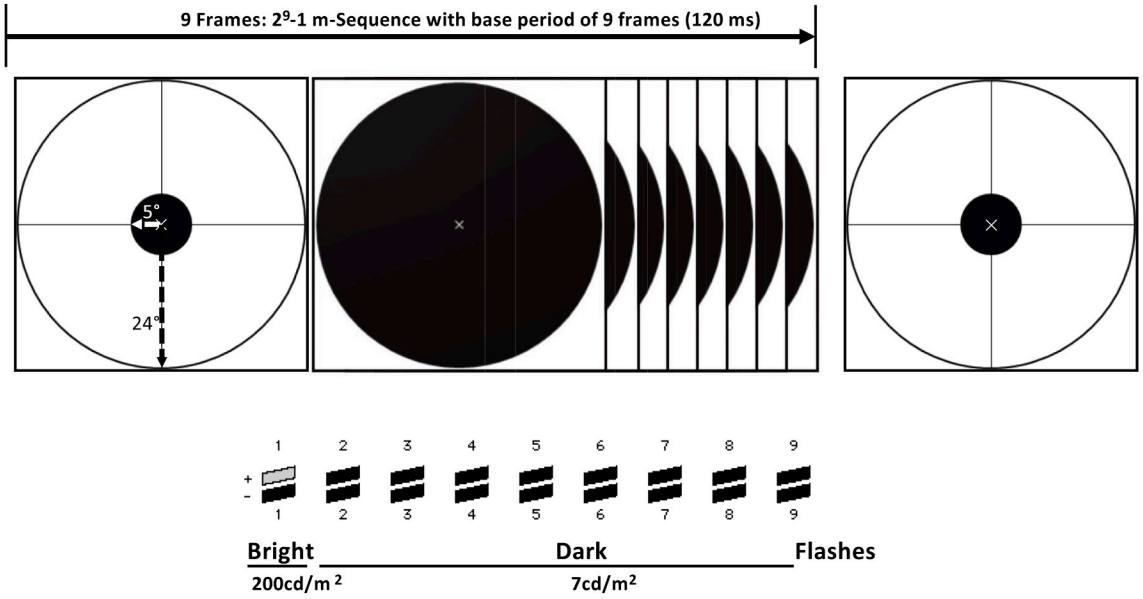

Fig. 1. Schematic of the mfPhNR stimulation paradigm. The multifocal stimulus array consisted of 5 visual field locations with inner diameter of 5° and outer of 24° and a small fixation cross in the center. Stimulation followed an m sequence with 2^9–1 elements, i.e., 511 stimulated patterns of black and white combinations. For the fast sequence protocol (C_{Fast_1}) each elements lasted for 9 frames, as depicted.

GmbH, Germany). Refractive correction optimized for a viewing distance of 33 cm for both mfPhNR and PERG recordings.

mfPhNR stimulation, recording and analysis. The stimulus display covered 48° and comprised 5 visual field locations (Fig. 1), a central (0°–5°) and four adjacent (from 5° to 24° eccentricity). The 5 fields of this display were stimulated independently with an m-sequence, a pseudo-random succession of 0 (no flash) and 1 (flash) states. In accordance with previous literature (Van Alstine and Viswanathan, 2017), we applied an m-sequence length of 2^9–1 (511) steps, each step lasted 13.3 ms. This resulted in a total recording ranging from 3 min to 23 s in the slowest protocol and 1 min and 1 s in the fastest protocol. The testing protocol was subdivided into 16 segments to allow blinking. Recording segments comprising artifacts, e.g. from eye movements or blinking, were re-recorded. VERIS Science 6.4.9d13 (EDI: Electro-Diagnostic Imaging, Redwood City, CA, USA) was used for stimulus delivery and electrophysiological recordings. For each area in the dartboard, the stimulus consisted of either 1, 2, or 5 bright frames, each occurring on 50% of the frame changes (75 Hz) followed by either 8 or 25 dark frames. This resulted in 3 fast conditions, i.e., 8 dark frames, with 1, 2 and 5 bright frames for stimulation (C_{Fast_1}, C_{Fast_2} and C_{Fast_3}, respectively) and 3 slow conditions, i.e., 25 dark frames, with 1, 2 and 5 bright frames for stimulation (C_{Slow_1}, C_{Slow_2} and C_{Slow_3}, respectively). The averaged stimulation frequency arising ranged from 1.3 to 4.2 Hz. Each condition was repeated twice in a counterbalanced sequence of conditions. The luminance of [i] white frames (stimulation), [ii] uniform grey background, and [iii] black frames (no stimulation) were set at 200, 100, and 7 cd/m^2, respectively, as checked with a calibrated photometer (CS-100A photometer; Konica Minolta Holdings, Inc.; Japan). Stimuli were presented on a monochrome CRT-monitor (MDG403, Philips; P45 phosphor) at a frame rate of 75 Hz, while the measurement was checked on a separate control monitor.

Using VERIS Science 6.4.9d13, the signals were amplified by 100 K (Grass Model 12, Astro-Med, Inc., West Warwick, RI, USA), band-pass filtered 3–100 Hz and digitized at 1200 Hz. The first order kernels were extracted using VERIS Science 6.4.9d13. Subsequent analyses were performed using Igor (WaveMetrics Inc., Lake Oswego, OR, USA). Traces were then digitally filtered (high pass filter: 3Hz; low pass filter: 45 Hz). Repetitions of each condition were averaged. Traces from right eyes were left-right flipped to match stimulated visual fields of traces recorded from left eyes of other participants.

We determined the amplitudes for the a-wave (1st negativity), b-wave (1st positivity) and the mfPhNR, within a time window of 15–35 ms, 20–50 ms, and 55–90 ms, respectively. For the determination of the latter time window we calculated, following Van Alstine and Viswanathan (Van Alstine and Viswanathan, 2017), the waveforms' grand means for the control group within each age bin and we summed all test location waveforms' grand means. This resulted in mfPhNRs to peak around 70–75 ms, adding 15 ms allowed covering the individually varying trace forms. Consequently, mfPhNR amplitude was localized within a time window of 55–90, which is similar to conventional PhNR amplitudes timing described previously (Machida et al., 2015). Following studies of mfPhNR (Kaneko et al., 2015) and full field (conventional) photopic ERG (Machida et al., 2008; Preiser et al., 2013), the PhNR amplitude was also evaluated in respect to b-wave measured from baseline (PhNR/b-wave ratio). Before normalizing mfPhNR to the b-wave, we first assessed the b-wave between groups. We found no significant differences of neither b-waves amplitudes nor peak times of all conditions across groups upon one-way ANVOA testing. All amplitudes were measured from trough to baseline. For an assessment of the visual field topography, we performed analyses for different groups of the stimulated visual field locations: We summed all visual field locations to represent the summed visual field locations response (VF_{SUM}), summed the pairs of visual field patches to cover four different visual field locations, i.e., upper, lower, nasal and temporal hemifields and periphery), and assessed the central response in isolation.

PERG stimulation, recording and analysis. Steady state PERGs were recorded following the international society for clinical electrophysiology of vision (ISCEV) standards for PERG recordings using EP2000 evoked potential system (Bach). By subtending an angle of 62 ° × 49 °, the stimulus was presented on 21-inch monochrome monitor with a 75 Hz frame rate (MDG403, Philips; P45 phosphor). Contrast-inverting (15 Hz) checkerboard patterns (mean luminance: 45 cd/m^2; contrast: 98%) with two checksizes, 0.8° and 15° were presented for stimulation at a viewing distance of 33 cm, as for the mfPhNR measurements. Signals exceeding ±90 μV were rejected and recollected. Two PERG blocks were recorded and averaged per subject. Only PERG 0.8° amplitude and PERG ratio (small/big checksizes' amplitudes) were used for analysis. Further description of analysis is given elsewhere

Table 2
Paired *t*-test comparisons of mfPhNR amplitudes and ratio of C_{Fast_1} vs. other stimulation condition in controls.

	C_{Fast_1} Mean ± SEM	vs. others	Mean ± SEM	Difference Mean ± SEM	t(23)	P* value
mfPhNR Amplitude	−9.86 ± 0.52	C_{Slow_3}	−10.63 ± 1.06	0.77 ± 1.03	0.75	0.46
		C_{Slow_2}	−11.62 ± 0.63	1.76 ± 0.47	3.76	0.004
		C_{Slow_1}	−11.31 ± 0.52	1.45 ± 0.39	3.76	0.001
		C_{Fast_3}	−9.21 ± 0.89	−0.65 ± 0.82	−0.80	0.43
		C_{Fast_2}	−9.16 ± 0.61	−0.70 ± 0.39	−1.80	0.09
mfPhNR/b-wave Ratio	0.41 ± 0.02	C_{Slow_3}	0.75 ± 0.08	−0.33 ± 0.08	−4.25	0.0009
		C_{Slow_2}	0.64 ± 0.04	−0.23 ± 0.03	−8.13	<0.00001
		C_{Slow_1}	0.51 ± 0.03	−0.10 ± 0.02	−5.88	0.00001
		C_{Fast_3}	0.58 ± 0.06	−0.17 ± 0.06	−2.89	0.016
		C_{Fast_2}	0.46 ± 0.03	−0.05 ± 0.02	−2.19	0.039

mfPhNR: multifocal photopic negative response; $C_{Fast\_1,\ Fast\_2,\ Fast\_3}$ (fast stimulation conditions with 1, 2, 5 bright and 8 dark frames, respectively); $C_{Slow\_1,\ Slow\_2,\ Slow\_3}$ (slow stimulation conditions with 1, 2, 5 bright and 25 dark frames, respectively); SEM: standard error of mean; *Paired *t*-test P value corrected for multiple testing.

(Bach and Hoffmann, 2008; Preiser et al., 2013; Al-Nosairy et al., 2020).

2.5. Statistics

mfPhNR responses and PERG amplitudes were transferred into Igor sheet and exported to SPSS 26 (statistical Package for the Social Sciences, IBM) or the R statistical system(R Core Team (2013)). Repeated measure analysis of variance (RM-ANOVA), analysis of variance (ANOVA), Kruskal-Wallis test for non-parametric testing, receiver operating characteristics analysis (ROC) and Post-hoc analysis were run between groups and protocols using SPSS 26 and R. P values were corrected with the Holm Bonferroni correction(Holm, 1979) for multiple testing. Pairwise comparisons of two AUCs were conducted to assess whether there is a significant difference by calculating a critical ratio z using the following formula(Hanley and McNeil, 1983):

$$z = \frac{Area_1 - Area_2}{\sqrt{SE^2_{Area1} + SE^2_{Area2} - 2r(SE_{Area1})(SE_{Area2})}}$$

and unpaired comparison of AUCs from 2 different data sets (controls vs GLA_S and Controls vs GLA_G) were done using the following formula (Motulsky):

$$z = \frac{|Area_1 - Area_2|}{\sqrt{SE^2_{Area1} + SE^2_{Area2}}}$$

where A_1 and A_2 refers to area under curve with their respective standard error (SE_1 &SE_2, respectively) for method 1 and 2, respectively, and r represents estimated correlation between A_1 and A_2. Z value is referred to the normal distribution tables and z value ≥ 1.96 means there is a true difference between both AUCs.

3. Results

3.1. Comparison of mfPhNR recording protocols

Multifocal stimulation settings that were previously applied for mfPhNR recordings ranged between fast (1–9 frames (Kamei and Nagasaka, 2010, 2014; Kamei et al., 2011; Kaneko et al., 2015; Kato et al., 2015; Tanaka et al., 2020)) and slow (30 frames (Rajagopalan et al., 2014; Van Alstine and Viswanathan, 2017)) sequences. In a first step, we performed a quantitative comparison of these settings and their transitions in order to identify the most effective stimulation condition. This condition subsequently entered the second step, i.e., a detailed analysis of the parameters determining the diagnostic potential.

Comparison of stimulation conditions. For an initial characterization of the mfPhNR for the different conditions, we compared response amplitudes between the different conditions for the controls. This was followed by an analysis of the discrimination performance and efficacy in the detection of glaucoma-related damage. We applied six different stimulation settings for mfPhNR recordings and compared the

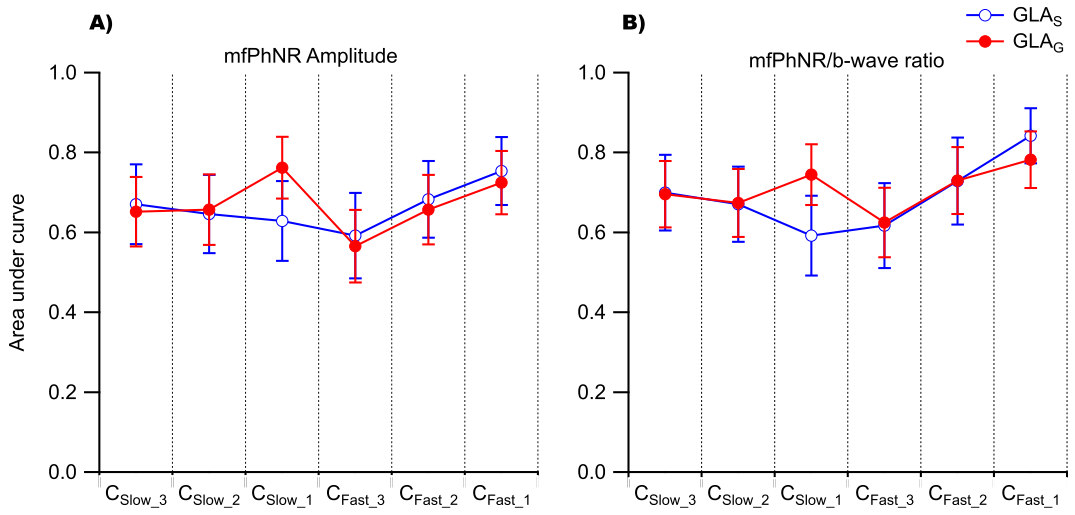

Fig. 2. Comparisons of AUCs ± SE for mfPhNR amplitudes (A) and mfPhNR/b-wave ratio (B) for the discrimination between controls vs glaucoma suspects (GLA_S) and glaucoma (GLA_G) across a range of stimulations conditions C_{Slow_3} (i.e., slowest condition with 25 dark frames and 5 bright flashes) to C_{Fast_1} (i.e., fastest condition with 8 dark frames and 1 bright flash). While for the mfPhNR amplitudes AUCs did not differ significantly, for the mfPhNR/b-wave ratio AUCs for C_{Fast_1} exceeded those for C_{Slow_1} (P = 0.02).

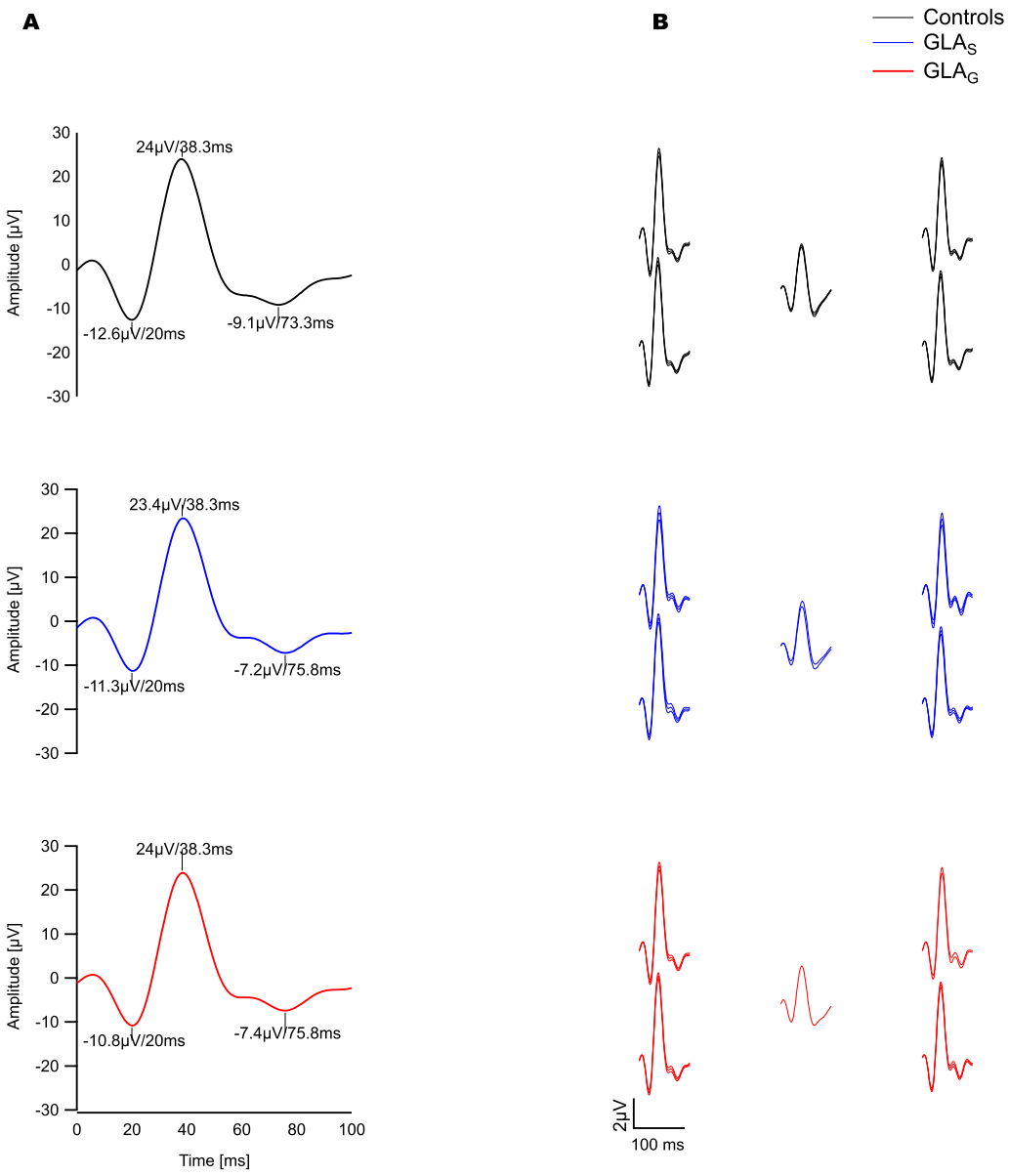

Fig. 3. Grand mean average traces of mfPhNR ("VF_{SUM} trace"; A; amplitudes of responses are referenced to the baseline) and grand mean trace arrays ± SEM (B) for controls, glaucoma suspects (GLA_S) and glaucoma (GLA_G) of the fastest condition responses (C_{Fast_1}).

mfPhNR amplitude and mfPhNR/b-wave ratio as detailed in Methods for the control group. A one-way repeated measure ANOVA [factor, *condition* (C_{Slow_3} to C_{Fast_1})] was conducted to determine the effect on mfPhNR amplitude and mfPhNR/b-wave ratio of the summed visual field locations' response (VF_{SUM}). There was a significant effect of condition on both mfPhNR amplitude [F (2.2, 51.7) = 4.3, P = 0.015] and mfPhNR/b-wave ratio [F (1.7, 38.8) = 12.6, P = 0.0001]. Post-hoc analyses were initially performed for the two most widely used conditions (C_{Fast_1} vs C_{Slow_1}) and demonstrated both mfPhNR amplitude and mfPhNR/b-wave ratio to be significantly lower for C_{Fast_1} [t (23) = 3.8 and −5.8, P = 0.001 and 0.00001, respectively]. Comparing C_{Fast_1} to the other conditions, mfPhNR-amplitudes were significantly lower than for C_{Slow_2} (P = 0.004), while mfPhNR/b-wave ratios were significantly lower than for all other conditions (see Table 2 for effect sizes). While amplitudes are informative to characterize the responses obtained for different stimulation conditions, an assessment of the discrimination performance between controls vs GLA_S and GLA_G is instrumental to identify the condition with the highest diagnostic power. Therefore, we conducted ROC analyses and used the area under curve (AUC) as a measure of the diagnostic performance for each condition for both mfPhNR amplitude and mfPhNR/b-wave ratio as depicted in Fig. 2. For most conditions, the ROC analyses yielded similar AUCs. Pairwise AUC-comparisons (see Methods), identified only the C_{Fast_1} for the mfPhNR/b-wave ratio to be significantly higher than the C_{Slow_1} in discriminating controls vs GLA_S, i.e. AUC ±SE: 0.84 ± 0.07 vs 0.59 ± 0.1, respectively (P = 0.02; Fig. 2 B). In summary, C_{Fast_1} had the highest discrimination performance, albeit not having the highest amplitudes and therefore entered the subsequent detailed analysis.

3.2. *Trace characteristics and topographical analysis for the C_{Fast_1} protocol*

Typical ERG trace shapes were obtained for C_{Fast_1} in all participant groups (controls, GLA_S, and GLA_G, see Fig. 3) with a negativity, positivity and negativity, termed, in accordance with the current literature (Machida et al., 2015; Van Alstine and Viswanathan, 2017), a-wave, b-wave, and PhNR, respectively. No significant group effects were observed for peak time and amplitude of a- and b-waves, neither for the

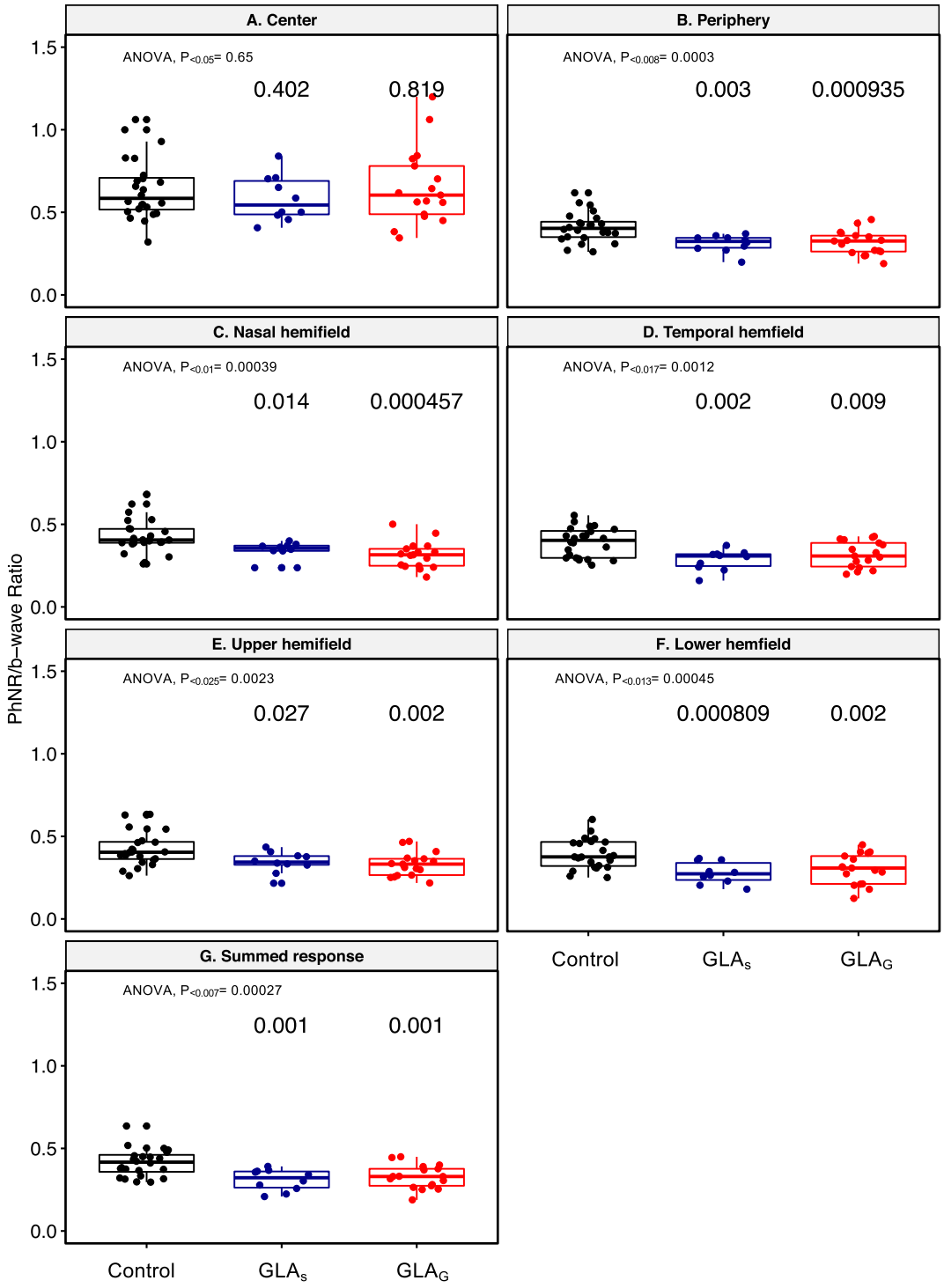

Fig. 4. Comparison of mfPhNR/b-wave ratio of the fastest condition across groups and topographic comparisons. Corrected alpha threshold is 0.025 for the more significant P value in each plot. mfPhNR/b-wave ratio is significantly different in all visual field locations across groups except for the center (for P values see panels). Controls' mfPhNR/b-wave ratio was significantly different vs either group, i.e., glaucoma suspects and glaucoma group. Box: 25%–75% interquartile range; horizontal line is the median value and the whiskers represent the range.

responses of each of the five visual field locations, nor for the summed response, i.e., VF_{SUM}. In contrast, both the mfPhNR VF_{SUM} amplitude and the mfPhNR/b-wave VF_{SUM} ratio were reduced in the patients groups (GLA_S and GLA_G) compared to controls upon ANOVA testing [mfPhNR VF_{SUM} amplitude: $F(2, 48) = 5.7$, $P = 0.018$; mfPhNR/b-wave VF_{SUM} ratio: $F(2, 48) = 9.8$, $P_{< 0.007} = 0.00027$]. For subsequent analyses, we focused in accordance to previous studies, on mfPhNR/b-wave ratio of VF_{SUM} response. Finally, no significant group effects were observed for mfPhNR VF_{SUM} peak times [$F(2, 48) = 2.9$, $P \geq 0.06$].

To assess whether the effects differed for specific hemifields and eccentricities, we subdivided the four peripheral visual field locations into upper, lower, nasal and temporal hemifields and center and periphery. As depicted in Fig. 4, in both GLA_S and GLA_G vs Controls the mfPhNR/b-wave ratio was significantly reduced for all sub-regions analyzed, except the center. The mfPhNR/b wave ratio of the VF_{SUM} response was also significantly different between in both GLA_S and GLA_G vs Controls upon ANOVA testing [$F(2, 48) = 9.8$, $P_{< 0.007} = 0.00027$] as detailed in Fig. 4G.

3.3. Cross-modal comparison of glaucoma-related damage

As our secondary aim, we determined the diagnostic accuracy of our measure, the mfPhNR/b-wave ratio of $C_{Fast\text{-}1}$, in comparison to other established diagnostic methods, i.e. PERG or pRNFL. Therefore, we conducted ROC analyses and determined the AUCs (±SE) for mfPhNR/b-wave ratio, PERG .8° amplitude and PERG ratio and pRNFL (Fig. 5A). In GLA_S, inspection of Fig. 5A suggested that mfPhNR/b-wave ratio was the measure with highest AUC, but statistical testing did not reveal a significant difference between modalities. In GLA_G, the highest AUC was reached for pRNFL, but without statistically significant differences from other measures. It is noteworthy that all our diagnostic measures showed no AUC difference between Controls vs GLA_S and Controls vs GLA_G based on unpaired AUC comparisons. Further, by combining mfPhNR/b-wave ratio and pRNFL measures, only 1 of 10 (10.0%) GLA_S was classified as normal, while separate assessments of mfPhNR/b-wave ratio and pRNFL result in 1 and 3 false negative cases, respectively. Similarly, 2 of 17 (11.8%) GLA_G eyes were classified as normal for the combined assessment, while separate assessments result in 6 and 2 false negative cases, respectively.

Subsequently, we compared the functional and structural parameters between both groups applying a one-way ANOVA and post-hoc analyses to compare each patient group vs controls. The mfPhNR/b-wave ratio differed significantly between controls, GLA_S and GLA_G ($P_{<0.025} = 0.00027$). Post-hoc tests (Fig. 5B) showed that mfPhNR/b-wave ratio were significantly reduced in GLA_S and GLA_G vs controls (T-test; $P_{<0.025} = 0.00118$, $P_{<0.05} = 0.00119$, respectively). Both PERG 0.8° amplitude and PERG ratio differed also significantly between controls and patient groups (ANOVA; $P_{<0.0166} = 0.00008$ and $P_{<0.05} = 0.03$, respectively; Fig. 5C/D). In GLA_S, PERG 0.8° amplitude and PERG ratio were significantly reduced compared to controls (T-test; $P_{<0.05} = 0.016$ and $P_{<0.025} = 0.013$, respectively). In GLA_G, PERG 0.8° amplitude and PERG ratio were significantly reduced compared to controls (T-test; $P_{<0.025} = 0.00005$ and $P_{<0.05} = 0.045$, respectively). Since PERG 0.8° amplitudes had a higher AUC than the PERG-ratio, we used only the PERG 0.8° amplitudes for the below analysis. As a measure of structural damage in glaucoma, mean pRNFL was also statistically different between groups (ANOVA; $P_{<0.0125} = 0.000042$), it was significantly reduced in GLA_S and GLA_G vs controls (T-test; $P_{<0.05} = 0.012$ and $P_{<0.025} = 0.00002$, respectively; Fig. 5E).

3.4. Correlation of PhNR/b-wave ratio and PERG 0.8° amplitude to VF MD, pRNFL thickness, and age

Finally, we tested the correlation of mfPhNR/b-wave ratio with other measures of retinal ganglion cell integrity, i.e. PERG 0.8°, pRNFL and VF-MD. All correlations reached significance as detailed in Fig. 6, indicating the relation of these measures. A stepwise linear regression was conducted to identify the measure of ganglion cell integrity predicts the mfPhNR/b-wave ratio best. This analysis indicated pRNFL [$t(48) = 4$, $P = 0.0002$] as a single significant predictor for VF_{SUM} mfPhNR/b-wave ratio. Subsequently, we concentrated on the relation of glaucomatous damage by excluding controls from the correlation analysis and found only mfPhNR vs pRNFL to be significantly correlated. Finally, we applied the same analysis steps to PERG 0.8 amplitudes. Significant correlations were found with all other structural and functional measures of retinal ganglion cell integrity, i.e. mfPhNR/b-wave ratio, pRNFL and MD, which holds significant after controls' exclusion from the correlation analysis. Again, stepwise linear regression indicated pRNFL [$t(48) = 3.4$, $P = 0.001$] as a single significant predictor for PERG 0.8° amplitude.

4. Discussion

4.1. Summary of findings

We assessed the effect of stimulus timing on mfPhNR recordings for glaucoma detection and compared a set of conditions with different stimulation rates. Analyzing the mfPhNR/b-wave ratio, we found the best discrimination performance between controls and glaucoma suspects for the fastest stimulation condition, i.e., C_{Fast_1}. A spatially resolved analysis of the multifocal responses rendered the analysis of the summed responses of all visual field locations (VF_{SUM}) preferable and the central responses least effective. A subsequent detailed assessment of the diagnostic potential of VF_{SUM} mfPhNR/b-wave ratio for C_{Fast_1} revealed a similar potential as PERG and pRNFL to differentiate between Controls and both glaucoma suspects and patients with glaucoma, i.e., GLA_S and GLA_G, respectively.

4.2. Comparisons between stimulation conditions

Our comparative approach was motivated by a variety of previous mfPhNR studies on glaucoma detection, that applied using slow (by inserting around 30 frames (Rajagopalan et al., 2014)) or fast sequences (1–9 frames (Kaneko et al., 2015; Kato et al., 2015; Tanaka et al., 2020)). Our study suggests advantages of the faster stimulation protocol (i.e. mfPhNR/b-wave ratio C_{Fast_1}) in the early detection of glaucoma, as it performed better than the other conditions tested for the discrimination GLA_S from controls. Additionally, it should be noted that C_{Fast_1} is the condition with the shortest recordings time (at equal m-sequence length for all conditions), i.e. 1 min and 1 s, which bears the potential to increase signal-to-noise and possibly discriminative power further by increasing recording time.

4.3. Topographical comparisons of PhNR/b-wave ratio of C_{Fast_1}

In the present study, mfPhNR/b-wave ratio of C_{Fast_1} remained unaltered in the central area for both patients' groups (GLA_S and GLA_G), compared to a decreased response in peripheral visual field locations. Previous studies reported reduced central retinal responses and unaltered peripheral mfPhNR/b-wave ratios glaucoma (Viswanathan et al., 2001; Kaneko et al., 2015; Kato et al., 2015). Recently the mfPhNR/b-wave ratio was reported (Tanaka et al., 2020) to be significantly different in all visual field locations, i.e., both central and peripheral responses in glaucoma patients [range of perimetric damage mean deviation [dB]: -29.26–2.02]. This might be related to methodological discrepancies between the studies possibly with diverging sensitivities to different damage sites.

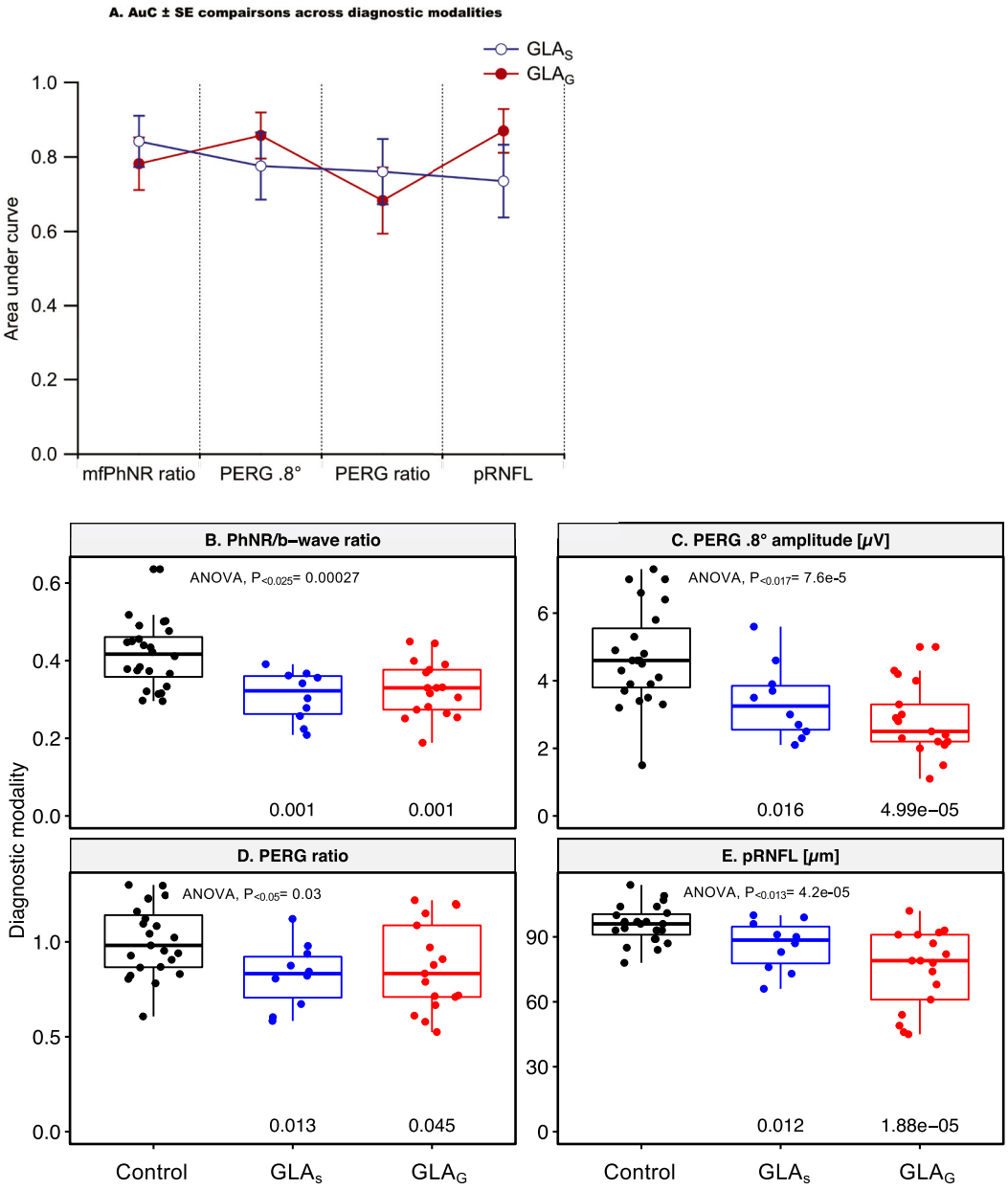

Fig. 5. A AUC ± SE comparison between diagnostic modalities [i.e., mfPhNR/b-wave ratio of fastest condition C_{Fast_1}, pattern electroretinogram (PERG) 0.8° amplitude, PERG ratio and peripapillary retinal nerve fiber layer thickness (pRNFL)] across groups. There were no significant differences of AUCs across modalities after multiple testing correction. Blue = glaucoma suspect (GLA_S), Red: Glaucoma group (GLA_G). **B-E** Comparisons of mfPhNR/b-wave ratio, PERG 0.8° amplitude, PERG ratio, and pRNFL across controls, glaucoma suspect and glaucoma group. ANOVA showed significant differences across groups (P values as indicated in the panels). Post-hoc analysis showed significant differences between control vs glaucoma suspect and control vs glaucoma (P values as indicated in the panels). Post hoc analysis corrected alpha value is 0.025 for the more significant P value in each plot. Box: 25%–75% interquartile range; horizontal line is the median value and the whiskers represent the range. Y-axis specified the diagnostic modality as indicated in the panel title.

4.4. PhNR ratio diagnostic performance

We obtained, based on the mfPhNR/b-wave ratio, similar AUCs for GLA_S and GLA_G (AUCs: 0.84 and 0.78, respectively). In our cross-modal comparison, we demonstrated similar AUCs for mfPhNR/b-wave ratio and PERG amplitude (at 0.8° checksize), pRNFL and PERG ratio for GLA_S as well as GLA_G. These AUCs correspond well to those of (Preiser et al., (2013)) employing the conventional recordings scheme. They reported AUCs for PhNR/b-wave ratios and the PERG ratio to be comparable for preperimetric (n: 11 and MD of 0.35 [dB]; AUCs: 0.80 and 0.73,

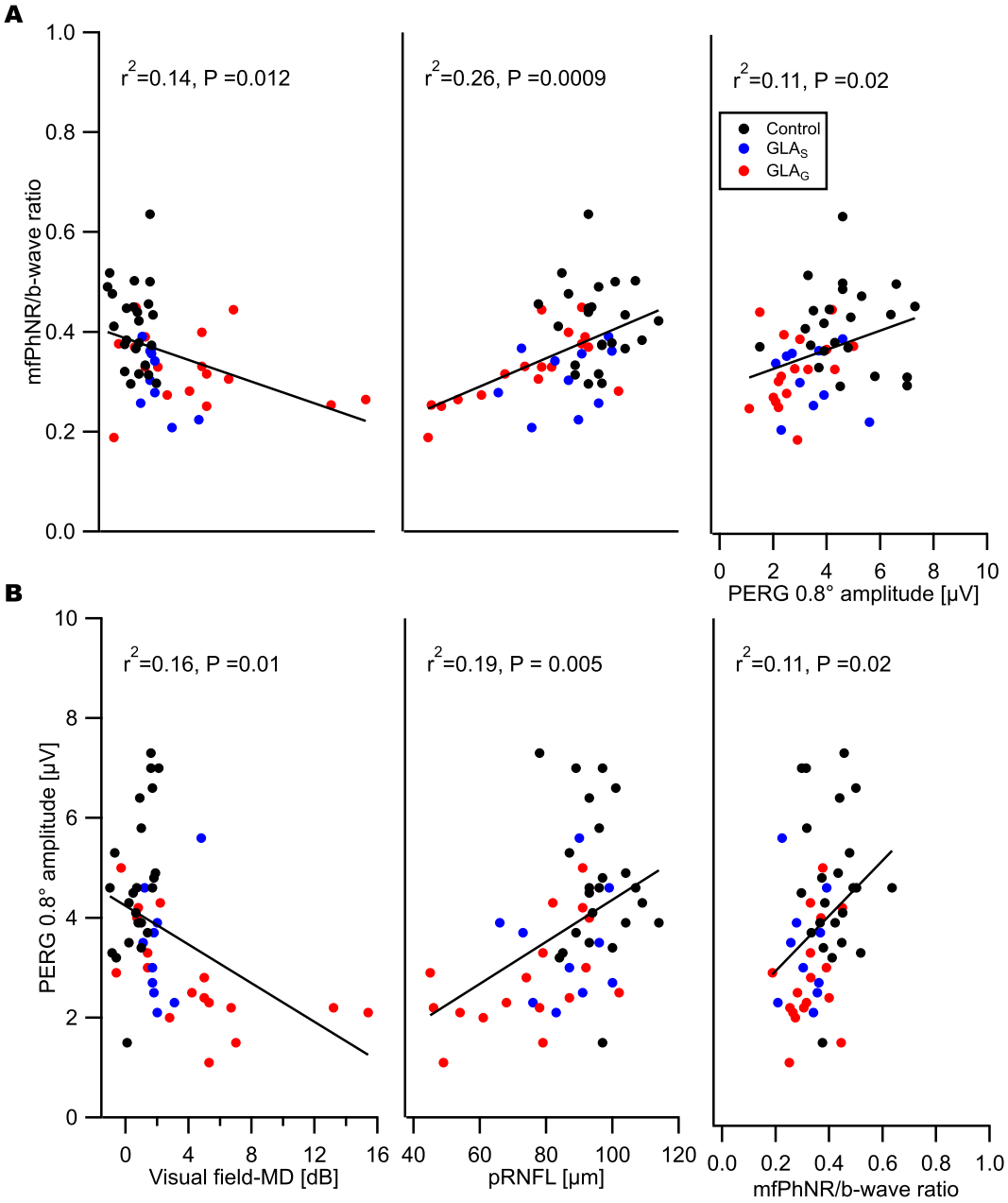

Fig. 6. **A** Correlation plots between mfPhNR/b-wave ratio fastest condition (C_{Fast_1}) and visual field mean deviation (VF-MD), peripapillary retinal nerve fiber layer thickness (pRNFL) & pattern electroretinogram (PERG) 0.8° amplitude. There were significant association between mfPhNR/b-wave ratio and the above-mentioned measures in which VF-MD, pRNFL and PERG 0.8° amplitude explained 14%, 26% and 11% of mfPhNR/b-wave ratio variance, respectively (see text). B-Correlation plots between PERG 0.8° amplitude and VF-MD, pRNFL and mfPhNR/b-wave ratio. There were significant association between PERG 0.8° amplitude and the above-mentioned measures in which VF-MD, pRNFL and mfPhNR/b-wave ratio explained 16%, 19% and 11% PERG 0.8° amplitude: variance respectively (see text).

respectively) and manifest glaucoma (n: 18 and MD of −4.48 [dB]; AUCs: 0.80 and 0.79, respectively). It must be noted, however, that caution must be exerted when comparing diagnostic methods across studies, e.g. based on AUCs, due different sample sizes and variable ranges of glaucomatous damage. Since our primary objective was to investigate which mfPhNR stimulation settings are superior for glaucoma detection, rather than multimodal AUC comparisons, we derived from our data a sample size for future studies to tackle this issue. Based on the current AUC of mfPhNR and pRNFL, the sample size giving an 80% power at a P-level of 0.05 to the AUCs' difference is 181 controls vs 78 glaucoma suspects and 338 controls vs 250 glaucoma patients (Obuchowski and McCLISH, 1997; Robin et al., 2011).

4.5. PhNR ratio association with other structural and functional measures

A correlation of PhNR and PERG measures in glaucoma has previously not been reported (Preiser et al., 2013). In our present study, we observed mfPhNR/b-wave ratios to be significantly correlated with both PERG 0.8° amplitude and PERG ratio ($r^2 = 0.11$, $P = 0.02$). Across patients' groups, however, mfPhNR/b-wave ratio and PERG showed no association implying that both measures might reflect different glaucomatous damage origins. Still, the cross-modal correlations of the electrophysiological measures with anatomical measures we observed in accordance with previous conventional PhNR studies (Machida et al., 2008; Kirkiewicz et al., 2016), PERG studies (Parisi et al., 2001; Toffoli et al., 2002; Elgohary et al., 2019) and another mfPhNR study (Kato et al., 2015). In fact, the observed pRNFL changes of this study were a predictor for both mfPhNR/b-wave ratio and PERG 0.8° amplitude.

5. Conclusion

We have shown that mfPhNR/b-wave ratio of C_{Fast_1} is superior to other stimulus frequencies in glaucoma diagnosis and might offer an additional value in GLA_s diagnosis besides structural measure (i.e. pRNFL). These findings thus serve to standardize mfPhNR recordings in future studies investigating the structure-function relationship of glaucomatous damage.

Declaration of competing interest

None.

Acknowledgements

This work was supported by European Union's Horizon 2020 research and innovation programme under the Marie Sklodowska-Curie grant agreement (No. 675033) and by funding of the German research foundation (DFG; HO2002/20–1) to MBH.

References

Al-Nosairy, K.O., van den Bosch, J.J.O.N., Pennisi, V., Mansouri, K., Thieme, H., Choritz, L., Hoffmann, M.B., 2020 Jul 29. Use of a novel telemetric sensor to study interactions of intraocular pressure and ganglion-cell function in glaucoma. Br. J. Ophthalmol. [cited 2020 Jul 30]; Available from: https://bjo.bmj.com/content/early/2020/07/29/bjophthalmol-2020-316136.

Bach, M.. Visual Evoked Potentials "EP2000" – Computer System by Michael Bach [Internet]. Available from: https://michaelbach.de/ep2000/.

Bach, M., Hoffmann, M., 2006. The origin of the pattern electroretinogram. In: Heckenlively, J.R., Arden, G.B. (Eds.), Principles and Practice of Clinical Electrophysiology of Vision, second ed. MIT Press, pp. 185–196.

Bach, M., Hoffmann, M.B., 2008 Jun. Update on the pattern electroretinogram in glaucoma. Optom. Vis. Sci. 85 (6), 386.

Bach, M., Mathieu, M., 2004 Jan 1. Different effect of dioptric defocus vs. light scatter on the Pattern Electroretinogram (PERG). Doc. Ophthalmol. 108 (1), 99–106.

Bach, M., Unsoeld, A.S., Philippin, H., Staubach, F., Maier, P., Walter, H.S., et al., 2006 Nov 1. Pattern ERG as an early glaucoma indicator in ocular hypertension: a long-term, prospective study. Invest. Ophthalmol. Vis. Sci. 47 (11), 4881–4887.

Bode, S.F.N., Jehle, T., Bach, M., 2011 Jun 1. Pattern electroretinogram in glaucoma suspects: new findings from a longitudinal study. Invest. Ophthalmol. Vis. Sci. 52 (7), 4300–4306.

Chauhan, B.C., Garway-Heath, D.F., Goñi, F.J., Rossetti, L., Bengtsson, B., Viswanathan, A.C., et al., 2008 Apr. Practical recommendations for measuring rates of visual field change in glaucoma. Br. J. Ophthalmol. 92 (4), 569–573.

Elgohary, A.M., Elbedewy, H.A., Saad, H.A., Eid, T.M., 2019 Sep 9. Pattern electroretinogram changes in patients with primary open-angle glaucoma in correlation with visual field and optical coherence tomography changes. Eur. J. Ophthalmol. 1120672119872606.

Flaxman, S.R., Bourne, R.R.A., Resnikoff, S., Ackland, P., Braithwaite, T., Cicinelli, M.V., et al., 2017 Dec 1. Global causes of blindness and distance vision impairment 1990–2020: a systematic review and meta-analysis. Lancet Glob Health 5 (12), e1221–e1234.

Hanley, J.A., McNeil, B.J., 1983 Sep. A method of comparing the areas under receiver operating characteristic curves derived from the same cases. Radiology 148 (3), 839–843.

Harwerth, R.S., Carter-Dawson, L., Smith, E.L., Barnes, G., Holt, W.F., Crawford, M.L.J., 2004 Sep 1. Neural losses correlated with visual losses in clinical perimetry. Invest. Ophthalmol. Vis. Sci. 45 (9), 3152–3160.

Holm, S., 1979. A simple sequentially rejective multiple test procedure. Scand. J. Stat. 6 (2), 65–70.

Kamei, A., Machida, S., Nagasaka, E., 2011 Apr 22. Multifocal photopic negative response (mfPhNR) and lineal visual sensitivity in patients with optic nerve lesions. Invest. Ophthalmol. Vis. Sci. 52 (14), 273–273.

Kamei, A., Nagasaka, E., 2010 Apr 17. Multifocal photopic negative response (mfPhNR) and retinal nerve fiber layer thickness (RNFLT) in patients with optic nerve lesions. Invest. Ophthalmol. Vis. Sci. 51 (13), 5473–5473.

Kamei, A., Nagasaka, E., 2014 Apr 30. Multifocal photopic negative response (mfPhNR) and ganglion cell-inner plexiform layer thickness (GCIPLT) in patients with optic nerve lesions. Invest. Ophthalmol. Vis. Sci. 55 (13), 6236–6236.

Kaneko, M., Machida, S., Hoshi, Y., Kurosaka, D., 2015 Jan 2. Alterations of photopic negative response of multifocal electroretinogram in patients with glaucoma. Curr. Eye Res. 40 (1), 77–86.

Kato, F., Miura, G., Shirato, S., Sato, E., Yamamoto, S., 2015 Dec. Correlation between N2 amplitude of multifocal ERGs and retinal sensitivity and retinal nerve fiber layer thickness in glaucomatous eyes. Doc. Ophthalmol. 131 (3), 197–206.

Kerrigan-Baumrind, L.A., Quigley, H.A., Pease, M.E., Kerrigan, D.F., Mitchell, R.S., 2000 Mar. Number of ganglion cells in glaucoma eyes compared with threshold visual field tests in the same persons. Invest. Ophthalmol. Vis. Sci. 41 (3), 741–748.

Kirkiewicz, M., Lubiński, W., Penkala, K., 2016 Feb 1. Photopic negative response of full-field electroretinography in patients with different stages of glaucomatous optic neuropathy. Doc. Ophthalmol. 132 (1), 57–65.

Machida, S., Gotoh, Y., Toba, Y., Ohtaki, A., Kaneko, M., Kurosaka, D., 2008 May 1. Correlation between photopic negative response and retinal nerve fiber layer thickness and optic disc topography in glaucomatous eyes. Investig Opthalmology Vis Sci 49 (5), 2201.

Machida, S., Kaneko, M., Kurosaka, D., 2015 Apr 3. Regional variations in correlation between photopic negative response of focal electroretinograms and ganglion cell complex in glaucoma. Curr. Eye Res. 40 (4), 439–449.

Machida, S., Tamada, K., Oikawa, T., Yokoyama, D., Kaneko, M., Kurosaka, D., 2010 Apr 17. Sensitivity and specificity of photopic negative response of focal electoretinogram to discriminate glaucomatous eyes. Invest. Ophthalmol. Vis. Sci. 51 (13), 3267–3267.

Motulsky, H.J.. GraphPad Prism 8 Statistics Guide - Comparing ROC Curves [Internet]. [cited 2020 Feb 18]. Available from: https://www.graphpad.com/guides/prism/8/statistics/stat_comparing_roc_curves.htm.

Obuchowski, N.A., McCLISH, D.K., 1997. Sample size determination for diagnostic accuracy studies involving binormal roc curve indices. Stat. Med. 16 (13), 1529–1542.

Parisi, V., Manni, G., Centofanti, M., Gandolfi, S.A., Olzi, D., Bucci, M.G., 2001 May. Correlation between optical coherence tomography, pattern electroretinogram, and visual evoked potentials in open-angle glaucoma patients. Ophthalmology 108 (5), 905–912.

Preiser, D., Lagrèze, W.A., Bach, M., Poloschek, C.M., 2013 Feb 1. Photopic negative response versus pattern electroretinogram in early glaucoma. Invest. Ophthalmol. Vis. Sci. 54 (2), 1182–1191.

Prum, B.E., Lim, M.C., Mansberger, S.L., Stein, J.D., Moroi, S.E., Gedde, S.J., et al., 2016 Jan 1. Primary open-angle glaucoma suspect preferred practice Pattern® guidelines. Ophthalmology 123 (1), P112–P151.

Prum, B.E., Rosenberg, L.F., Gedde, S.J., Mansberger, S.L., Stein, J.D., Moroi, S.E., et al., 2016 Jan. Primary open-angle glaucoma preferred practice Pattern(®) guidelines. Ophthalmology 123 (1), P41–P111.

Quigley, H.A., Dunkelberger, G.R., Green, W.R., 1989 May 1. Retinal ganglion cell atrophy correlated with automated perimetry in human eyes with glaucoma. Am. J. Ophthalmol. 107 (5), 453–464.

R Core Team, 2013. In: R: the R Project for Statistical Computing [Internet]. R: A Language and Environment for Statistical Computing. R Foundation for Statistical Computing, Vienna, Austria. Available from: https://www.r-project.org/.

Rajagopalan, L., Patel, N.B., Viswanathan, S., Harwerth, R.S., Frishman, L., 2014 Apr 30. Comparison of multifocal photopic negative response (mfPhNR) with structural and functional measures in experimental glaucoma. Invest. Ophthalmol. Vis. Sci. 55 (13), 5128–5128.

Robin, X., Turck, N., Hainard, A., Tiberti, N., Lisacek, F., Sanchez, J.-C., et al., 2011 Mar 17. pROC: an open-source package for R and S+ to analyze and compare ROC curves. BMC Bioinf. 12 (1), 77.

Sutter, E.E., 2001. Imaging visual function with the multifocal m-sequence technique. Vis. Res. 41 (10–11), 1241–1255.
Sutter, E.E., Tran, D., 1992 Mar. The field topography of ERG components in man-I. The photopic luminance response. Vis. Res. 32 (3), 433–446.
Tanaka, H., Ishida, K., Ozawa, K., Sawada, A., Mochizuki, K., Yamamoto, T., 2020. Relationship between structural and functional changes in glaucomatous eyes: a multifocal electroretinogram study [Internet]. In Review; 2020 Jan. Available from: https://www.researchsquare.com/article/c39a0970-ca9d-4cb4-864d-e04c4a860e46/v1.
Toffoli, G., Vattovani, O., Cecchini, P., Pastori, G., Rinaldi, G., Ravalico, G., 2002 Jun. Correlation between the retinal nerve fiber layer thickness and the pattern electroretinogram amplitude. Ophthalmol J Int Ophtalmol Int J Ophthalmol Z Augenheilkd 216 (3), 159–163.
Van Alstine, A.W., Viswanathan, S., 2017 Feb. Test–retest reliability of the multifocal photopic negative response. Doc. Ophthalmol. 134 (1), 25–36.
Viswanathan, S., Frishman, L.J., Robson, J.G., Harwerth, R.S., Smith, E.L., 1999 May 1. The photopic negative response of the macaque electroretinogram: reduction by experimental glaucoma. Invest. Ophthalmol. Vis. Sci. 40 (6), 1124–1136.
Viswanathan, S., Frishman, L.J., Robson, J.G., Walters, J.W., 2001 Feb. The photopic negative response of the flash electroretinogram in primary open angle glaucoma. Invest. Ophthalmol. Vis. Sci. 42 (2), 514–522.

Chapter 7

Multimodal assessment of glaucoma

This study has been published in the Translational Vision Science & Technology (TVST) Journal - Transl Vis Sci Technol. November 2020, Vol.9, 7.- and entitled "**Combined Multi-Modal Assessment of Glaucomatous Damage with Electroretinography and Optical Coherence Tomography/Angiography**" reprinted in this thesis with permission and is cited as follows:

Al-Nosairy, K. O., Prabhakaran, G. T., Pappelis, K., Thieme, H., & Hoffmann, M. B. (2020). Combined Multi-Modal Assessment of Glaucomatous Damage With Electroretinography and Optical Coherence Tomography/Angiography. Translational Vision Science & Technology, 9(12), 7–7. https://doi.org/10.1167/tvst.9.12.7

tvst

Article

Combined Multi-Modal Assessment of Glaucomatous Damage With Electroretinography and Optical Coherence Tomography/Angiography

Khaldoon O. Al-Nosairy[1], Gokulraj T. Prabhakaran[1], Konstantinos Pappelis[2], Hagen Thieme[1], and Michael B. Hoffmann[1,3]

[1] Department of Ophthalmology, Otto-von-Guericke University, Magdeburg, Germany
[2] Department of Ophthalmology, University of Groningen, University Medical Center, Groningen, The Netherlands
[3] Center for Behavioral Brain Sciences, Magdeburg, Germany

Correspondence: Michael B. Hoffmann, Department of Ophthalmology, Otto-von-Guericke University, Magdeburg, Germany.
e-mail: michael.hoffmann@med.ovgu.de

Received: June 19, 2020
Accepted: August 30, 2020
Published: November 2, 2020

Keywords: glaucoma; multifocal photopic negative response; pattern electroretinogram; OCT-angiography; vessel density

Citation: Al-Nosairy KO, Prabhakaran GT, Pappelis K, Thieme H, Hoffmann MB. Combined multi-modal assessment of glaucomatous damage with electroretinography and optical coherence tomography/angiography. Trans Vis Sci Tech. 2020;9(12):7, https://doi.org/10.1167/tvst.9.12.7

Purpose: To compare the diagnostic performance and to evaluate the interrelationship of electroretinographical and structural and vascular measures in glaucoma.

Methods: For 14 eyes of 14 healthy controls and 15 eyes of 12 patients with glaucoma ranging from preperimetric to advanced stages optical coherence tomography (OCT), OCT-angiography (OCT-A), and electrophysiological measures (multifocal photopic negative response ratio [mfPhNR] and steady-state pattern electroretinography [ssPERG]) were applied to assess changes in retinal structure, microvasculature, and function, respectively. The diagnostic performance was assessed via area-under-curve (AUC) measures obtained from receiver operating characteristics analyses. The interrelation of the different measures was assessed with correlation analyses.

Results: The mfPhNR, ssPERG amplitude, parafoveal (pfVD) and peripapillary vessel density (pVD), macular ganglion cell inner plexiform layer thickness (mGCIPL) and peripapillary retinal nerve fiber layer thickness (pRNFL) were significantly reduced in glaucoma. The AUC for mfPhNR was highest among diagnostic modalities (AUC: 0.88, 95% confidence interval: 0.75–1.0, $P < 0.001$), albeit not statistically different from that for macular (mGCIPL: 0.76, 0.58–0.94, $P < 0.05$; pfVD: 0.81, 0.65–0.97, $P < 0.01$) or peripapillary imaging (pRNFL: 0.85, 0.70–1.0, $P < 0.01$; pVD: 0.82, 0.68–0.97, $P < 0.01$). Combined functional/vascular measures yielded the highest AUC (mfPhNR-pfVD: 0.94, 0.85–1.0, $P < 0.001$). The functional/structural measure correlation (mfPhNR-mGCIPL correlation coefficient [r_s]: 0.58, $P = 0.001$; mfPhNR-pRNFL r_s: 0.66, $P < 0.001$) was stronger than the functional-vascular correlation (mfPhNR-pfVD r_s: 0.29, $P = 0.13$; mfPhNR-pVD r_s: 0.54, $P = 0.003$).

Conclusions: The combination of ERG measures and OCT-A improved diagnostic performance and enhanced understanding of pathophysiology in glaucoma.

Translational Relevance: Multimodal assessment of glaucoma damage improves diagnostics and monitoring of disease progression.

Introduction

Glaucoma is a progressive optic neuropathy characterized by the loss of retinal ganglion cells (RGCs) and eventually visual field (VF) defects.[1] Damage to RGCs is attributed to an increase in intraocular pressure (IOP) (mechanical theory) or primary vascular dysfunction (vascular theory).[2–5] Elevated IOP is an important risk factor for the development of primary open angle glaucoma (POAG),[6] the most prevalent glaucoma type,[7] although vascular dysfunction might be particularly critical for normal tension glaucoma (NTG).[2] However, vascular changes were also proposed for POAG.[8–10] Surrogate measures in clinical practice to estimate glaucomatous damage are

macular ganglion cell inner plexiform layer (mGCIPL) and peripapillary retinal nerve fiber layer (pRNFL) thickness measures obtained via optical coherence tomography (OCT)[11–13]; however, conventional structural OCT assessment does not enable the quantification of vascular changes in glaucoma.[14] Using the OCT platform for three-dimensional angiography allows for optical coherence tomography angiography (OCT-A), a recent innovation in imaging technology. In fact, OCT-A has opened the possibility of noninvasive evaluations of retina and optic nerve vasculature in glaucoma[15–19] to further our understanding of the underlying pathophysiology and to improve glaucoma detection. Vessel density parameters of macular and peripapillary areas measured with OCT-A have a similar diagnostic performance as retinal thickness measures obtained with conventional OCT (A review[20]). In fact, vessel density measures of OCT-A were strongly correlated with both structural OCT measures and functional indexes (standard automated perimetry).[20]

Although it is well known that OCT-A correlates with visual field measures,[21–23] there is limited information of OCT-A measures correlation with direct measures of retinal ganglion cell function. This gap can be filled by combining OCT-A parameters with electroretinographic (ERG) measures. Two ERG-based approaches provide sensitive information about the pathophysiology of glaucoma damage,[24] i.e. pattern ERG (PERG) and photopic negative responses (PhNR). They are therefore of paramount importance for the objective assessment of retinal function in glaucoma. The PERG is an established method with promising outcomes for glaucoma diagnosis.[25,26] The PhNR is a more recent development to quantify glaucomatous damage,[26–28] which has been applied in a conventional manner and in combination with the multifocal stimulation technique[29], that is, multifocal photopic negative response ratio (mfPhNR).[30–32]

Taken together, a combined approach of structural, vascular and functional assessment of glaucomatous retinal damage employing OCT, OCT-A and PERG/mfPhNR is of great promise to uncover the interrelationship between the different components of ocular damage in glaucoma and to shed light on the underlying patho-mechanisms. A recent study[33] demonstrated that in NTG the PhNR amplitude was correlated with macular vessel density and concluded that vascular changes might precede structural measures in early NTG. We aimed to assess such relationships for POAG. For this purpose, we correlated two types of ERG methods (PERG and mfPhNR) vs structural (OCT based) and vascular (OCT-A based) changes of macular and peripapillary areas. This multimodal approach opens a window to assess how these structural, vascular and functional measures of retinal damage are linked to peripapillary and macular damage sites, and to each other. The aim of the present study was twofold: (i) to compare the diagnostic performance of individual measures and of combined measures of ERG and structural or vascular parameters and (ii) to elucidate the interrelation of ERG measures of retinal ganglion cell function with structural and vascular parameters and their association with macular and peripapillary sites.

Methods

Participants

Twelve glaucoma patients and 14 age-matched healthy controls were included in this observational study after giving written consent to participate in the study. The procedures followed the tenets of the declaration of Helsinki, and the protocol was approved of by the ethical committee of the Otto-von-Guericke University of Magdeburg, Germany. The study was performed in the ophthalmological department of the Otto-von-Guericke University Hospital, Magdeburg. ERG data of the study participants were acquired as part of another study.[34] In two sessions, all participants underwent best corrected visual acuity testing (BCVA) for far and near, visual field testing, OCT/-A measurements, and an ophthalmic examination.

Healthy Controls

Fourteen eyes of 14 subjects (mean age ± standard deviation [SD]: 50.2 years, 14.3) with BCVA $\geq$ 1 were included in the study.

Glaucoma-Group

Fifteen eyes of 12 patients (mean age ± SD: 56.8 years, 14.5; no age difference to control group [$P = 0.26$; t-test]), with open angle glaucoma were enrolled in this study. The group comprised seven preperimetric and eight perimetric glaucomatous eyes. The seven preperimetric glaucoma patients with an open anterior chamber had a glaucomatous optic disc damage defined via a vertical cup-to-disc ratio $\geq$ 0.7, a retinal fiber layer defect, or a local notching of the rim. The eight perimetric glaucoma eyes had glaucomatous visual field defects manifested as a cluster of three or more non-edge points all depressed on the pattern deviation plot <5% and one of which depressed <1% or abnormal corrected pattern standard deviation <5% on the Humphrey Swedish interactive threshold algorithm 24-2 (SITA fast).[35] According to the

selection criteria for the glaucoma patients' eyes (see above), incidentally only their left eyes (with three exceptions where both eyes had different stages of glaucoma damage) were included and, consequently, compared to the left eyes of the controls. An additional analysis including only the left eyes of the 12 glaucoma patients, to assess confounds of interocular correlations, yielded highly comparable results (Supplementary Tables S2 and S3).

Exclusion criteria were any systemic diseases, ocular diseases or surgeries that might affect electrophysiological recordings except cataract surgery and, in the glaucoma group, glaucoma surgery or BCVA < 0.8[36] and refractive error exceeding ± 5 D or astigmatism >2 D. Insufficient quality of OCT images was also an exclusion criteria. An overview of participants' characteristics is given in Supplementary Table S1.

Visual Field Testing

Visual field sensitivities were assessed using the Swedish Interactive Threshold Algorithm 24-2 protocol (SITA-Fast) of the Humphrey Field Analyzer 3 (Carl Zeiss Meditec AG, Jena, Germany). In one control subject, visual field was tested with Octopus perimeter (dG2; dynamic strategy; Goldmann size III; OCTOPUS Perimeter 101, Haag-Streit International, Bern, Switzerland).

OCT Angiography Acquisition and Image Analysis

OCT images were acquired using the Spectralis HRA+OCT (Heidelberg Engineering, Heidelberg, Germany) equipped with the Angiography, the Glaucoma, and the Flex Module. Both eyes were scanned for macula and disc scans. OCT structural measures and angiographical images were then exported for further analysis.

Structural Measures

Averaged macular retinal nerve fiber layer thickness and ganglion cell inner plexiform layer thickness were assessed inside the 3 mm (pfRNFL and pfGCIPL, respectively) and 6 mm (mRNFL and mGCIPL, respectively) rings of ETDRS scan and exported for further analysis (Figs. 1I, 1J). The averaged peripapillary retinal nerve fiber layer thickness (pRNFL) was calculated within a 3.4 mm circle around the disc. Global indexes of macula and peripapillary structure measures, that is, mGCIPL and pRNFL thickness, respectively, were compared to other parameters.

Angiographical Measures

Spectralis OCT-A enables distinctive mapping of three vascular layers of the retina, superficial vascular plexus (SVP), intermediate capillary plexus (ICP), and deep capillary plexus (DCP).[37] We focused our analysis on the SVP layer that nourishes macular GCLIPL (mGCIPL) and peripapillary superficial vascular complex (SVC) layer, which includes the peripapillary radial capillaries supplying the pRNFL.[38,39] OCT-A images were exported in the form of transverse analysis from the Heidelberg Engineering interface. High-speed scans (20°) were used, and 768 × 768 pixel images were used. SVP (Fig. 1A), ICP, and DCP of parafovea were evaluated. Each layer was analyzed separately with a MATLAB- script[40] described below. Only the SVC of the peripapillary perfusion area was evaluated with the current script (Fig. 1D).

With the MATLAB-based script[40] used for analysis, images were imported, and one region of interest (ROI) (see below) was defined after determining the center of macula and disc for macular and disc perfusion quantification by the same investigator, respectively. SVP, ICP, and DCP were calculated automatically once the ROI center was determined manually by the investigator. Binary images of macula and optic disc were generated, and each vessel pixel and tissue pixel were represented as white and black, respectively. A local Otsu threshold[41] to binarize an image was applied to flow and no-flow signals. The ROI of the macula was a circle with 3 mm diameter centered on the macula (Figs. 1 B, 1C) and the ROI around the optic disc was a ring shaped with inner and outer radii of 1.03 and 1.84 mm (Figs. 1E, 1F). The big blood vessels of the optic nerve head (ONH) images were masked out with a Frangi vesselness filter using eigenvectors of the Hessian filter response of image[42] (Figs. 1G, 1H). To assess the reproducibility of the applied script, repeated analysis of the same OCT-A images were compared between the OCT-A data of the study population. Pairwise comparisons did not identify significant differences between the 2 iterations of image processing ($P > 0.05$). Intraclass correlations between both data sets of SVP, ICP and DCP and SVC showed excellent agreement of all measures (95% confidence interval [CI] of ICC: 0.99–1.0, $P < 0.001$).

The following parameters were evaluated: (1) Fractal dimension (FD): FD is an index of the branching complexity of the capillary network and ranges from 1 to 2, with a higher FD indicating a greater vessel branching pattern. FD was calculated based on a box-counting technique where the image is subdivided into square boxes of equal sizes and the number of boxes covering a vessel segment is counted. This was repeated for different box sizes. The logarithmized box

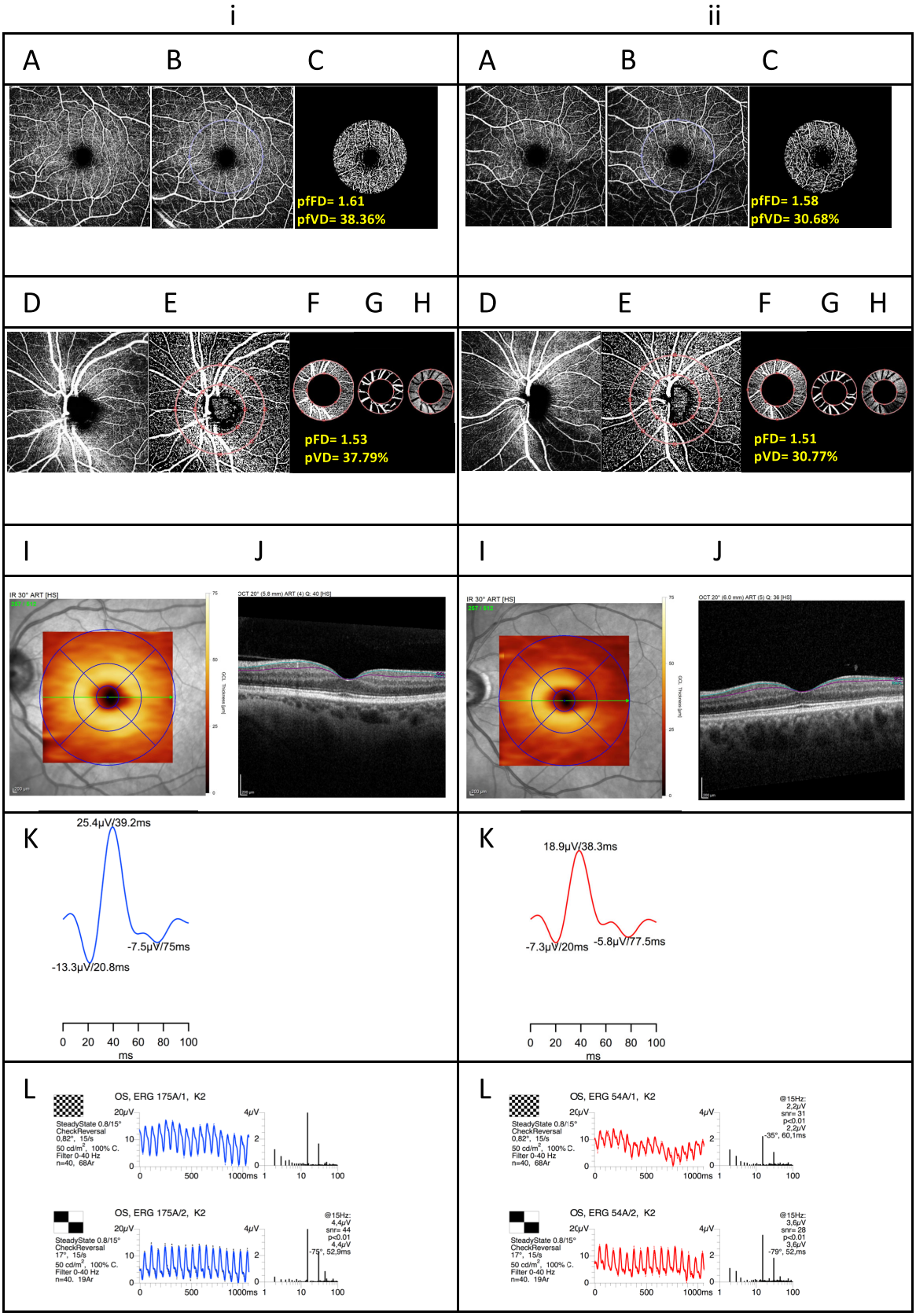

Figure 1. (**A**) OCT angiography image of the parafovea analyzing superficial vascular plexus (SVP) of (i) a representative control's and (ii) a glaucoma participant's left eye. In (**B**, **C**) offline postprocessed images (see text for details) are depicted, where (**B**) the ROI is delineated and (**C**) the ROI is used for subsequent analyses. (**D**) OCT-A of the peripapillary area extracting the superficial vascular complex. In (**E**, **F**) →

←
offline processed images are depicted, where (**E**) is an image of the disc with delineation of ROI, (**F**) ROI of disc selected, (**G**) exclusion of big vessels from the analyzed area (**H**). In (**I**) the ETDRS scans of the macula are depicted, with a visualization of the 1, 3, 6 mm circles used for the analyses. In (**J**) a macular OCT image is shown with the ganglion cell layer embraced between the lines. (**K**) Summed mfPhNR trace with the first negativity, i.e., a wave, the first positivity, i.e., b wave, and the second negativity, i.e., the mfPhNR component. (**L**) ssPERG to 0.8 check size (*upper panel*) and 15° check size stimuli (*lower panel*) together with the frequency plot with the dominant response at the stimulation frequency, i.e., 15 Hz, and the corresponding *P* values of each response.

number was plotted vs logarithmized box size, where the FD equals the slope of the regression line.[43,44] (2) Vessel density (VD) [%]: VD is the percentage of the area occupied by capillaries. The peripapillary parameters of FD and VD were denoted as pFD and pVD to differentiate them from parafovea pfFD and pfVD parameters. In the literature, the most frequently reported measure of microvasculature in glaucoma is VD. Consequently, we focused on VD in Discussion, specifically because we obtained similar findings for FD and VD.

Visual Stimuli, Procedure, and Recordings of mfPhNR and Steady-State Pattern ERG (ssPERG)

mfPhNR

For mfPhNR recording, VERIS Science 6.4.9d13 (EDI; Electro-Diagnostic Imaging, Redwood City, CA, USA) was used for stimulus delivery and electrophysiological recordings. The stimulus comprised five visual field locations covering 48° of visual field with central and four quadrants (0°–5° and 5°–48°, respectively). A binary m-sequence of 0 (no flash) and 1 (flash) states was used for stimulation with a length of 2^9-1 steps and 9 frames (frequency of stimulation: 4.2 Hz). Each step lasted 13.3 ms resulting in total recording time of 61 seconds. Two mfPhNR blocks were recorded and averaged. A monochrome CRT monitor (MDG403, Philips; P45 phosphor) was used for the stimulus presentation at 75 Hz frame rate, and the measurements were inspected in real-time on a separate monitor. In accordance with previous studies, mfPhNR were normalized to b-wave amplitude, both measured from the baseline, defined as the initial 10 ms of the epoch. The resulting mfPhNR ratio was compared between groups. We reported only the mfPhNR ratio of the summed response of five visual field locations (Fig. 1K), as a previous investigation did not reveal benefits from a spatially resolved analysis for mfPhNR-based glaucoma diagnostics.[34] The multifocal approach has the benefit to offer higher stimulation rates than conventional stimulation. Because in the present investigation we compare the ERG responses to global structural and vascular measures, we decided beforehand to report the mfPhNR ratio of the summed response across visual field locations.

ssPERG

The EP2000 evoked potential system was used for stimulation, recording and analysis of ssPERGs[45] following the PERG-standard of the international society for clinical electrophysiology of vision.[46] The stimuli were presented at a frame rate of 75 Hz on a monochrome monitor (MDG403; Philips, Amsterdam, the Netherlands; P45 phosphor) subtending a visual angle of 62° × 49°. A 15 Hz checkerboard pattern stimulus with two check sizes (0.8° and 15°) was used for stimulation (Fig. 1L). Following established procedures,[47] the PERG ratio is calculated as an amplitude ratio of check sizes 0.8° to 15°.

In separate sessions, mfPhNR and ssPERG were recorded binocularly using active DTL (Dawson, trick Litzkow 1979, Thompson, Drasdo, 1987) electrodes (DTL Electrode ERG; Unimed Electrode Supplies, Ltd, Farnham, UK). The pupils were dilated only for the mfPhNR recordings. Further details on the procedure and recording, analysis of mfPhNR and ssPERG are given in references 26, 34, and 48.

Statistics

The mfPhNR ratio (mfPhNR) and ssPERG 0.8° amplitude (ssPERG) were calculated using IGOR (IGOR Pro; WaveMetrics, Portland, OR, USA) and exported to SPSS 26 (Statistical Package for the Social Sciences; IBM, Armonk, NY, USA), and R statistical system[49] for further analysis. The normality of the data was checked by applying the Shapiro-Walk test. Either *t*-tests or Mann-Whitney tests were conducted for cross-modal comparisons between groups, and effect sizes of these tests were also reported as a d value and U [%], which represented the probability percentage of non-overlap between two distributions.[50] Correlations between measures were calculated using Spearman's coefficient (r_s) and the 95% CI of the coefficient was calculated using a bootstrapping method. The variances explained by the correlations (r_s^2) were also calculated and reported. Receiver operating characteristics analyses were conducted

using SPSS to calculate area under curve (AUC) to discriminate between controls and glaucoma. Pairwise comparisons of all measures' AUCs were assessed to check for any significant difference between them.[51] P values were corrected for multiple testing with adjusted α-levels (P_α) using the Bonferroni-Holm correction[52] where applicable. To verify the reproducibility of the applied MATLAB analysis script, intraclass correlation of analyses between two sets of repeated analysis of the same OCT-A images and 95% CI were calculated based on absolute-agreement and two-way mixed-effects model.[53] MATLAB R2019b (MathWorks, Natick, MA, USA) was used for OCT-A image processing.

Results

Functional and Structural Parameters versus Electrophysiological and Vascular Measures

Electrophysiology

The electrophysiological measures of retinal ganglion cell function showed differential responses between the groups. The mfPhNR ratio was significantly different in glaucoma and the difference between the groups represented 75% of the nonoverlapping distribution (d = 1.7, $P_{\leq 0.025} = 0.0002$). Similarly, the difference between healthy and glaucoma ssPERG amplitudes was statistically significant (d = 1.1, $P_{\leq 0.05}$=0.006), for effect sizes see Figures 2A and 2B.

Perimetry

On average, functional measures of glaucoma in terms of VF-MD and pattern standard deviation were statistically different between the study groups (d = 2.3, $P_{\leq 0.025} < 0.0001$ and d = 1.3, $P_{\leq 0.05} = 0.004$, respectively; see Table 1).

OCT

pRNFL thickness were significantly lower in glaucoma patients with a substantial effect size of 1.8 ($P_{\leq 0.025} = 0.001$) (Figs. 2C, 2D). The mRNFL thickness was not statistically different between the groups (P > 0.05). In contrast, mGCIPL thickness was significantly lower in glaucoma (d = 1.4, $P_{\leq 0.05} = 0.009$; see Table 1).

OCT-Angiography

In terms of vascular estimates for the parafoveal ROI, we were particularly interested in the inner retinal layer supplied by parafoveal SVP and peripapillary SVC (for effect sizes see Figs. 2E, 2H). Parafoveal FD (pfFD) (d = 1.3, $P_{\leq 0.025} = 0.0037$) and parafoveal VD (pfVD) (d = 1.1, $P_{\leq 0.05} = 0.008$) were significantly reduced in glaucoma. For the peripapillary ROI perfused by SVC, pFD showed a significant decrease (d = 1.7, $P_{\leq 0.025} = 0.0016$), as well as pVD (d = 1.5, $P_{\leq 0.05} = 0.0019$) in glaucoma patients. It is notable that both ICP and DCP showed significant pfFD and pfVD reductions in glaucoma ($P < 0.01$) compared to controls (Table 1).

Discriminatory Performance of ERG, Structural Parameters, and Vascular Parameters

In terms of the discriminatory performance between controls and glaucoma, we applied receiver operating characteristics (ROC)-analyses to compare ERG measures of RGC-function (mfPhNR ratio, ssPERG amplitude), established structural (i.e., mGCLIPL thickness, pRNFL thickness) and vascular measures of parafoveal and peripapillary areas (pfFD and pfVD as well as pFD and pVD). With respect to the ERG measures of RGC-function, there was a non-significant trend for higher AUC (AUC, 95% CI, P value) for the mfPhNR ratio (0.88, 0.75–1.0, $P_{\leq 0.025} < 0.001$) than for the ssPERG amplitude (0.81, 0.64-0.99, $P_{\leq 0.05} = 0.004$). Therefore our further analyses were focused on the mfPhNR ratio. With respect to the structural assessment, there was a nonsignificant trend for higher AUC for pRNFL (0.85, 0.70–1.0, $P_{\leq 0.025} = 0.001$) than for mGCIPL (0.76, 0.58–0.94, $P_{\leq 0.05} = 0.018$). AUCs for vascular parameters were calculated for pfFD (0.82, 0.66–0.98, $P_{\leq 0.025} = 0.0037$) and for pfVD (0.81, 0.65-0.97, $P_{\leq 0.05} = 0.005$) compared to pFD (0.86, 0.72–0.99, $P_{<0.025} = 0.001$) and pVD (0.82, 0.68–0.97, $P_{\leq 0.05} = 0.003$; see Fig. 3). Finally, by conducting pairwise comparisons of ERG measures of RGC-function, structural and vascular AUCs, we found no significant differences ($P > 0.05$) between these measures, indicating a similar and complementary performance in terms of differentiating glaucoma from controls. By testing the combined approach to identify the highest discriminatory performance, mfPhNR-pfVD had the highest AUC for the differentiation between glaucoma and controls (AUC: 0.94; $P < 0.001$).

Association between ERG, Structural Parameters and Vascular Parameters

To elucidate associations between functional and other metrics, we investigated the correlation between vascular estimates of inner layers macula and peripapillary zones versus other structural and ERG

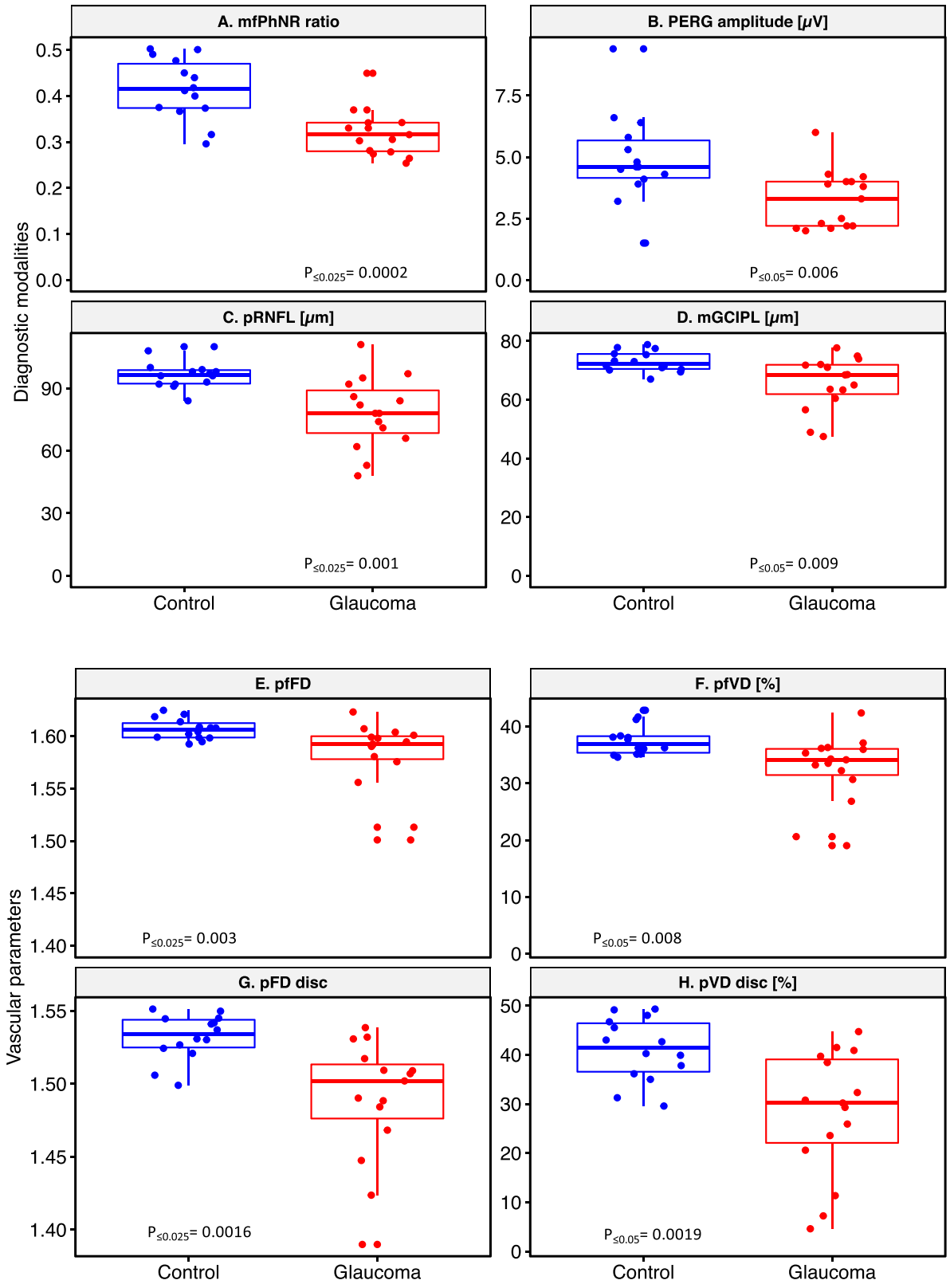

Figure 2. Cross-modal comparison of diagnostic performance. (**A**) The mfPhNR, (**B**) PERG amplitude for 0.8° check size, (**C**) averaged peripapillary retinal nerve fiber layer thickness in micrometer, and (**D**) averaged mGCIPL in micrometers. Vascular metrics of (**E**) pfFD and (**F**) pfVD. Vascular metrics of (**G**) pFD and (**H**) pVD. Independent *t*-tests were conducted except for parafoveal FD where Mann-Whitney test was performed (alpha-thresholds corrected for multiple comparisons are shown as subscripts). Panel title specifies the y-axis for each plot.

Table 1. Measures Differences Between Normal and Glaucoma Participants

Measure	Category		N	Mean	SD	t(24)	M.Diff.	d	U	P[a]
Functional	MD	C	14	0.01[b]	1.48[b]	4.06[c]	2.02	2.3	85	<0.0001[c]
		G	15	−2.03[b]	4.06[b]					
	PSD	C	14	1.36[b]	0.25[b]	−2.88[c]	−0.66	1.3	65	0.004[c]
		G	15	2.02[b]	9.49[b]					
	mfPhNR	C	14	0.42	0.07	4.37	0.10	1.7	75	0.0002
		G	15	0.32	0.05					
	PERG 0.8°	C	14	4.93	1.82	2.95	1.67	1.1	59	0.006
		G	15	3.26	1.17					
	PERG ratio	C	14	1.04	0.17	2.18	0.17	0.8	47	0.038
		G	15	0.87	0.24					
Structural	pRNFL	C	14	96.71	6.66	3.86	18.25	1.8	77	0.001
		G	15	78.47	16.98					
	pfGCIPL	C	14	79.94	4.67	2.46	7.52	1.1	59	0.023
		G	15	72.43	10.80					
	mGCIPL	C	14	72.99	3.53	2.94	7.43	1.4	68	0.009
		G	15	65.56	9.07					
	pfRNFL	C	14	19.01	1.11	−0.11	−0.07	0.04	3	0.91
		G	15	19.08	1.98					
	mRNFL	C	14	25.08	1.71	1.07	1.10	0.5	33	0.30
		G	15	23.98	3.56					
Vascular	SVP pfFD	C	14	1.61[b]	0.02[b]	2.9[c]	0.03	1.3	65	0.0037[c]
		G	15	1.58[b]	0.03[b]					
	SVP pfVD	C	14	37.60	2.68	2.84	5.08	1.1	59	0.008
		G	15	32.52	6.17					
	ICP pfFD	C	14	1.58[b]	0.01[b]	3.1[c]	0.01	1.4	68	0.0016[c]
		G	15	1.57[b]	0.01[b]					
	ICP pfVD	C	14	29.48	1.93	2.84	2.97	1.1	59	0.009
		G	15	26.50	3.45					
	DCP pfFD	C	14	1.59	0.01	3.20	0.02	1.2	62	0.0034
		G	15	1.57	0.02					
	DCP pfVD	C	14	31.14	2.55	3.22	3.50	1.2	62	0.0033
		G	15	27.64	3.23					
	SVC pFD	C	14	1.53	0.02	3.70	0.04	1.7	75	0.0016
		G	15	1.49	0.04					
	SVC pVD	C	14	41.01	6.46	3.51	12.95	1.5	71	0.0019
		G	15	28.06	12.65					

P values not corrected for multiple testing due to explorative nature. C, control participants; G, glaucoma participants; d, effect size with U[%]: probability percentage of non-overlap between the two distributions; MD [dB]: mean deviation; PSD [dB], pattern standard deviation; m/pfGCIPL[µm], averaged macular/parafoveal thickness of ganglion cell layer and inner plexiform layer within 6/3 mm ETDRS scans; m/pfRNFL [µm], averaged macular/parafoveal retinal nerve fiber layer thickness within 6/3 mm ETDRS scans; PERG 0.8° [µV], steady-state pattern electroretinogram of 0.8° check size amplitude [µV]; pf/pFD, parafoveal/peripapillary fractal dimension; pf/pVD, parafoveal/peripapillary vessel density [%]; M.Diff., mean difference; n, number of eyes.

[a]T-test *P* value.

[b]Median and interquartile range.

[c]Mann-Whitney test z and *P* values.

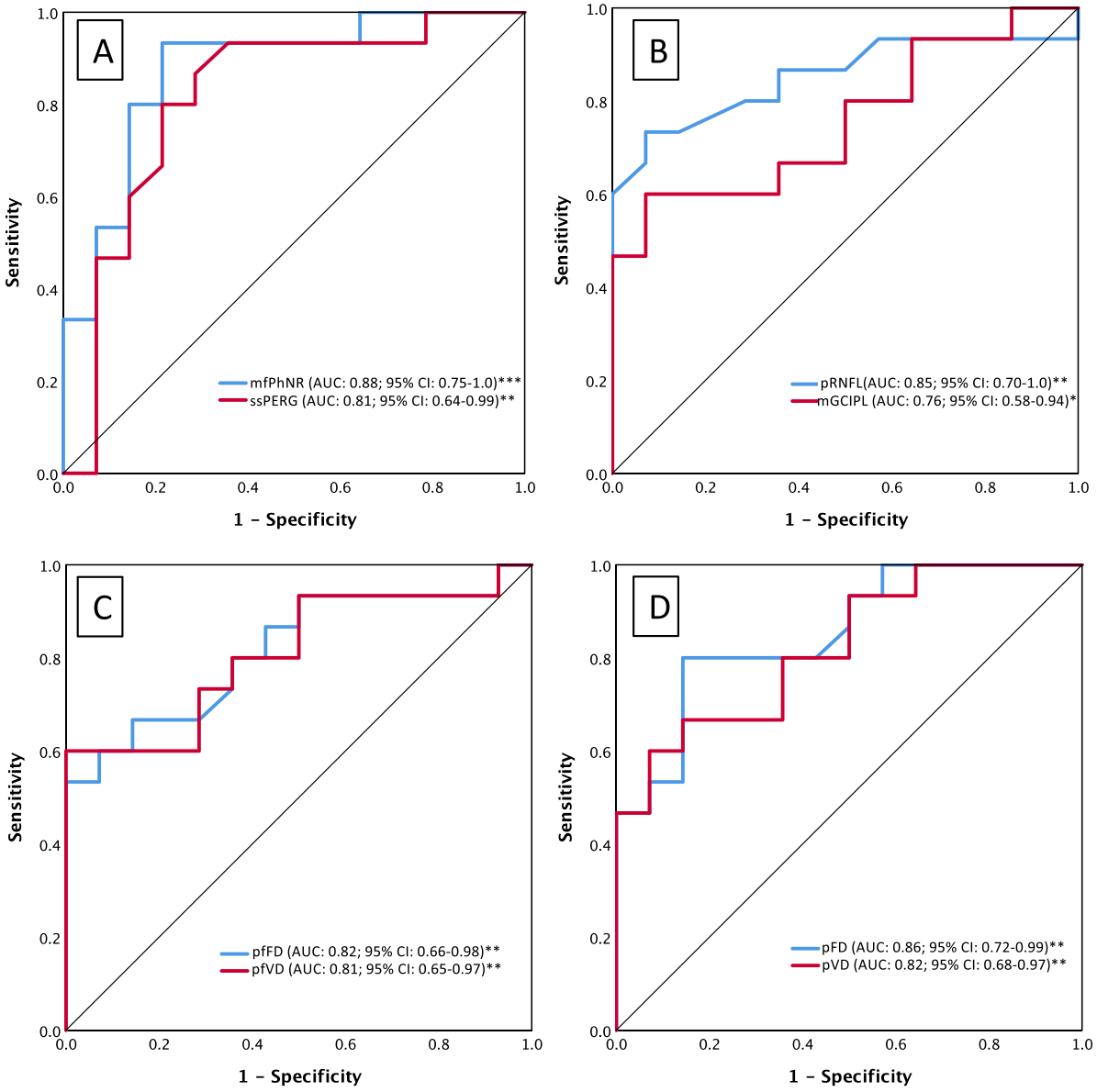

Figure 3. AUC of ROC and AUC 95% CI. (**A**) Electrophysiological parameters, mfPhNR and pattern electroretinogram 0.8° amplitude (ssPERG). (**B**) Structural measures of pRNFL and mGCIPL. (**C**, **D**) vascular metrics of parafovea, which are (**C**) pfFD and pfVD versus peripapillary vascular metrics which are (**D**) pFD and pVD. *P* value significance levels are indicated where * indicates $P \leq 0.05$, ** indicates $P < 0.01$, and *** indicates $P < 0.001$ where the null hypothesis is that true area = 0.5.

measures of RGC-function. Both pfFD and pfVD were strongly correlated with pf/mGCLIPL thickness ($P \leq 0.001$; Table 2). Similarly vascular estimates of peripapillary perfusion showed a strong significant association with pRNFL thickness ($P \leq 0.001$). Our ERG measure of RGC-function, the mfPhNR ratio, was strongly correlated with all structural macula and peripapillary disc parameters as well as visual field-MD ($P \leq 0.001$). ssPERG amplitude was also significantly correlated to pRNFL, mGCIPL and VF-MD ($P = 0.003$, 0.027, and 0.003, respectively), but not to pfGCIPL ($P = 0.09$). Out of the vascular measures, the mfPhNR ratio and the ssPERG amplitude were significantly correlated only with pFD and pVD ($P < 0.01$; see Table 2 and Fig. 4). The exclusion of the two extreme data points of the correlation plots left the results essentially unchanged.

To further elucidate glaucomatous damage mechanisms, we investigated the association between ERG-based functional indexes with anatomical indexes at damage sites. ERG-based functional measures at the peripapillary site (i.e., mfPhNR-pRNFL r_s: 0.66,

Table 2. Correlations Between Functional, Structural, and Vascular Parameters

				Functional			Structural			Vascular			
Spearman's rho				PhNR	PERG	MD	pRNFL	pfGCIPL	mGCIPL	pfFD	pfVD	pFD	pVD
Functional	PERG	r		0.60[a]	1								
		P		0.001									
		B[b] 95% CI	L	0.34									
			U	0.78									
	MD	r		0.76[a]	0.53[a]	1							
		P		< .001	0.003								
		B[b] 95% CI	L	0.53	0.19								
			U	0.89	0.80								
Structural	pRNFL	r		0.66[a]	0.53	0.62[a]	1						
		P		<0.001	0.003	<0.001							
		B[b] 95% CI	L	0.26	0.20	0.27							
			U	0.90	0.78	0.87							
	pfGCIPL	r		0.58[a]	0.32	0.48[a]	0.56[a]	1					
		P		0.001	0.09	0.008	0.002						
		B[b] 95% CI	L	0.29	−0.05	0.07	0.23						
			U	0.77	0.66	0.79	0.78						
	mGCIPL	r		0.58[a]	0.41[c]	0.51[a]	0.73[a]	0.93[a]	1				
		P		0.001	0.027	0.005	<0.001	<0.001					
		B[b] 95% CI	L	0.28	0.06	0.13	0.49	0.84					
			U	0.79	0.70	0.81	0.86	0.97					
Vascular	pfFD	r		0.34	0.24	0.52[a]	0.30	0. 57[a]	0.57[a]	1			
		P		0.07	0.20	<0.001	0.12	0.001	0.001				
		B[b] 95% CI	L	0.001	−0.17	0.17	−0.11	0.27	0.25				
			U	0.62	0.58	0.76	0.64	0.76	0.78				
	pfVD	r		0.29	0.21	0.52[a]	0.29	0.56[a]	0.57[a]	0.99[a]	1		
		P		0.13	0.27	0.004	0.12	0.001	0.001	<0.001			
		B[b] 95% CI	L	−0.05	−0.18	0.20	−0.12	0.25	0.25	0.98			
			U	0.58	0.55	0.74	0.63	0.76	0.80	1.0			
	pFD	r		0.56[a]	0.52[a]	0.54[a]	0.80[a]	0.49[a]	0.65[a]	0.39[c]	0.37[c]	1	
		P		0.002	0.004	0.002	<0.001	0.007	< 0.001	0.037	0.046		
		B[b] 95% CI	L	0.19	0.19	0.18	0.60	0.12	0.33	0.04	0.02		
			U	0.82	0.75	0.79	0.92	0.76	0.86	0.067	0.65		
	pVD	R		0.54[a]	0.49[a]	0.48[a]	0.79[a]	0.45[c]	0.64[a]	0.35	0.34	0.99[a]	1
		P		0.003	0.007	0.008	<0.001	0.014	<0.001	0.07	0.07	<0.001	
		B[b] 95% CI	L	0.14	0.19	0.08	0.57	0.06	0.34	−0.07	−0.07	0.98	
			U	0.82	0.74	0.78	0.93	0.73	0.84	0.66	0.65	1.0	

Included eyes: 14 eyes of 14 control subjects and 15 eyes (12 left/3 right eyes) of 12 glaucoma subjects. Peripapillary measures: Blue font; macular/parafoveal measures: green fonts. Conventions as Table 1. U, upper limit of 95% CI; L, lower limit of 95% CI.

[a]Correlation is significant at the 0.01 level (uncorrected, 2-tailed, blue background).

[b]Bootstrap results are based on 1000 bootstrap samples.

[c]Correlation is significant at the 0.05 level (uncorrected, 2-tailed, light blue background).

P value > 0.05 White background.

$P = 0.0001$ and mfPhNR-pVD r_s: 0.54, $P = 0.003$) exceeded those at the macular site (i.e. mfPhNR-mGCIPL r_s: 0.58, $P = 0.001$ and mfPhNR-pfVD r_s: 0.29, $P = 0.13$).

Discussion

Applying a set of complementary retinal imaging modalities we demonstrated a significant effect of glaucoma on vascular (OCT-A; parafoveal vessel density "pfVD" and fractal dimension "pfFD" and peripapillary pVD and pFD), electrophysiological (mfPhNR ratio and ssPERG amplitude) and structural measures (OCT; mGCIPL/pRNFL). These measures had equivalently high discriminatory performance, which further improved for the combination of the methods. The ERG measures of retinal ganglion cell function were more strongly associated with structural than with vascular measures.

Our findings of significant changes in the ocular microvasculature (VD) in glaucoma support previous studies, that demonstrated glaucomatous changes in the VD of the macular/parafoveal superficial layers[16,18,54–56] and the peripapillary area.[22,54–57]

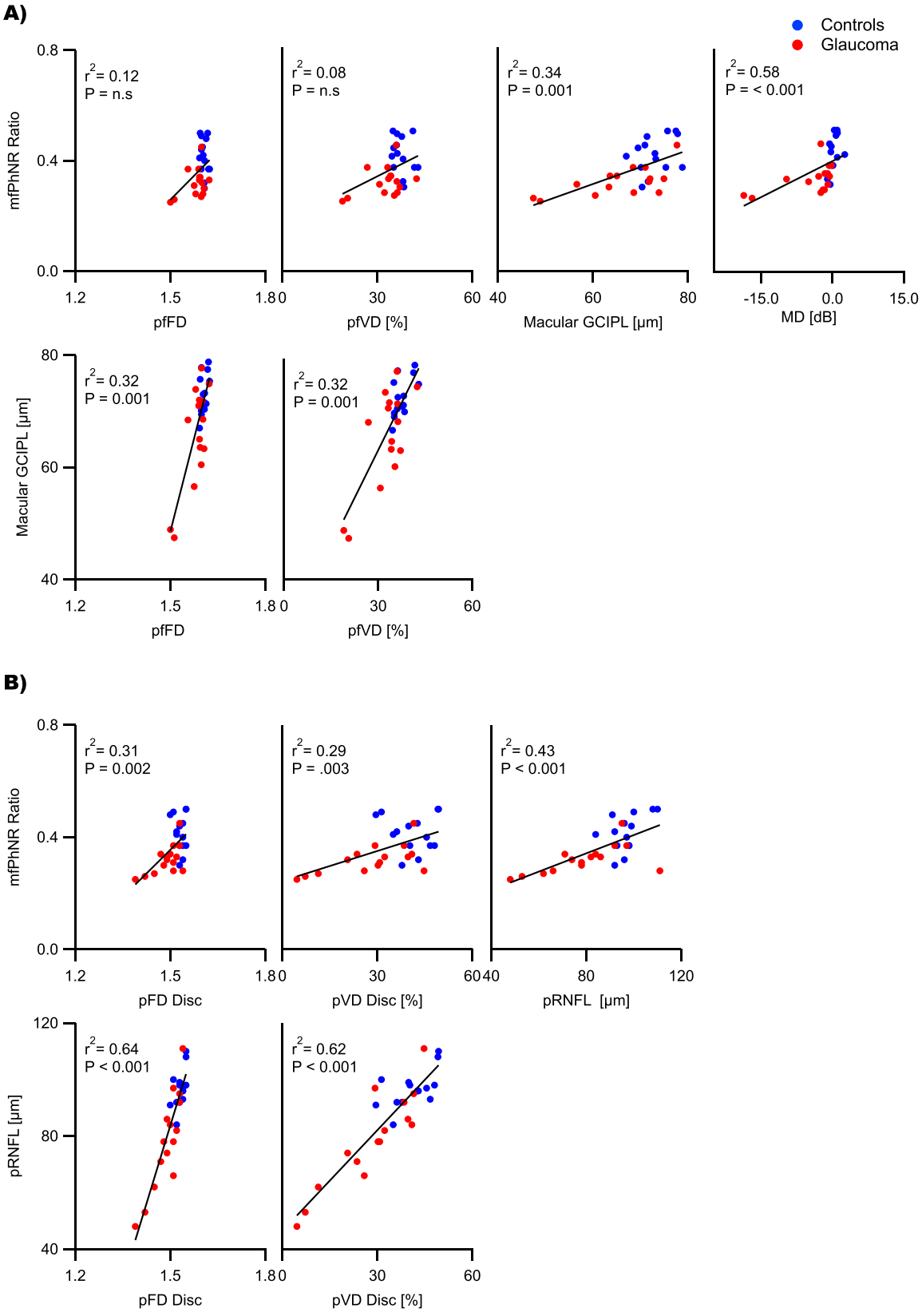

Figure 4. (**A**) Correlation plots of mfPhNR (*upper panel*) versus pfFD and pfVD mGCIPL and visual field mean deviation (dB) and of mGCIPL (*bottom*) versus pfFD and pfVD measures. (**B**) Correlation plots of mfPhNR (*top*) versus peripapillary perfusion metrics and pRNFL and of pRNFL (*bottom*) versus pFD and pVD. r_s^2 = coefficient of determination. n.s= nonsignificant association.

Furthermore, they are in agreement with investigations that demonstrated glaucoma associated changes in mfPhNR and PERG[25,26,34] and mGCIPL and pRNFL.[11–13] We considerably extended these studies by demonstrating an association between ERG-based functional and anatomical indexes, as well as an enhanced diagnostic efficacy of combined ERG-based functional indexes with vascular indexes.

Cross-Modal Comparison of Glaucoma Detection

To assess the benefit of any of the applied modalities for glaucoma detection, we conducted ROC analyses and compared their outcome measures, that is, AUC. The only previous cross-modal study addressing this for early glaucoma detection,[58] demonstrated ssPERG to have a higher performance (AUC = 0.92) than whole image VD in macula and disc (AUC= 0.80 and 0.74, respectively) and ganglion cell complex thickness (AUC = 0.74). In the current study, the highest discrimination performance was observed for the mfPhNR (not tested in[58]; AUC = 0.88), albeit not being significantly different from other measures' AUCs. Subsequently, we investigated the effect of combining ERG measures of RGC-function with structural or vascular measures. In fact, the combination of mfPhNR with pfVD AUCs yielded the highest AUC (0.94; $P < 0.001$), indicating an improvement of diagnostic performance. In addition to its relevance for glaucoma diagnosis, the improved performance for the combined assessment with pfVD might also suggest that the ERG measures of RGC-function and OCT-A measures reflect distinctive glaucomatous damage mechanisms within the retina. It should be noted, however, that, as an alternative, the enhancement might also be due to decreasing the effect of noise by pooling data from different modalities.

Association of ERG, Structural, and Vascular Measures in Glaucoma

Given the relation of vascular changes with glaucoma, it is currently still unresolved, whether these are secondary or primary events associated with RGCs damage.[2] Previous OCT-A studies are inconclusive because they found structural changes either to precede[17,59,60] or succeed[33,61] vascular changes in glaucoma. We investigated the interrelation of these measures with the sensitive measures of RGC-function, mfPhNR, and ssPERG amplitude to elucidate glaucomatous damage mechanisms. For this purpose, we compared the association of retinal ganglion cell dysfunction with specific changes (i) in fundus anatomy, that is, microvasculature (OCT-A) and retinal structure (OCT), and (ii) at damage sites, that is, macular and peripapillary sites: (i) Fundus anatomy: We reported a stronger correlation of RGC-function (mfPhNR/ssPERG) with retinal structure ($r_s \leq 0.66$) than with the microvasculature ($r_s \leq 0.56$). In contrast, for NTG the reverse pattern was recently reported,[33] that is, a stronger association of PhNR with measures of macular/parafoveal microvasculature ($r \leq 0.42$). Taken together, these findings support the current view that NTG is more strongly associated with vascular damage mechanisms than POAG. (ii) Damage sites: The measures of RGC-function were more strongly associated with peripapillary than with macular structural and vascular measures (mfPhNR with pRNFL and pVD r_s: 0.66 and 0.54, respectively; mfPhNR with mGCIPL and pfVD r_s: 0.58 and 0.29, respectively). This suggests that damage mechanisms exert their action preferentially at the peripapillary zone. It must be noted, however, that in the present study glaucomatous damage ranged from preperimetric to advanced glaucoma, such that, for example, early-stage changes of the macula[13,62,63] might not have been relevant.

Limitations

A small sample size, because of strict inclusion criteria and extensive diagnostic methods used, is a limiting factor for the findings of this study.

Practical Considerations and Potential Applications

We provide proof-of-concept for the use of ERG to further our understanding of glaucoma pathophysiology. Because we demonstrated that the combined use of ERG and vascular measures improved the detection of glaucomatous damage, it is of great promise to study their diagnostic role in borderline cases, such as glaucoma suspects, as well as for the follow-up of glaucomatous damage because ERG offers means to monitor RGC dysfunction that might precede vascular/structural damage.

In conclusion, combining ERG and OCT-A measures may improve the assessment and eventually the management of glaucoma. Follow-up studies comparing the effects of glaucoma on retinal electrophysiology, microvasculature, and structure with larger sample sizes and using longitudinal designs are of promise to further explore the pathophysiology of glaucoma.

Acknowledgments

Supported by European Union's Horizon 2020 Research and Innovation Programme under the Marie Sklodowska-Curie Grant agreement (No. 675033) and by funding of the German Research Foundation (DFG; HO2002/20-1) to MBH.

Disclosure: **K.O. Al-Nosairy,** None; **G.T. Prabhakaran,** None; **K. Pappelis,** None; **H. Thieme,** None; **M.B. Hoffmann,** None

References

1. Kwon YH, Fingert JH, Kuehn MH, Alward WLM. Primary Open-Angle Glaucoma. *N Engl J Med*. 2009;360(11):1113–1124.
2. Mansouri K. Optical coherence tomography angiography and glaucoma: searching for the missing link. *Expert Rev Med Devices*. 2016;13(10):879–880.
3. Flammer J. The vascular concept of glaucoma. *Surv Ophthalmol*. 1994;38:S3–S6.
4. Flammer J, Orgül S, Costa VP, et al. The impact of ocular blood flow in glaucoma. *Prog Retin Eye Res*. 2002;21(4):359–393.
5. Halpern DL, Grosskreutz CL. Glaucomatous optic neuropathy: mechanisms of disease. *Ophthalmol Clin N Am*. 2002;15(1):61–68.
6. Bahrami H. Causal inference in primary open angle glaucoma: specific discussion on intraocular pressure. *Ophthalmic Epidemiol*. 2006;13(4):283–289.
7. Tham Y-C, Li X, Wong TY, Quigley HA, Aung T, Cheng C-Y. Global prevalence of glaucoma and projections of glaucoma burden through 2040: a systematic review and meta-analysis. *Ophthalmology*. 2014;121(11):2081–2090.
8. Mroczkowska S, Benavente-Perez A, Negi A, Sung V, Patel SR, Gherghel D. Primary open-angle glaucoma vs normal-tension glaucoma: the vascular perspective. *JAMA Ophthalmol*. 2013;131(1):36–43.
9. Bonomi L, Marchini G, Marraffa M, Bernardi P, Morbio R, Varotto A. Vascular risk factors for primary open angle glaucoma: the Egna-Neumarkt Study. *Ophthalmology*. 2000;107(7):1287–1293.
10. Salowe R, Salinas J, Farbman NH, et al. Primary open-angle glaucoma in individuals of African descent: a review of risk factors. *J Clin Exp Ophthalmol*. 2015;6(4):450.
11. Mwanza J-C, Durbin MK, Budenz DL, et al. Glaucoma diagnostic accuracy of ganglion cell-inner plexiform layer thickness: comparison with nerve fiber layer and optic nerve head. *Ophthalmology*. 2012;119(6):1151–1158.
12. Oddone F, Lucenteforte E, Michelessi M, et al. Macular versus retinal nerve fiber layer parameters for diagnosing manifest glaucoma: a systematic review of diagnostic accuracy studies. *Ophthalmology*. 2016;123(5):939–949.
13. Kim YK, Ha A, Na KI, Kim HJ, Jeoung JW, Park KH. Temporal relation between macular ganglion cell-inner plexiform layer loss and peripapillary retinal nerve fiber layer loss in glaucoma. *Ophthalmology*. 2017;124(7):1056–1064.
14. Gao SS, Jia Y, Zhang M, et al. Optical coherence tomography angiography. *Invest Ophthalmol Vis Sci*. 2016;57(9):OCT27–OCT36.
15. Jia Y, Tan O, Tokayer J, et al. Split-spectrum amplitude-decorrelation angiography with optical coherence tomography. *Opt Express*. 2012;20(4):4710–4725.
16. Penteado RC, Zangwill LM, Daga FB, et al. Optical coherence tomography angiography macular vascular density measurements and the central 10-2 visual field in glaucoma. *J Glaucoma*. 2018;27(6):481–489.
17. Kim SB, Lee EJ, Han JC, Kee C. Comparison of peripapillary vessel density between preperimetric and perimetric glaucoma evaluated by OCT-angiography. *PloS One*. 2017;12(8):e0184297.
18. Akil H, Chopra V, Al-Sheikh M, et al. Swept-source OCT angiography imaging of the macular capillary network in glaucoma. *Br J Ophthalmol*. 2018;102(4):515–519.
19. Yarmohammadi A, Zangwill LM, Diniz-Filho A, et al. Optical coherence tomography angiography vessel density in healthy, glaucoma suspect, and glaucoma eyes. *Invest Ophthalmol Vis Sci*. 2016;57(9):OCT451–OCT459.
20. Van Melkebeke L, Barbosa-Breda J, Huygens M, Stalmans I. Optical coherence tomography angiography in glaucoma: a review. *Ophthalmic Res*. 2018;60(3):139–151.
21. Ghahari E, Bowd C, Zangwill LM, et al. Association of macular and circumpapillary microvasculature with visual field sensitivity in advanced glaucoma. *Am J Ophthalmol*. 2019;204:51–61, doi:10.1016/j.ajo.2019.03.004.
22. Liu L, Jia Y, Takusagawa HL, et al. Optical coherence tomography angiography of the peri-

papillary retina in glaucoma. *JAMA Ophthalmol*. 2015;133(9):1045–1052.
23. Yarmohammadi A, Zangwill LM, Diniz-Filho A, et al. Relationship between optical coherence tomography angiography vessel density and severity of visual field loss in glaucoma. *Ophthalmology*. 2016;123(12):2498–2508.
24. Wilsey LJ, Fortune B. Electroretinography in glaucoma diagnosis. *Curr Opin Ophthalmol*. 2016;27(2):118–124.
25. Bode SFN, Jehle T, Bach M. Pattern electroretinogram in glaucoma suspects: new findings from a longitudinal study. *Invest Ophthalmol Vis Sci*. 2011;52(7):4300–4306.
26. Preiser D, Lagrèze WA, Bach M, Poloschek CM. Photopic negative response versus pattern electroretinogram in early glaucoma. *Invest Ophthalmol Vis Sci*. 2013;54(2):1182–1191.
27. Viswanathan S, Frishman LJ, Robson JG, Walters JW. The photopic negative response of the flash electroretinogram in primary open angle glaucoma. *Invest Ophthalmol Vis Sci*. 2001;42(2):514–522.
28. Kirkiewicz M, Lubiński W, Penkala K. Photopic negative response of full-field electroretinography in patients with different stages of glaucomatous optic neuropathy. *Doc Ophthalmol*. 2016;132(1):57–65.
29. Sutter EE. Imaging visual function with the multifocal m-sequence technique. *Vis Res*. 2001;41(10-11):1241–1255.
30. Kaneko M, Machida S, Hoshi Y, Kurosaka D. Alterations of photopic negative response of multifocal electroretinogram in patients with glaucoma. *Curr Eye Res*. 2015;40(1):77–86.
31. Kato F, Miura G, Shirato S, Sato E, Yamamoto S. Correlation between N2 amplitude of multifocal ERGs and retinal sensitivity and retinal nerve fiber layer thickness in glaucomatous eyes. *Doc Ophthalmol Adv Ophthalmol*. 2015;131(3):197–206.
32. Van Alstine AW, Viswanathan S. Test-retest reliability of the multifocal photopic negative response. *Doc Ophthalmol*. 2017;134(1):25–36.
33. Honda H, Anraku A, Ishida K, Enomoto N, Tomita G. Relationship between macular vessel density and focal electroretinograms in early normal tension glaucoma. *Curr Eye Res*. 2019;44(7):753–759.
34. Al-Nosairy KO, Thieme H, Hoffmann MB. Diagnostic performance of multifocal photopic negative response, pattern electroretinogram and optical coherence tomography in glaucoma. *Experimental Eye Research*. 2020;200:108242.
35. Anderson DR, Patella VM. *Automated static perimetry*. St. Louis: Mosby; 1999.
36. Bach M, Mathieu M. Different effect of dioptric defocus vs. light scatter on the pattern electroretinogram (PERG). *Doc Ophthalmol*. 2004;108(1):99–106.
37. Hosari S, Hohberger B, Theelke L, Sari H, Lucio M, Mardin CY. OCT angiography: measurement of retinal macular microvasculature with Spectralis II OCT angiography—reliability and reproducibility. *Ophthalmol J Int Ophtalmol Int J Ophthalmol Z Augenheilkd*. 2020;243(1):75–84.
38. Iwasaki M, Inomata H. Relation between superficial capillaries and foveal structures in the human retina. *Invest Ophthalmol Vis Sci*. 1986;27(12):1698–1705.
39. Campbell JP, Zhang M, Hwang TS, et al. Detailed vascular anatomy of the human retina by projection-resolved optical coherence tomography angiography. *Sci Rep*. 2017;7:42201.
40. Pappelis K, Jansonius NM. Quantification and repeatability of vessel density and flux as assessed by optical coherence tomography angiography. *Transl Vis Sci Technol*. 2019;8(3):3.
41. Otsu N. A threshold selection method from gray-level histograms. *IEEE Trans Syst Man Cybern*. 1979;9(1):62–66.
42. Frangi AF, Niessen WJ, Vincken KL, Viergever MA. Multiscale vessel enhancement filtering. In: Wells WM, Colchester A, Delp S, eds. *Medical Image Computing and Computer-Assisted Intervention — MICCAI'98*. Lecture Notes in Computer Science. Berlin: Springer; 1998:130–137.
43. Masters BR. Fractal analysis of the vascular tree in the human retina. *Annu Rev Biomed Eng*. 2004;6(1):427–452.
44. Reif R, Qin J, An L, Zhi Z, Dziennis S, Wang R. Quantifying optical microangiography images obtained from a spectral domain optical coherence tomography system. *Int J Biomed Imaging*. 2012;2012:509783.
45. Bach M. Bach-Freiburg evoked potentials. Available at: http://localhost:4000/ep2000/. Accessed January 14, 2019.
46. Bach M, Brigell MG, Hawlina M, et al. ISCEV standard for clinical pattern electroretinography (PERG): 2012 update. *Doc Ophthalmol*. 2013;126(1):1–7.
47. Bach M, Hoffmann MB. Update on the pattern electroretinogram in glaucoma. *Optom Vis Sci*. 2008;85(6):386.
48. Al-Nosairy KO, van den Bosch JJON, Pennisi V, et al. Use of a novel telemetric sensor to study interactions of intraocular pressure and ganglion-cell

function in glaucoma [published online ahead of print July 29, 2020]. *Br J Ophthalmol*, doi:10.1136/bjophthalmol-2020-316136.
49. R Core Team. *R: The R Project for Statistical Computing. R: A language and environment for statistical computing*. Vienna, Austria: R Foundation for Statistical Computing; 2013.
50. Fritz CO, Morris PE, Richler JJ. Effect size estimates: current use, calculations, and interpretation. *J Exp Psychol Gen*. 2012;141(1):2–18.
51. Hanley JA, McNeil BJ. A method of comparing the areas under receiver operating characteristic curves derived from the same cases. *Radiology*. 1983;148(3):839–843.
52. Holm S. A simple sequentially rejective multiple test procedure. *Scand J Stat*. 1979;6(2):65–70.
53. Koo TK, Li MY. A guideline of selecting and reporting intraclass correlation coefficients for reliability research. *J Chiropr Med*. 2016;15(2):155–163.
54. Rao HL, Pradhan ZS, Weinreb RN, et al. Regional comparisons of optical coherence tomography angiography vessel density in primary open-angle glaucoma. *Am J Ophthalmol*. 2016;171:75–83.
55. Yarmohammadi A, Zangwill LM, Manalastas PIC, et al. Peripapillary and macular vessel density in patients with primary open-angle glaucoma and unilateral visual field loss. *Ophthalmology*. 2018;125(4):578–587.
56. Chung JK, Hwang YH, Wi JM, Kim M, Jung JJ. Glaucoma diagnostic ability of the optical coherence tomography angiography vessel density parameters. *Curr Eye Res*. 2017;42(11):1458–1467.
57. Scripsema NK, Garcia PM, Bavier RD, et al. Optical coherence tomography angiography analysis of perfused peripapillary capillaries in primary open-angle glaucoma and normal-tension glaucoma. *Invest Ophthalmol Vis Sci*. 2016;57(9):OCT611–OCT620.
58. Kurysheva NI, Maslova EV, Zolnikova IV, Fomin AV, Lagutin MB. A comparative study of structural, functional and circulatory parameters in glaucoma diagnostics. *PloS One*. 2018;13(8):e0201599.
59. Lee EJ, Kim S, Hwang S, Han JC, Kee C. Microvascular compromise develops following nerve fiber layer damage in normal-tension glaucoma without choroidal vasculature involvement. *J Glaucoma*. 2017;26(3):216–222.
60. Akagi T, Iida Y, Nakanishi H, et al. Microvascular density in glaucomatous eyes with hemifield visual field defects: an optical coherence tomography angiography study. *Am J Ophthalmol*. 2016;168:237–249.
61. Shoji T, Zangwill LM, Akagi T, et al. Progressive macula vessel density loss in primary open angle glaucoma: a longitudinal study. *Am J Ophthalmol*. 2017;182:107–117.
62. Hood DC, Raza AS, de Moraes CGV, Liebmann JM, Ritch R. Glaucomatous damage of the macula. *Prog Retin Eye Res*. 2013;32:1–21.
63. Kim YK, Jeoung JW, Park KH. Inferior macular damage in glaucoma: its relationship to retinal nerve fiber layer defect in macular vulnerability zone. *J Glaucoma*. 2017;26(2):126–132.

Chapter 8

General Discussion

Visual impairment and visual loss is reported to reduce the quality of life (Ramrattan et al., 2001) and to affect the educational and economic opportunities (Eckert et al., 2015). With a global prevalence of 3.5% (Tham et al., 2014), glaucoma ranks second next to cataract as a cause of blindness worldwide (Quigley and Broman, 2006). There are yet unmet clinical needs in glaucoma. Among these are the early identification of an ideal time window to start the therapy as well as basic knowledge of the temporal sequence leading to glaucomatous damage. This thesis addresses these issues with respect to the role of functional and anatomical measures.

8.1 Summary of main findings and discussion

8.1.1 Postural influence on glaucoma

The major and only modifiable risk factor for glaucoma is IOP (Leske et al., 2003). The IOP is a dynamic parameter and subject to diurnal, long term and positional fluctuations (Yanoff and Duker, 2018). Several studies demonstrated an elevated IOP in different body positions e.g. supine, prone and LDP (Park et al., 2019; Lee et al., 2013; Malihi and Sit, 2012; Lee et al., 2012; Tsukahara and Sasaki, 1984) without tracking IOP changes continuously and without monitoring RGCs changes. It is well established that -10º head down tilt increases IOP with a consequent RGC dysfunction manifested on the pattern electroretinogram (PERG) in glaucoma (Porciatti et al., 2017; Ventura et al., 2013). This testing protocol can actually predict the conversion of glaucoma suspects into glaucoma 4 years ahead (Porciatti et al., 2017).

A more flexible positioning approach was used in my study, i.e. lateral decubitus positioning (LDP), and combined with continual IOP measurements using a novel IOP sensor (eyemate-IO sensor®, Implandata) coupled with the PERG to assess the postural-related IOP and RGC changes, respectively, in glaucoma with and without an IO-eyemate sensor implant and in healthy controls.

In chapter 5, I have demonstrated the feasibility of such synchronous measurements specifically in patients with IO sensors where the electromagnetic intrusions from the IO-sensor had no relevant effects on steady-state PERG recording. This is attributed to the robustness of the steady state PERG where responses could be separately extracted at the frequency of 15 Hz which is different from that elicited by the IO-reader, i.e. 9 Hz. I also found LDP coupled with IOP and PERG measurements could contribute to decipher the direct IOP-RGC relationship. In this regard, I demonstrated that IOP increased during LDP resulting in distinctive changes in the RGC function determined via PERG recordings in controls [IOP increase of 1.6 ± 0.6 mmHg (P = 0.02) and a reversible reduction of the RGC function of -17 ± 5% (P = 0.005) for right eye changes during right LDP in comparison to the levels during sitting]. Glaucomatous eyes with the sensor implant showed a similar trend [an IOP increase of 5.1 ± 0.6 mmHg, P = 0.00004 and a reversible reduction of the RGC function of -25 ± 10% (P = .02) for right eye changes during right LDP in comparison to the levels during sitting].

These findings corroborated the fact that positional changes induce physiological changes in glaucomatous eyes. These posture induced changes were in part consistent with previous studies albeit using another testing protocol and no continual IOP monitoring (Porciatti et al., 2017; Ventura et al., 2013). In conclusion, the IOP and RGC relationship was, for the first time, investigated with synchronous continual readings. Furthermore, this study demonstrated short term effects of the IOP increase on the RGC function during LDP.

Future studies with a larger sample size are of promise to test long term effects and to evaluate the LDP paradigm as a provocative test in glaucoma suspects. If LDP is proven to be of value in screening glaucoma suspects, it might have implications in the risk stratifications of glaucoma.

8.1.2 mfPhNR in glaucoma diagnosis

Clinical ERG measures of visual function can provide key findings in the detection of glaucoma, e.g. PERG predicted the OHT conversion to glaucoma 4 years earlier (Bode et al., 2011). Another ERG method addressing the photopic negative response (PhNR) of mfERG (mfPhNR), can also provide insights into RGC function including an analysis of the visual field topography. Previous works on the mfPhNR used various stimulation sequences either fast, 1 to 9 interleaved frames (Kamei et al., 2011; Kamei and Nagasaka,

2014, 2010; Kaneko et al., 2015; Kato et al., 2015; Tanaka et al., 2020), or slow stimulation sequences with around 30 interleaved frames (Rajagopalan et al., 2014; Van Alstine and Viswanathan, 2017). I extended these studies (chapter 6) by investigating: i) both fast and slow protocols during the multifocal stimulation and ii) the comparison of the diagnostic performance of the mfPhNR vs other established methods, i.e. the PERG and the pRNFL thickness. I found that the mfPhNR/b-wave ratio with a faster stimulation (9 interleaved frames) outperforms the slower stimuli protocols in differentiating the glaucoma from the healthy controls. I also demonstrated that the mfPhNR/b-wave ratio had the highest diagnostic performance, in particular for glaucoma suspects [AUC = 0.84, P = 0.008], compared to 0.8º checksize PERG amplitude [AUC = 0.78, P = 0.039], and the surrogate structural measure in clinical practice, i.e. pRNFL [AUC = 0.74, $P \leq 0.05$]. The respective AUCs for differentiating glaucoma from controls were 0.78 (P = 0.004), 0.85 ($P \leq 0.001$) and 0.87 ($P \leq 0.001$). It was also found that the RGC functional changes could be predicted by the estimation of pRNFL thickness changes, i.e. for the mfPhNR/b-wave ratio [t(48) = 4, P = 0.0002] and the 0.8º checksize PERG amplitude [t(48) = 3.4, P = 0.001]. I also assessed the selective damage for different regions of the retina and found no superiority of the specially resolved multifocal assessment vs grouping multifocal responses to the retinal sum response. In short, the findings of chapter 6 contribute to the optimization of mfERG diagnostics in glaucoma. Indeed, the mfPhNR was deemed to be of higher value in the detection of glaucoma suspects and hence has the potential to improve the glaucoma management.

Future studies with a prospective collection of data and a longitudinal design should be performed with a larger sample size to evaluate the mfPhNR diagnostic performance for the recognition of patients at a higher risk for glaucoma conversions. Further, the topographical analysis of glaucoma damage deserves further investigations to possibly recognize local defects in glaucoma and to test the benefit of multifocal ERG-techniques in glaucoma investigations.

8.1.3 Multimodal assessment of glaucoma

In glaucoma pathogenesis, the vascular dysfunction is a major contributing factor next to the elevated IOP (Flammer et al., 2002; Sommer et al., 1991). In chapter 7, a recent innovation and a promising tool in glaucoma diagnostic, the OCT-A, is highlighted. Previous studies reported the presence of vascular dysfunction even prior to the structural

damage (Honda et al., 2019; Shoji et al., 2017) and demonstrated stronger ties with functional metrices of vision (Yarmohammadi et al., 2017). Several studies reported a reduced vessel density at the macular, peripapillary area or optic disc in glaucomatous eyes; however, its diagnostic performance compared to conventional OCT measurements is still inconclusive (Chen et al., 2017; Rao et al., 2017b, 2017a; Shoji et al., 2017; Wan et al., 2018; Yarmohammadi et al., 2017). Likewise, the association of functional visual field measures with either macular thickness or vascular density is still a point of controversy. In this thesis, I expanded these studies by the additional assessment of mfPhNR and PERG as direct functional measures of the RGC in comparison to the surrogate clinical structural (mGCIPL and pRNFL) and vasculature measures [parafoveal VD (pfVD) and peripapillary VD (pVD)]. I found that mfPhNR had a stronger association with structural measures [mfPhNR ratio/mGCIPL correlation of 0.58 ($P = 0.001$) and mfPhNR ratio/pRNFL correlation of 0.66 ($P \leq 0.001$)] than with vascular measures [mfPhNR ratio/pfVD correlation of 0.29 ($P = 0.13$) and mfPhNR ratio-pVD correlation of 0.54 ($P = 0.003$)] a finding that is consistent (Wan et al., 2018) and inconsistent (Honda et al., 2019; Yarmohammadi et al., 2017) with previous studies. Further, I demonstrated that combined ERG functional and vascular measures had the highest AUC for the detection of glaucoma [mfPhNR ratio + pVD AUC = 0.94 ($P \leq 0.001$)]. In brief, the use of ERG along with OCT/A could provide valuable insights into glaucoma pathogenesis and diagnosis.

The OCT-A is a promising tool in ophthalmology practice but currently there is a lack of longitudinal studies to assess the vascular damage in glaucoma. Future studies should also attempt the combination of ERG and OCT/A to ascertain the temporal aspects of the glaucomatous damage, i.e. whether the vascular damage precedes/concedes the RGC degenerations, but with a larger sample size in a longitudinal design. These studies will transform the use of OCT-A and ERG from promising to useful clinical tools for a potentially complementation of the already established structural and functional tools used in glaucoma diagnosis and management.

8.2 Concluding remarks

Glaucoma is the leading cause of irreversible visual blindness and poses a major public health problem. Its early detection is essential to halt or slow disease progression. ERG measures of visual function reflect RGC function and are complementary to other morphological technologies in glaucoma diagnostics. In this thesis, I investigated the potential utility of ERG measures of vision along with structural and vascular retinal measures (OCT/A) in the assessment of the glaucomatous damage. In regards to glaucoma diagnosis, mfPhNR and PERG hold promise to early detection of glaucoma cases even at the glaucoma suspect stage. Furthermore, ERGs along with OCT/A might be of assistance to elucidate damage mechanisms and might help deciphering the temporal relationship of the damage that may have implications in the monitoring and the treatment of glaucoma. In short, clinical ERG measures of visual function alongside OCT/A might be indispensable tools in the field of ophthalmology and provides a paradigm to integrate various aspects of glaucoma damage for the enhancement of the clinical management and the advancement of vision research.

Bibliography

Aptel F, Musson C, Zhou T, Lesoin A, Chiquet C. 24-hour Intraocular Pressure Rhythm in Patients With Untreated Primary Open Angle Glaucoma and Effects of Selective Laser Trabeculoplasty. Journal of Glaucoma 2017;26:272–7. https://doi.org/10.1097/IJG.0000000000000604.

Asrani S, Zeimer R, Wilensky J, Gieser D, Vitale S, Lindenmuth K. Large diurnal fluctuations in intraocular pressure are an independent risk factor in patients with glaucoma. J Glaucoma 2000;9:134–42.

Bach M, Hoffmann M. The origin of the Pattern Electroretinogram. In: Heckenlively JR, Arden GB, editors. Principles and Practice of Clinical Electrophysiology of Vision. 2nd ed., MIT Press; 2006, p. 185–96.

Bach M, Hoffmann MB. Update on the Pattern Electroretinogram in Glaucoma. Optometry and Vision Science 2008;85:386. https://doi.org/10.1097/OPX.0b013e318177ebf3.

Bach M, Poloschek CM. Electrophysiology and glaucoma: current status and future challenges. Cell and Tissue Research 2013;353:287–96. https://doi.org/10.1007/s00441-013-1598-6.

Bach M, Unsoeld AS, Philippin H, Staubach F, Maier P, Walter HS, et al. Pattern ERG as an Early Glaucoma Indicator in Ocular Hypertension: A Long-Term, Prospective Study. Invest Ophthalmol Vis Sci 2006;47:4881–7. https://doi.org/10.1167/iovs.05-0875.

Banitt MR, Ventura LM, Feuer WJ, Savatovsky E, Luna G, Shif O, et al. Progressive Loss of Retinal Ganglion Cell Function Precedes Structural Loss by Several Years in Glaucoma Suspects. Invest Ophthalmol Vis Sci 2013;54:2346–52. https://doi.org/10.1167/iovs.12-11026.

Bode SFN, Jehle T, Bach M. Pattern Electroretinogram in Glaucoma Suspects: New Findings from a Longitudinal Study. Invest Ophthalmol Vis Sci 2011;52:4300–6. https://doi.org/10.1167/iovs.10-6381.

Bourne RRA, Taylor HR, Flaxman SR, Keeffe J, Leasher J, Naidoo K, et al. Number of People Blind or Visually Impaired by Glaucoma Worldwide and in World Regions 1990 – 2010: A Meta-Analysis. PLOS ONE 2016;11:e0162229. https://doi.org/10.1371/journal.pone.0162229.

Brar VS, Law, Simon K, Lindsey, Jennifer L, Schulze, Robert L, Silverstein, Evan, Singth, Ravi S.J, et al. 2019-2020 Basic and Clinical Science Course, Section 2: Fundamentals and Principles of Ophthalmology. American Academy of Ophthalmology; 2019.

Burgoyne CF, Downs JC, Bellezza AJ, Suh J-KF, Hart RT. The optic nerve head as a biomechanical structure: a new paradigm for understanding the role of IOP-related stress and strain in the pathophysiology of glaucomatous optic nerve head damage.

Prog Retin Eye Res 2005;24:39–73. https://doi.org/10.1016/j.preteyeres.2004.06.001.

Chen HS-L, Liu C-H, Wu W-C, Tseng H-J, Lee Y-S. Optical Coherence Tomography Angiography of the Superficial Microvasculature in the Macular and Peripapillary Areas in Glaucomatous and Healthy Eyes. Invest Ophthalmol Vis Sci 2017;58:3637–45. https://doi.org/10.1167/iovs.17-21846.

Denniston AKO, Murray PI. Oxford Handbook of Ophthalmology. Oxford University Press; 2018.

Eckert KA, Carter MJ, Lansingh VC, Wilson DA, Furtado JM, Frick KD, et al. A Simple Method for Estimating the Economic Cost of Productivity Loss Due to Blindness and Moderate to Severe Visual Impairment. Ophthalmic Epidemiol 2015;22:349–55. https://doi.org/10.3109/09286586.2015.1066394.

Flammer J. The vascular concept of glaucoma. Survey of Ophthalmology 1994;38:S3–6. https://doi.org/10.1016/0039-6257(94)90041-8.

Flammer J, Orgül S, Costa VP, Orzalesi N, Krieglstein GK, Serra LM, et al. The impact of ocular blood flow in glaucoma. Prog Retin Eye Res 2002;21:359–93. https://doi.org/10.1016/s1350-9462(02)00008-3.

Forrester JV, Dick AD, McMenamin PG, Roberts F, PhD EP BSc. The Eye: Basic Sciences in Practice. Elsevier Health Sciences; 2015.

Girkin CA, Bhorade, Anjali M, Crowston, Jonathan Guy, Giaconi, JoAnn A, Medeiros, Felipe A, Sit, Arthur J, et al. 2019-2020 Basic and Clinical Science Course, Section 10: Glaucoma. S.l.: American Academy of Ophthalmology; 2019.

Halpern DL, Grosskreutz CL. Glaucomatous optic neuropathy: mechanisms of disease. Ophthalmol Clin North Am 2002;15:61–8. https://doi.org/10.1016/s0896-1549(01)00012-8.

Harwerth RS, Quigley HA. Visual Field Defects and Retinal Ganglion Cell Losses in Human Glaucoma Patients. Arch Ophthalmol 2006;124:853–9. https://doi.org/10.1001/archopht.124.6.853.

Harwerth RS, Wheat JL, Fredette MJ, Anderson DR. Linking Structure and Function in Glaucoma. Prog Retin Eye Res 2010;29:249–71. https://doi.org/10.1016/j.preteyeres.2010.02.001.

Heijl A, Leske MC, Bengtsson Bo, Hyman L, Bengtsson Boel, Hussein M, et al. Reduction of intraocular pressure and glaucoma progression: results from the Early Manifest Glaucoma Trial. Arch Ophthalmol 2002;120:1268–79. https://doi.org/10.1001/archopht.120.10.1268.

Hiss P, Fahl G. [Changes in the pattern electroretinogram in glaucoma and ocular hypertension are dependent on stimulus frequency]. Fortschritte Der Ophthalmologie: Zeitschrift Der Deutschen Ophthalmologischen Gesellschaft 1991;88:562–5.

Hoffmann MB. Investigating Visual Function with Multifocal Visual Evoked Potentials. In: Lorenz B, Borruat F-X, editors. Pediatric Ophthalmology, Neuro-Ophthalmology, Genetics, Berlin, Heidelberg: Springer; 2008, p. 139–59. https://doi.org/10.1007/978-3-540-33679-2_9.

Hoffmann MB, Heinrich SP, Thieme H, Al-Nosairy KO. Mit klinischer Elektrophysiologie hinter die Netzhaut. Klin Monbl Augenheilkd 2018;235:1229–34. https://doi.org/10.1055/a-0715-8072.

Honda H, Anraku A, Ishida K, Enomoto N, Tomita G. Relationship between Macular Vessel Density and Focal Electroretinograms in Early Normal Tension Glaucoma. Curr Eye Res 2019;44:753–9. https://doi.org/10.1080/02713683.2019.1593464.

Hood DC. Improving our understanding, and detection, of glaucomatous damage: An approach based upon optical coherence tomography (OCT). Prog Retin Eye Res 2017;57:46–75. https://doi.org/10.1016/j.preteyeres.2016.12.002.

Jonas JB, Aung T, Bourne RR, Bron AM, Ritch R, Panda-Jonas S. Glaucoma. Lancet 2017;390:2183–93. https://doi.org/10.1016/S0140-6736(17)31469-1.

Joukal M. Anatomy of the Human Visual Pathway. In: Skorkovská K, editor. Homonymous Visual Field Defects, Cham: Springer International Publishing; 2017, p. 1–16. https://doi.org/10.1007/978-3-319-52284-5_1.

Kamei A, Machida S, Nagasaka E. Multifocal Photopic Negative Response (mfPhNR) and Lineal Visual Sensitivity in Patients with Optic Nerve Lesions. Invest Ophthalmol Vis Sci 2011;52:273–273.

Kamei A, Nagasaka E. Multifocal Photopic Negative Response (mfPhNR) and Ganglion Cell-Inner Plexiform Layer Thickness (GCIPLT) in Patients with Optic Nerve Lesions. Invest Ophthalmol Vis Sci 2014;55:6236–6236.

Kamei A, Nagasaka E. Multifocal Photopic Negative Response (mfPhNR) and Retinal Nerve Fiber Layer Thickness (RNFLT) in Patients with Optic Nerve Lesions. Invest Ophthalmol Vis Sci 2010;51:5473–5473.

Kaneko M, Machida S, Hoshi Y, Kurosaka D. Alterations of Photopic Negative Response of Multifocal Electroretinogram in Patients with Glaucoma. Current Eye Research 2015;40:77–86. https://doi.org/10.3109/02713683.2014.915575.

Kass MA, Heuer DK, Higginbotham EJ, Johnson CA, Keltner JL, Miller JP, et al. The Ocular Hypertension Treatment Study: a randomized trial determines that topical ocular hypotensive medication delays or prevents the onset of primary open-angle glaucoma. Arch Ophthalmol 2002;120:701–13; discussion 829-830.

Kato F, Miura G, Shirato S, Sato E, Yamamoto S. Correlation between N2 amplitude of multifocal ERGs and retinal sensitivity and retinal nerve fiber layer thickness in glaucomatous eyes. Doc Ophthalmol 2015;131:197–206. https://doi.org/10.1007/s10633-015-9519-5.

Kd B, Pp C, Jc W. Optical coherence tomography angiography in glaucoma. Curr Opin Ophthalmol 2019;30:110–6. https://doi.org/10.1097/icu.0000000000000554.

Kerrigan-Baumrind LA, Quigley HA, Pease ME, Kerrigan DF, Mitchell RS. Number of ganglion cells in glaucoma eyes compared with threshold visual field tests in the same persons. Invest Ophthalmol Vis Sci 2000;41:741–8.

Koustenis A, Harris A, Gross J, Januleviciene I, Shah A, Siesky B. Optical coherence tomography angiography: an overview of the technology and an assessment of applications for clinical research. The British Journal of Ophthalmology 2017;101:16–20. https://doi.org/10.1136/bjophthalmol-2016-309389.

Koutsonas A, Walter P, Plange N. Selbsttonometrie mit einem telemetrischen, intraokularen Drucksensor bei Patienten mit Glaukom. Klin Monatsbl Augenheilkd 2016;233:743–8. https://doi.org/10.1055/s-0041-106191.

Koutsonas A, Walter P, Roessler G, Plange N. Long-term follow-up after implantation of a telemetric intraocular pressure sensor in patients with glaucoma: a safety report. Clinical & Experimental Ophthalmology 2018;46:473–9. https://doi.org/10.1111/ceo.13100.

Lee JY, Yoo C, Jung JH, Hwang YH, Kim YY. The effect of lateral decubitus position on intraocular pressure in healthy young subjects. Acta Ophthalmol 2012;90:e68-72. https://doi.org/10.1111/j.1755-3768.2011.02208.x.

Lee JY, Yoo C, Kim YY. The effect of lateral decubitus position on intraocular pressure in patients with untreated open-angle glaucoma. Am J Ophthalmol 2013;155:329-335.e2. https://doi.org/10.1016/j.ajo.2012.08.003.

Leske MC, Heijl A, Hussein M, Bengtsson B, Hyman L, Komaroff E, et al. Factors for Glaucoma Progression and the Effect of Treatment: The Early Manifest Glaucoma Trial. Arch Ophthalmol 2003;121:48–56. https://doi.org/10.1001/archopht.121.1.48.

Machida S, Kaneko M, Kurosaka D. Regional Variations in Correlation between Photopic Negative Response of Focal Electoretinograms and Ganglion Cell Complex in Glaucoma. Current Eye Research 2015;40:439–49. https://doi.org/10.3109/02713683.2014.922196.

Malihi M, Sit AJ. Effect of head and body position on intraocular pressure. Ophthalmology 2012;119:987–91. https://doi.org/10.1016/j.ophtha.2011.11.024.

Mansouri K. Optical coherence tomography angiography and glaucoma: searching for the missing link. Expert Review of Medical Devices 2016;13:879–80. https://doi.org/10.1080/17434440.2016.1230014.

McCannel CA, Berrocal, Audina M, Holder GE, Kim,Stephan J, Leonard, Brian C, Spaide, Richard F, et al. 2019-2020 Basic and Clinical Science Course, Section 10: Retina and vitreous. American Academy of Ophthalmology; 2019.

Melki S, Todani A, Cherfan G. An Implantable Intraocular Pressure Transducer: Initial Safety Outcomes. JAMA Ophthalmol 2014;132:1221–5. https://doi.org/10.1001/jamaophthalmol.2014.1739.

Müller PL, Meigen T. M-sequences in ophthalmic electrophysiology. Journal of Vision 2016;16:15–15. https://doi.org/10.1167/16.1.15.

Park J-H, Yoo C, Yoo E, Kim YY. Intraocular Pressure Elevation during Lateral Body Posture in Side-sleeping Glaucoma Patients. Optom Vis Sci 2019;96:62–70. https://doi.org/10.1097/OPX.0000000000001322.

Porciatti V, Feuer WJ, Monsalve P, Triolo G, Vazquez L, McSoley J, et al. Head-down Posture in Glaucoma Suspects Induces Changes in IOP, Systemic Pressure, and PERG That Predict Future Loss of Optic Nerve Tissue: Journal of Glaucoma 2017;26:459–65. https://doi.org/10.1097/IJG.0000000000000648.

Porciatti V, Ventura LM. Normative data for a user-friendly paradigm for pattern electroretinogram recording. Ophthalmology 2004;111:161–8. https://doi.org/10.1016/j.ophtha.2003.04.007.

Quigley HA, Broman AT. The number of people with glaucoma worldwide in 2010 and 2020. British Journal of Ophthalmology 2006;90:262–7. https://doi.org/10.1136/bjo.2005.081224.

Rajagopalan L, Patel NB, Viswanathan S, Harwerth RS, Frishman L. Comparison of multifocal photopic negative response (mfPhNR) with structural and functional measures in experimental glaucoma. Invest Ophthalmol Vis Sci 2014;55:5128–5128.

Ramrattan RS, Wolfs RC, Panda-Jonas S, Jonas JB, Bakker D, Pols HA, et al. Prevalence and causes of visual field loss in the elderly and associations with impairment in daily functioning: the Rotterdam Study. Arch Ophthalmol 2001;119:1788–94. https://doi.org/10.1001/archopht.119.12.1788.

Rao HL, Pradhan ZS, Suh MH, Moghimi S, Mansouri K, Weinreb RN. Optical Coherence Tomography Angiography in Glaucoma. Journal of Glaucoma 2020;29:312–321. https://doi.org/10.1097/IJG.0000000000001463.

Rao HL, Pradhan ZS, Weinreb RN, Dasari S, Riyazuddin M, Venugopal JP, et al. Optical Coherence Tomography Angiography Vessel Density Measurements in Eyes With Primary Open-Angle Glaucoma and Disc Hemorrhage. J Glaucoma 2017a;26:888–95. https://doi.org/10.1097/IJG.0000000000000758.

Rao HL, Pradhan ZS, Weinreb RN, Riyazuddin M, Dasari S, Venugopal JP, et al. A comparison of the diagnostic ability of vessel density and structural measurements of optical coherence tomography in primary open angle glaucoma. PLoS One 2017b;12. https://doi.org/10.1371/journal.pone.0173930.

Salmon J. Kanski's Clinical Ophthalmology E-Book: A Systematic Approach. Elsevier Health Sciences; 2019.

Shah NN, Bowd C, Medeiros FA, Weinreb RN, Sample PA, Hoffmann EM, et al. Combining Structural and Functional Testing for Detection of Glaucoma. Ophthalmology 2006;113:1593–602. https://doi.org/10.1016/j.ophtha.2006.06.004.

Sharma, Priya, Sergott RC. Optical Coherence Tomography. Springer International Publishing; 2016. https://doi.org/10.1007/978-3-319-24817-2.

Shoji T, Zangwill LM, Akagi T, Saunders LJ, Yarmohammadi A, Manalastas PIC, et al. Progressive Macula Vessel Density Loss in Primary Open Angle Glaucoma: A Longitudinal Study. Am J Ophthalmol 2017;182:107–17. https://doi.org/10.1016/j.ajo.2017.07.011.

Snell RS, Lemp MA. The Eyeball. Clinical Anatomy of the Eye, John Wiley & Sons, Ltd; 2013, p. 132–213. https://doi.org/10.1002/9781118690987.ch6.

Sommer A, Tielsch JM, Katz J, Quigley HA, Gottsch JD, Javitt J, et al. Relationship between intraocular pressure and primary open angle glaucoma among white and black Americans. The Baltimore Eye Survey. Arch Ophthalmol 1991;109:1090–5. https://doi.org/10.1001/archopht.1991.01080080050026.

Spaide RF, Klancnik JM, Cooney MJ. Retinal vascular layers imaged by fluorescein angiography and optical coherence tomography angiography. JAMA Ophthalmology 2015;133:45–50. https://doi.org/10.1001/jamaophthalmol.2014.3616.

Sutter EE. Imaging visual function with the multifocal m-sequence technique. Vision Res 2001;41:1241–55. https://doi.org/10.1016/s0042-6989(01)00078-5.

Sutter EE, Tran D. The field topography of ERG components in man--I. The photopic luminance response. Vision Res 1992;32:433–46. https://doi.org/10.1016/0042-6989(92)90235-b.

Tanaka H, Ishida K, Ozawa K, Sawada A, Mochizuki K, Yamamoto T. Relationship between structural and functional changes in glaucomatous eyes: A multifocal electroretinogram study. In Review; 2020. https://doi.org/10.21203/rs.2.20694/v1.

Tham Y-C, Li X, Wong TY, Quigley HA, Aung T, Cheng C-Y. Global Prevalence of Glaucoma and Projections of Glaucoma Burden through 2040: A Systematic Review and Meta-Analysis. Ophthalmology 2014;121:2081–90. https://doi.org/10.1016/j.ophtha.2014.05.013.

Tojo N, Abe S, Ishida M, Yagou T, Hayashi A. The Fluctuation of Intraocular Pressure Measured by a Contact Lens Sensor in Normal-tension Glaucoma Patients and Nonglaucoma Subjects. Journal of Glaucoma 2017;26:195–200. https://doi.org/10.1097/IJG.0000000000000517.

Trattler WB, Friedman NJ, Kaiser PK. Review of Ophthalmology E-Book: Expert Consult. Elsevier Health Sciences; 2016.

Trick GL. Retinal potentials in patients with primary open-angle glaucoma: physiological evidence for temporal frequency tuning deficits. Invest Ophthalmol Vis Sci 1985;26:1750–8.

Tsukahara S, Sasaki T. Postural change of IOP in normal persons and in patients with primary wide open-angle glaucoma and low-tension glaucoma. Br J Ophthalmol 1984;68:389–92.

Van Alstine AW, Viswanathan S. Test–retest reliability of the multifocal photopic negative response. Documenta Ophthalmologica 2017;134:25–36. https://doi.org/10.1007/s10633-016-9569-3.

Ventura LM, Golubev I, Lee W, Nose I, Parel J-M, Feuer WJ, et al. Head-down posture induces PERG alterations in early glaucoma. J Glaucoma 2013;22:255–64. https://doi.org/10.1097/IJG.0b013e318232973b.

Viswanathan S, Frishman LJ, Robson JG. The uniform field and pattern ERG in macaques with experimental glaucoma: removal of spiking activity. Investigative Ophthalmology & Visual Science 2000;41:2797–810.

Viswanathan S, Frishman LJ, Robson JG, Harwerth RS, Smith EL. The photopic negative response of the macaque electroretinogram: reduction by experimental glaucoma. Invest Ophthalmol Vis Sci 1999;40:1124–36.

Viswanathan S, Frishman LJ, Robson JG, Walters JW. The photopic negative response of the flash electroretinogram in primary open angle glaucoma. Invest Ophthalmol Vis Sci 2001;42:514–22.

Wan KH, Lam AKN, Leung CK-S. Optical Coherence Tomography Angiography Compared With Optical Coherence Tomography Macular Measurements for Detection of Glaucoma. JAMA Ophthalmol 2018;136:866–74. https://doi.org/10.1001/jamaophthalmol.2018.1627.

Wang DL, Raza AS, Moraes CG de, Chen M, Alhadeff P, Jarukatsetphorn R, et al. Central Glaucomatous Damage of the Macula Can Be Overlooked by Conventional OCT Retinal Nerve Fiber Layer Thickness Analyses. Trans Vis Sci Tech 2015;4:4–4. https://doi.org/10.1167/tvst.4.6.4.

Weinreb RN, Aung T, Medeiros FA. The Pathophysiology and Treatment of Glaucoma: A Review. JAMA 2014;311:1901–11. https://doi.org/10.1001/jama.2014.3192.

Wilsey LJ, Fortune B. Electroretinography in glaucoma diagnosis. Curr Opin Ophthalmol 2016;27:118–24. https://doi.org/10.1097/ICU.0000000000000241.

Wright KW. Textbook of ophthalmology. Lippincott: Williams & Wilkins; 1997.

Yanoff M, Duker JS. Ophthalmology E-Book. Elsevier Health Sciences; 2018.

Yarmohammadi A, Zangwill LM, Diniz-Filho A, Saunders LJ, Suh MH, Wu Z, et al. Peripapillary and Macular Vessel Density in Patients with Glaucoma and Single-Hemifield Visual Field Defect. Ophthalmology 2017;124:709–19. https://doi.org/10.1016/j.ophtha.2017.01.004.

Declaration of honor

I hereby declare that I prepared this thesis without the impermissible help of third parties and that none other than the aids indicated have been used; all sources of information are clearly marked, including my own publications.

in particular I have not consciously:

- fabricated data or rejected undesirable results,
- misused statistical methods with the aim of drawing other conclusions than those warranted by the available data,
- plagiarized external data or publications,
- presented the results of other researchers in a distorted way.

I am aware that violations of copyright may lead to injunction and damage claims by the author and also to prosecution by the law enforcement authorities. I hereby agree that the thesis may be electronically reviewed with the aim of identifying plagiarism.

This work has not yet been submitted as a doctoral thesis in the same or a similar form in Germany nor in any other country. And it has not yet been published as a whole.

Magdeburg, January 13th, 2021

Khaldoon Al-Nosairy

Publications

*Al-Nosairy, K. O., Bosch, J. J. O. N. van den, Pennisi, V., Mansouri, K., Thieme, H., Choritz, L., & Hoffmann, M. B. (2020). Use of a novel telemetric sensor to study interactions of intraocular pressure and ganglion-cell function in glaucoma. British Journal of Ophthalmology. https://doi.org/10.1136/bjophthalmol-2020-316136

*Al-Nosairy, K. O., Thieme, H., & Hoffmann, M. B. (2020). Diagnostic performance of multifocal photopic negative response, pattern electroretinogram and optical coherence tomography in glaucoma. Experimental Eye Research, 108242. https://doi.org/10.1016/j.exer.2020.108242

*Al-Nosairy, K. O., Prabhakaran, G. T., Pappelis, K., Thieme, H., & Hoffmann, M. B. (2020). Combined Multi-Modal Assessment of Glaucomatous Damage With Electroretinography and Optical Coherence Tomography/Angiography. Translational Vision Science & Technology, 9(12), 7–7. https://doi.org/10.1167/tvst.9.12.7

Pawlitzki, M., Horbrügger, M., Loewe, K., Kaufmann, J., Opfer, R., Wagner, M., Al-Nosairy, K. O., Meuth, S. G., Hoffmann, M. B., & Schippling, S. (2020). MS optic neuritis-induced long-term structural changes within the visual pathway. *Neurology(R) Neuroimmunology & Neuroinflammation*, *7*(2). https://doi.org/10.1212/NXI.0000000000000665

Hoffmann, M. B., Heinrich, S. P., Thieme, H., & Al-Nosairy, K. O. (2018). Mit klinischer Elektrophysiologie hinter die Netzhaut. *Klinische Monatsblätter für Augenheilkunde*, *235*(11), 1229–1234. https://doi.org/10.1055/a-0715-8072

* Publications presented in this thesis.